AD-A172 732 STRUCTURE DYNAMIC THEORIES OF FRACTURE DIAGNOSIS(U) NEW 1/2
MEXICO UNIV ALBUQUERQUE DEPT OF MECHANICAL ENGINEERING
F D JU 03 MAR 86 ME-134(85)AFOSR-993-2 AFOSR-TR-86-0090
UNCLASSIFIED AFOSR-85-0085 F/G 20/11 NL

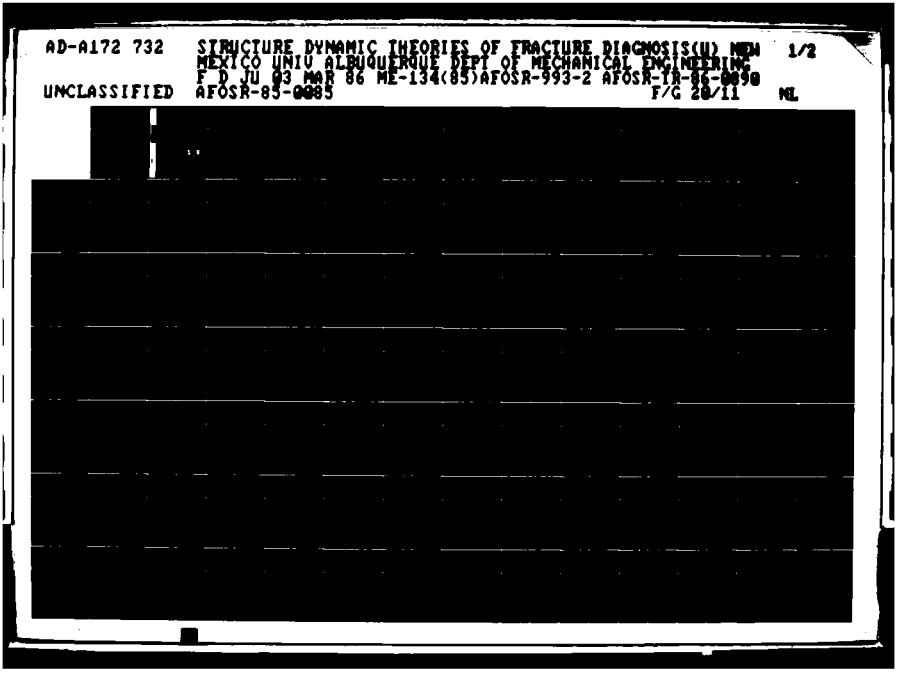

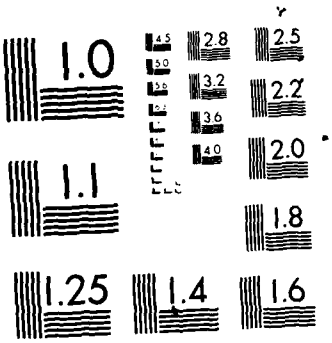

(2)

AFOSR-TR- 86-0890

THE UNIVERSITY OF NEW MEXICO
COLLEGE OF ENGINEERING

BUREAU OF ENGINEERING RESEARCH

STRUCTURE DYNAMIC THEORIES OF FRACTURE DIAGNOSIS

by
Frederick D. Ju
Mechanical Engineering Department
The University of New Mexico

Technical Report
~~ME-134(09)AFOSR-993-2~~

Work Supported by Air Force Office of Scientific Research
Grant No. AFOSR-85-0085

March 3, 1986

DISCLAIMER NOTICE

THIS DOCUMENT IS BEST QUALITY PRACTICABLE. THE COPY FURNISHED TO DTIC CONTAINED A SIGNIFICANT NUMBER OF PAGES WHICH DO NOT REPRODUCE LEGIBLY.

Unclassified
SECURITY CLASSIFICATION OF THIS PAGE

AD-A172 732

REPORT DOCUMENTATION PAGE

1a. REPORT SECURITY CLASSIFICATION: Unclassified	1b. RESTRICTIVE MARKINGS
2a. SECURITY CLASSIFICATION AUTHORITY	3. DISTRIBUTION/AVAILABILITY OF REPORT: Approved for Public Release Distribution Unlimited
2b. DECLASSIFICATION/DOWNGRADING SCHEDULE	
4. PERFORMING ORGANIZATION REPORT NUMBER(S): ME 134(85)AFOSR-993-2	5. MONITORING ORGANIZATION REPORT NUMBER(S): AFOSR-TR- 86-0890
6a. NAME OF PERFORMING ORGANIZATION: University of New Mexico; 6b. OFFICE SYMBOL (If applicable)	7a. NAME OF MONITORING ORGANIZATION: Directorate of Aerospace Sciences, Air Force Office of Scientific Research
6c. ADDRESS (City, State and ZIP Code): Albuquerque, NM 87131	7b. ADDRESS (City, State and ZIP Code): Bolling AFB, DC 20332
8a. NAME OF FUNDING/SPONSORING ORGANIZATION: Air Force Office of Scientific Research; 8b. OFFICE SYMBOL (If applicable): AROSR/NA	9. PROCUREMENT INSTRUMENT IDENTIFICATION NUMBER: AFOSR-85-0085
8c. ADDRESS (City, State and ZIP Code): Bolling AFB, DC 20332	10. SOURCE OF FUNDING NOS.

PROGRAM ELEMENT NO.	PROJECT NO.	TASK NO.	WORK UNIT NO.
6110F	2302	C2	

11. TITLE (Include Security Classification): Struct. Dyn., Th. of Fracture Diagnosis	
12. PERSONAL AUTHOR(S): Ju, Frederick D.	

13a. TYPE OF REPORT	13b. TIME COVERED	14. DATE OF REPORT (Yr., Mo., Day)	15. PAGE COUNT
Technical	FROM 01/85 TO 12/85	86-3-3	121

16. SUPPLEMENTARY NOTATION

17. COSATI CODES			18. SUBJECT TERMS (Continue on reverse if necessary and identify by block number)
FIELD	GROUP	SUB. GR.	
			Modal Frequency, Transmissibility, Fracture Hinge, Circuit Analogy

19. ABSTRACT (Continue on reverse if necessary and identify by block number)

Two modal theories of damage diagnosis are presented. The modal frequency theory, based on the changes in a modal frequencies of a structure due to damage, can identify both the location and the intensity of a crack for simple fracture configurations. The transmissibility theory, which utilizes the changes in transmissibilities across a structure, is proposed as a feasible method for large structures. The report reveals the uncertainties of the modal frequency theory. The transmissibility theory is illustrated with a frame structure in localizing a fracture damage.

20. DISTRIBUTION/AVAILABILITY OF ABSTRACT	21. ABSTRACT SECURITY CLASSIFICATION
UNCLASSIFIED/UNLIMITED. ☒ SAME AS RPT. ☐ DTIC USERS ☐	Unclassified

22a. NAME OF RESPONSIBLE INDIVIDUAL	22b. TELEPHONE NUMBER (Include Area Code)	22c. OFFICE SYMBOL
Col. Lawrence D. Hokanson	(202) 767-4935	AFOSR/NA

DD FORM 1473, 83 APR EDITION OF 1 JAN 73 IS OBSOLETE.

SECURITY CLASSIFICATION OF THIS PAGE

STRUCTURAL DYNAMIC THEORIES OF FRACTURE DAMAGE DIAGNOSIS

ABSTRACT

In this report, two modal theories of damage diagnosis in simple and complex structures are presented. The modal frequency theory, based on the changes in the modal frequencies of a structure due to damage, is shown to be a suitable method for simple fracture configurations, but not for complex ones. The transmissibility theory, which utilizes the changes in transmissibilities across a structure, is, on the other hand, proposed as a feasible method for damage diagnosis in large structures.

The modal frequency theory is applied to multiple cracks in simple beams to demonstrate its intrinsic uncertainties. It is shown that closely spaced multiple cracks behave as one single crack as far as the modal frequencies are concerned. Uncertainties may arise in the diagnosis of multiple cracks when an inadequate number of frequency measurements are available. When the structure has one major crack in addition to minor ones, however, the major crack is diagnosable.

In the transmissibility theory, the effects of (1) the excitation location and frequency, (2) the locations of the response stations where transmissibilities are computed, (3) the crack location and severity, and (4) damping on the transmissibility changes are studied for a three-story four-span frame structure. It is found that best results are obtained when the frame is excited near the joints at its modal frequencies and when the response stations are located in the vicinity of the minimum deflection points. The largest transmissibility changes are shown to occur at the response stations nearest the crack. This result allows the crack to be

located within one or two cells of a frame structure. The regions of the frame which, when cracked, are undiagnosable at the fundamental frequency are established in the study. The advantage of exciting the structure at a higher modal frequency, in such cases, is demonstrated. It is shown that undiagnosable regions become larger for less severe cracks.

The structures are modeled without loss of generality as composed of generalized Bernoulli-Euler beams, undamped in the application of the modal frequency theory and damped in that of the transmissibility theory. Damping is incorporated by means of the complex Young's modulus. In the analysis, the general theory of circuit is utilized to represent simple beams with basic electric circuits, and the fracture hinge by an electrical resistor. The damage analysis of a complex frame structure is thus formalized and adaptive for computer programming. A formalized program for the computation of frame deformation is enclosed.

TABLE OF CONTENTS

LIST OF FIGURES

LIST OF TABLES

Nomenclature

a	crack length
b	half depth of a flexural member
e	location of the crack on a beam with only one crack
$\mathbf{e}$	a column vector with all zeros except for the last entry which is unity
$e_i (=L_i / L)$	distance between $(i-1)$th and ith cracks on a simple beam; relative length of the ith beam segment in a frame structure
e_{eq}	location of the single crack which is equivalent to a group of cracks (the definition of equivalence is given on p. 56)
E	complex Young's modulus
E_d	dynamic Young's modulus
E_{i1}, E_{i2}	voltage sources in an analog T circuit for the ith beam segment (no subscript i for a one-member structure)
F	sinusoidal excitation force
F_m	sinusoidal force amplitude
G_i, G_{i0}	conductances in an analog Π circuit for the ith beam segment (no subscript i for a one-member structure)
h	$L^2 / EI\beta^2$ (subscripted when referring to the ith segment)
h_f	h value for the beam element with the force
$\mathbf{i}$	vector of current sources
I	area moment of inertia
I_{i1}, I_{i2}	current sources in an analog Π circuit for the ith beam segment (no subscript i for a one-member structure)
k	total number of cracks on a structure
$k_c (k_g)$	total number of column(girder) cracks on a frame structure
L_i	distance between $(i-1)$th and ith cracks on a simple beam; length of the ith beam segment in a structure

L length of a beam

m number of spans of a frame structure

$\mathbf{m}$ vector of unknown moments

M_i resisting moment at the (i-1)th crack in a cantilever

M_{i1}, M_{i2} resisting moments at the two ends of the $i$the beam segment (no subscript i for a one-member structure)

n number of stories of a frame structure

P, P', Q, Q' variables of the analog Π circuit; subscripted when referring to the ith segment

R_j $1-\omega_j/\omega_{uj}$, relative change in jth modal frequency

$R_{j_{eq}}$ relative change in jth frequency due to an equivalent crack causing the same change in two other frequencies as the actual damage

R_T relative transmissibility change

S, S', T, T' variables of the analog T circuit; subscripted when referring to the ith segment

T transmissibility

t time

U matrix of resistances or conductances

V_{i1}, V_{i2} resisting cross-shears at the two ends of the ith beam (no subscript i for a one-member structure)

W, W' variables of the analog Π circuit; subscripted when referring to the ith segment

X coefficient matrix of $\mathbf{m}$ or $\mathbf{y}'$

y complex modal shape or complex deflection(real when δ=0

y^* nondimensional complex deflection, Equation 4.7

y_i deflection at the ith crack; horizontal displacement of the ith floor

y_m amplitude of complex deflection

y_f complex deflection under the excitation force

y_t complex deflection at a response station

y_{i1}, y_{i2} transverse deflections at the two ends of the ith beam segment (no subscript i for a one-member structure)

$\mathbf{y}$ vector of deflections

y_i' rotation of the ith node

y_r' rotation of the node r' immediately to the right of or above a crack

y_{i1}', y_{i2}' rotations at the two ends of the ith beam segment (no subscript i for a one-member structure)

$\mathbf{y}'$ vector of rotations

Z_i, Z_{ic} resistances in T circuit for the ith segment

$\mathbf{Z}$ coefficient matrix of $\mathbf{y}$

α defined in Equation 2.31

β complex characteristic value(real when $\delta=0$), $\beta^4=\omega^2\rho L^4/EI$

β_d undamped characteristic value, $\beta_d^4=\omega^2\rho L^4/E_dI$

β_u characteristic value of the undamaged structure

$\beta^{(j)}$ jth characteristic value

$\beta_{eq}^{(j)}$ jth characteristic value for the structure with an equivalent crack having two other characteristic values in common with the actual damaged structure

$\beta_{act}^{(j)}$ jth characteristic value for the actual damaged structure

β_i characteristic value for the ith beam segment

δ damping factor

ε strain

η_{ij} defined in Equation (2.51)

γ a/b , relative crack depth

κ torsional spring constant of a fracture hinge (subscripted for the ith crack)

Λ_i $\dfrac{1}{\Theta_i\beta_c(1+i\delta)}$

λ_i $\dfrac{\beta_i/L_i}{\beta_c/L_c}$

ν Poisson's ratio

ρ lineal mass density

σ stress

Θ_i sensitivity number for the ith crack on a simple beam;
sensitivity number for the crack on the ith member of a frame structure

ω_j jth modal frequency

ω_{uj} jth modal frequency of the undamaged structure

ξ normalized length coordinate

ξ_f location on the beam element where force is applied

ξ_i location of the response station on the ith beam element

Subscripts :

0 reference value when used on β, EI, L, h; no-crack case when used on T, y

c value with crack

CHAPTER 1

INTRODUCTION

Fracture damage diagnosis stems from the need to ensure safety of structural components or structures, or from the requirements of quality control in production. Structures may develop cracks from aging but most likely as a result of some strong excitations such as in earthquake, blast loading, wind loading and the like. Diagnosis of flaws is thus essential in assessing the reliability and integrity of the structure. The diagnostic method must be of such a nature that it is nondestructive. The present report summarizes two diagnostic theories for fracture damage in structures based on the modal theory of structure dynamics. The first one is the modal frequency theory. The second one is the transmissibility theory.

Nondestructive testing began gaining importance in industry after World War I even though there were earlier studies to detect cracks in metals nondestructively [1]. Nondestructive testing had no great impetus, however, until World War II. Since then, it has become a major area of research and development. Nondestructive test techniques include the categories of radiography, sonic-ultrasonic methods, visual methods-penetrants, electromagnetic methods and thermal methods. The current ASME code for the inspection of boilers and pressure vessels recognizes some of the existing methods which fall into the first four of these categories [2]. None of these methods, however, yield good results when the surfaces of the crack are nearly parallel to the direction of propagation of waves or magnetic flux lines. On the other hand, all of these methods are local methods, that is, the excitation (X-rays, ultrasonic transmitter, magnetic coil, or heat flux)

and the sensor must be physically near the flaw. As a result, a scanning of the structure or the component is necessary to cover all areas which are likely to contain flaws. A global full-scale testing method is, therefore, needed for diagnosis of damage in large structures such as bridges, offshore platforms, buildings and the likes. By a global method is meant a method whereby the location and possibly the severity of flaws in a structure can be determined by exciting the structure at an arbitrary point and monitoring the responses at various stations on the structure, without the need for scanning. An ultrasonic technique described as global was proposed [3,4] for the inspection of tubular K-joints, where globalism is defined as the capability to monitor an entire joint rather than an entire structure. The proposed method, however, is not capable of detecting cracks which are located around the periphery of the major tubular column near the joint [4].

A global method of damage detection studied recently is the random decrement technique [5,6]. The random decrement process is a signal processing technique which extracts the free decay responses from the random dynamic responses. The changes in the free decay responses at several locations on an experimental scale model of an offshore platform were used to detect the damage in the structure [5]. The scale model consisted of six levels with K-joints at the mid-span of each girder. The predictions of the damage locations in various damage scenarios were not very specific with the random decrement method. The cross random decrement method was later employed as an improvement [6]. This technique utilizes two simultaneous response measurements from two different positions on the structure. Experiments were carried out on a similar platform model. Relative phase shifts between every two neighboring response locations were computed using the cross random decrement technique before and after damage was introduced.

The largest changes in the relative phase shifts, in general, occurred at locations near the damage. Both studies by Yang et al. [5] and Tsai et al. [6] were purely experimental. Experiments of this nature are costly and cannot be carried out for a significant number of damage configurations. Consequently, neither of the studies was able to reach a general conclusion. It was concluded, "due to the complexity of the large structure configuration, the relationship between phase changes and the damage location still needs more research effort" [6].

The report will cover two modal theories of damage diagnosis developed by the author and his co-workers, using the change of dynamic characteristics of the damaged structure. The modal frequency theory uses the change of modal frequencies to establish damage functions, from which the intensity and location of individual crack damage are diagnosed [7,8]. The application of the theory to large structures and to multiple crack problems was made possible with the development of a general theory of circuit analogy [9,10,11]. For complex structures or crack damage configurations, there are intrinsic uncertainties of the modal frequency theory to be included in the present report, portion of which was presented by Ju [12]. The transmissibility theory uses the change of the transmissibility between a known excitation station and a number of response stations to diagnose the fracture damage. Details of the theory and application are included in this report. The feasibility and application of the theory were earlier presented by Akgun and Ju [13,14].

It is well-known that a structural member deminishes its load-carrying capacity when a crack is developed in the member [15,16,17]. It was shown in the case history of a large structure that the frequencies of the structure decreased after an earthquake [18]. Numerous studies have been

reported in the literature on the effect of notches and cracks on beam behavior. Static deflection of beams with abruptly changing cross sections was studied by analyzing an equivalent uniform beam with modified loading [19]. This approach was extended to vibration of bars with narrow slots [20]. An experimental and analytical study was conducted earlier on narrow cracks, in which bending frequencies of a beam with a 1.6 mm wide crack at the center were measured [21]. It was found, for this particular configuration, that analytical and experimental natural frequencies agreed when an equivalent slot width of five times the actual width was used. Such a relationship cannot be generalized, however, since it omits the effect of slot depth [20]. A combination of the finite element and transfer matrix methods was used recently to determine the effect of grooves on the natural frequencies of beams and, as an example, changes in the fundamental frequency of a free-free beam with a slot at mid-span were determined as a function of the slot depth and width [22]. The method of representing a slot with modified loading [19,20] was extended to a study of the effect of a crack on the stresses and deflections in cylindrical shells and beams under dynamic loading [23,24]. In the model, the cracked structure was represented by an uncracked structure with the local reduction in stiffness due to crack being accounted for by a pair of concentrated couples M located a small distance c/2 on either side of the physical crack location. The method requires the knowledge of static radial deflections at two points in the case of a circular cylindrical shell from which the product Mc is determined and the model is calibrated [23]. The static modes of deformation are then used to compute the dynamic response of the structure. The required static deflections of the cracked structure need to be measured experimentally or computed numerically to establish the dependence of Mc on the crack depth for the particular structure.

Chondros et al. [25] investigated the effect of a crack in a welded joint on the dynamic flexural behavior of beams. Their model was a massless cantilever beam with a tip mass. The crack at the welded joint was modeled as a torsional spring. The spring constant was experimentally determined from the changes in the natural frequency for different crack depths. Gudmundson [26] using a first order perturbation method for small cracks, showed that the frequency changes are functions of the static strain energy due to the crack. Gudnundson like Ju et al. [7,8] related the strain energy to the crack depth via the stress intensity factor. In the case of a cantilever beam, his analytical results showed excellent agreement with the results of an experimental study except when the crack was close to the built-in end. He explained the disagreement near the built-in end by the influence of the built-in boundary on the static stress intensity factor. Gudmundson [27] recently modeled a crack by a static flexibility matrix which accounts for the dicontinuity in the generalized displacements at the crack location. He obtained the flexibility matrix for a cantilever beam by using static stress intensity factors. For the case of torsional vibrations, he used the finite element mehtod to obtain the flexibility matrix. Gudmundson's experiments with a cantilever beam confirmed his analytical results very well.

Ju [7,8] proposed the theory that the stiffness-softening effect of crack damage in structures can be effectively represented quantitatively by a spring-loaded hinge at the cracked section of the structure. He further postulated in his theory that the spring constant is completely defined by the configuration of the crack and is independent of its location or of the frequency of osicllation. The determination of the effective spring constant, hence, can be made experimentally or analytically. One of the analytical techniques for the determination of the spring constant is by

equating the strain energy stored in the spring with the surface energy gained through the creation of the crack surface. The fracture-hinge theory has recently been verified by experiment to be reported later. A portion of the work will be presented by Ju and Mimovich [28] at the International Modal Analysis Conference and published in its proceedings.

The numerical analysis, used in the present report, is based on the general theory of circuit analogy, which was initially developoed in Russia [29] and was later generalized for structural dynamics by Ju and Akgün [9,10,11]. The fundamental principle lies in that the beam equations with the assumption of modal shapes become algebraic and are mathematically equivalent to the Kirchhoff's circuit theory equations. Details were reported in [11]. The work has been generalized to include damping and extended to beams of non-uniform properties (geometrical or material). In this revised form, the general theory of circuit analogy is included.

CHAPTER 2

GENERAL THEORY OF CIRCUIT ANALOGY

The structures considered in this study are beams and plane frames whose motions are described by the Bernoulli-Euler equation with damping. The method used to analyze the structures is the electrical analogy method. The present chapter is devoted to the development of the analog circuits and circuit equations for a beam and for a general frame with and without cracks. First, the complex Young's modulus and the types of damping which can be incorporated in the structure model are studied in the next section.

2.1. Types of Damping Encompassed by the Model

2.1.1. Internal Damping - Complex Young's Modulus

Metals at low stress display linear viscoelastic behavior [30] The general stress-strain relation for a linear viscoelastic material is given by [31].

$$(a_0+a_1D_1+\cdots+a_nD_n+\ldots)\sigma = (b_0+b_1D_1+\cdots+b_mD_m+\ldots)\varepsilon \qquad (2.1)$$

where a_k and b_k are constants and D_k denotes the kth partial derivative with respect to time. When σ and ε vary sinusoidally with time, $D_k = (i\omega)^k$, and

$$\frac{\sigma}{\varepsilon} = E(\omega) = E_d(\omega)\,[1 + i\,\delta(\omega)] \qquad (2.2)$$

where $E(\omega)$ is the complex Young's modulus, $E_d(\omega)$ is the dynamic Young's modulus and $\delta(\omega)$ is the loss or damping factor. The real part of $E(\omega)$ is termed the storage modulus and the imaginary part is the loss modulus. For low damping materials (δ of the order 0.1 or less), variation of E with frequency is slow. For many materials of engineering interest, E_d and δ may be treated as constants. Common metals such as aluminum and magnesium, for which δ is very small, fall into this category [31, pp.27,137]. A type of damping which is sometimes used in flexural and longitudinal

vibrations is the internal strain velocity damping (viscous) for which the constitutive equation is

$$\sigma = E_d\, \varepsilon + bD_1\, \varepsilon \tag{2.3}$$

where the second term on the right is the damping stress [32] For harmonic vibrations,

$$\frac{\sigma}{\varepsilon} = E = E_d\,(1 + \frac{ib\omega}{E_d}) \tag{2.4}$$

which yields a damping factor proportional to frequency. Experimental evidence contradicts such dependence of damping on frequency. A more realistic damping factor may result if higher order time derivatives are used in Eq. (2.3). However, the damping force in real structures appears to be in phase with the velocity but proportional to the displacement [32 p.76]. Such damping is termed structural or hysteretic damping. The constitutive equation can then be written as

$$\sigma = E_d\, \varepsilon + id\,\varepsilon. \tag{2.5}$$

The complex modulus for structural damping then follows from Eq. (2.5); that is,

$$E = E_d\,(1 + \frac{id}{E_d}) \tag{2.6}$$

where $\frac{d}{E_d}$ is the structural damping factor which is independent of frequency. In this study, E will be used in the form given by eq. (2.2) without referring to the type of damping.

The deflection of a beam under transverse vibration, excited by a sinusoidal force, is governed by [31 p.196]

$$\left[\frac{d^4y}{d\xi^4} - \beta^4 y\right] e^{i\omega t} = 0 \tag{2.7}$$

where $\xi = \frac{x}{L}$ is the normalized axial coordinate, $y = y(\xi)$ is the complex modal shape and

$$\beta^4 = \frac{\rho\omega^2 L^4}{EI} = \frac{\beta_d^4}{(1 + i\delta)} \tag{2.8}$$

where $\beta_d^4 = \frac{\rho\omega^2 L^4}{E_d I}$ and β_d, at resonance, is the undamped characteristic value. β, near resonance, will be called the "complex characteristic value". When δ is small,

$$\beta \approx \beta_d(1 - i\,\frac{\delta}{4}). \tag{2.9}$$

In the study, however, exact values of β are used.

At this point, a clarification on terminology will be made. It is appropriate to call y the complex modal shape, and this term has been used in the literature. The physical shape of a damped beam under forced vibration, however, cannot, in general, be referred to as the modal shape. This is a consequence of the fact that the physical beam deflection cannot, in general, be expressed as the product of a time function and a space function. The argument can be illustrated by taking the real part of the complex deflection. Namely,

$$w_r = \mathrm{Re}\,[y\ e^{i\omega t}\ ] = y_m(\xi)\cos\,[\omega\, t - \varphi(\xi)] \tag{2.10}$$

where w_r is the physical deflection, and y_m and φ are the magnitude and phase angle of the complex modal shape y, both of which are functions of ξ and ω. Only when $\varphi = 0$ (i.e., no damping), can y_m be referred to as the modal shape. In this study, y_m is termed the amplitude of deflection.

2.1.2. External Viscous Damping

When there is external viscous resistance to the transverse harmonic vibration of a uniform beam, the governing equation is again of the form of Equation (2.7) where β is now defined as

$$\beta^4 = \frac{(\rho\omega^2 - i\,c\,\omega)\,L^4}{EI} \tag{2.11}$$

where c is the coefficient of viscous damping. Therefore, the methods of this study are also valid when the damping is of the external viscous type or a combination of external and internal types.

In the remaining part of the chapter, the basic circuit analogs of a beam and a general frame with cracks are derived based on Eq. (2.7). In the frequency theory (Chapter 3), the structures are assumed undamped and therefore β is real. In the transmissibility theory (Chapter 4), damped structures are considered, for which β is complex. The same analog circuits, however, are used in both methods, with β chosen properly.

2.2. Basic Analog Circuits

Keropyan and Chegolin gave the T- and Π-circuit analogs of vibrating beams [29]. The analog circuits will be rederived here. The complex mode shapes of a Bernoulli-Euler beam element under transverse vibration are given by the solution to Equation (2.7). That is,

$$y(\xi) = \bar{A}\cosh\beta\xi + \bar{B}\sinh\beta\xi + \bar{C}\cos\beta\xi + \bar{D}\sin\beta\xi \tag{2.12}$$

Four variables are associated with each end of the beam element, namely, deflection, y, slope (or angle of rotation), y', resisting moment, M, and shear force, V (Figure 1). From Equation (2.12) and its appropriate derivatives at $\xi = 0$, the variables at the left end are obtained:

$$\begin{aligned} y_1 &= \bar{A} + \bar{C} & y_1' &= (\bar{B} + \bar{D})\frac{\beta}{L} \\ M_1 &= (\bar{A} - \bar{C})\frac{EI\,\beta^2}{L^2} & V_1 &= (\bar{D} - \bar{B})\frac{EI\,\beta^3}{L^3} \end{aligned} \tag{2.13}$$

From the equations in (2.13), the four coefficients can be solved for in terms of the four variables. Namely,

$$\begin{aligned} \bar{A} &= \frac{(y_1 + h\,M_1)}{2} & \bar{B} &= \frac{(y_1' - h\,V_1)L}{2\beta} \\ \bar{C} &= \frac{(y_1 - h\,M_1)}{2} & \bar{D} &= \frac{(y_1' + h\,V_1)L}{2\beta} \end{aligned} \tag{2.14}$$

where $h = \dfrac{L^2}{EI\beta^2}$. The variables at the right-end of the beam element are obtained from Equations (2.12) and (2.14) with $\xi = 1$. The result is

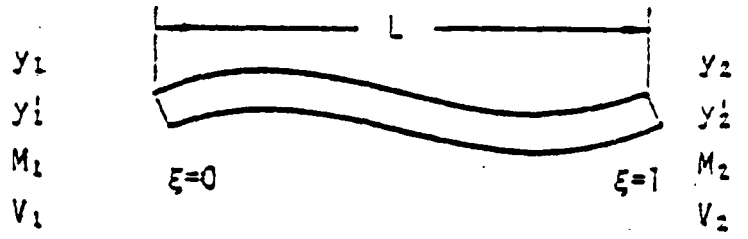

Figure 1. Beam element under free vibration.

$$y_2 = Ay_1 + By_1'\frac{L}{\beta} + CM_1h - DV_1h\frac{L}{\beta}$$

$$y_2' = Dy_1\frac{\beta}{L} + Ay_1' + \frac{BM_1L}{EI\beta} - CV_1h$$

$$M_2 = C\frac{y_1}{h} + Dy_1'EI\frac{\beta}{L} + AM_1 - BV_1\frac{L}{\beta}$$

$$V_2 = -By_1\frac{\beta}{hL} - C\frac{y_1'}{h} - DM_1\frac{\beta}{L} + AV_1 \qquad (2.15)$$

where

$$A = \frac{(\cosh\beta + \cos\beta)}{2} \qquad B = \frac{(\sinh\beta + \sin\beta)}{2}$$

$$C = \frac{(\cosh\beta - \cos\beta)}{2} \qquad D = \frac{(\sinh\beta - \sin\beta)}{2} \qquad (2.16)$$

Any four of the eight variables in Equation (2.15) can be solved for in terms of the remaining four variables. The mathematical analogy between electrical circuits and beams is based on the liner transform (2.15). The type and properties of the resulting circuit depend on the choice of the independent variables. In this study, angles of rotation are analogous to voltages and resisting moments are analogous to electrical currents.

2.2.1. T Circuit

When the condition $\sin\beta \neq 0$ is imposed, (β is real for an undamped beam) slopes and shears can be expressed in terms of resisting moments and deflections. Thus,

from Equation (2.15)

$$\begin{Bmatrix} y_1' \\ y_2' \\ V_1 \\ V_2 \end{Bmatrix} = \frac{\beta}{2L} \begin{bmatrix} -hS & -hT & -S' & T' \\ hT & hS & -T' & S' \\ S' & -T' & S/h & T/h \\ T' & -S' & -T/h & -S/h \end{bmatrix} \begin{Bmatrix} M_1 \\ M_2 \\ y_1 \\ y_2 \end{Bmatrix} \tag{2.17}$$

where $h = \frac{L^2}{EI\beta^2}$ and

$$S = \coth \beta - \cot \beta$$

$$S' = \coth \beta + \cot \beta$$

$$T = \csc \beta - \operatorname{csch} \beta$$

$$T' = \csc \beta + \operatorname{csch} \beta \tag{2.18}$$

The first two equations in (2.17) can be rewritten as

$$y_1' = (Z + Z_0)M_1 - Z_0 M_2 + E_1 \quad , \quad y_2' = Z_0 M_1 - (Z + Z_0)M_2 + E_2 \tag{2.19}$$

where

$$Z = -(S+T)\frac{L}{2EI\beta} \quad , \quad Z_0 = \frac{TL}{2EI\beta} \tag{2.20}$$

$$E_1 = (T'y_2 - S'y_1)\frac{\beta}{2L} \quad , \quad E_2 = (S'y_2 - T'y_1)\frac{\beta}{2L} \tag{2.21}$$

The two equations in (2.19) are the Kirchhoff's equations for the active three terminal network shown in Figure 2 (T circuit) with slope and moment (y', M) being analogous to electrical voltage and current, respectively. The quantities Z and E denote electrical impedance and voltage source, respectively. Negative resistance (real part of Z) poses no difficulty in analytical and numerical analyses. The ends of a beam segment are simulated by the ports of the circuit. It must be observed that the electromechanical analogy described above does not simulate the differential equation of motion, but instead the solution based on the assumption of harmonic motion [29].

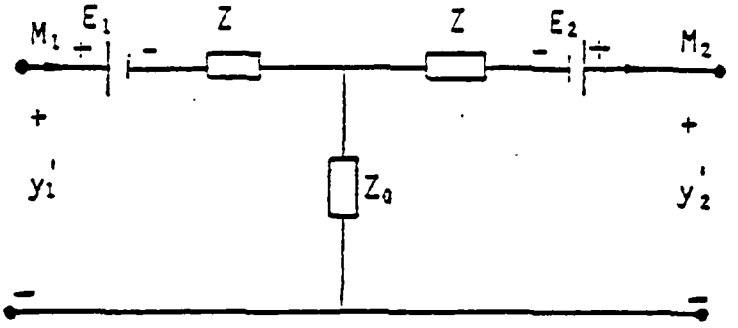

Figure 2. T-circuit analog of a beam under free vibration

Boundary conditions at the ends of a beam element can be simulated as follows:

a. Free end or simply-supported end, $M=0$: the corresponding port of the circuit is left open, which results in zero electrical current.

b. Fixed end, $y'=0$: The corresponding port is short-circuited, which results in zero voltage. The other boundary conditions at these ends and the last two Equations in (2.17) are utilized to express the voltage sources, Equation (2.21), in terms of the moments, as will be illustrated with an undamped cantilever beam vibrating freely (Figure 3). All of the circuit variables are real in this case. The Kirchoff's voltage law applied to the loop yields

$$(Z + Z_0)M_1 + E_1 = 0 \tag{2.22}$$

where Z is the analog resistance. From the last equation in (2.17) with $y_1 = M_2 = 0$,

$$V_2 = 0 = (T'M_1 - S\frac{y_2}{h})\frac{\beta}{2L} \tag{2.23}$$

from which

$$y_2 = hT'\frac{M_1}{S} \qquad \text{and} \qquad E_1 = (T')^2 M_1 \frac{L}{2EI\beta S} \tag{2.24}$$

The second equation in (2.24) is obtained from Equation (2.21).

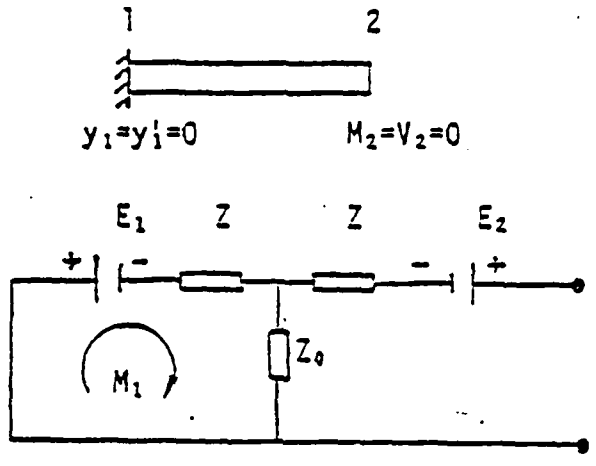

Figure 3. Cantilever beam and its T-circuit analog

The substitution of Equations (2.20) and (2.24) into (2.22) and the fact that $M_1 \neq 0$ result in

$$\frac{(T')^2}{S} - S = 0 \tag{2.25}$$

which yields the characteristic equation of a cantilever beam, $1 + \cosh\beta \csc\beta = 0$.

In the derivation of Equation (2.17), it is theoretically sound to impose $\sin\beta \neq 0$. However, during the numerical search of the undamped natural frequencies, $\sin\beta$ may get very small at some point, or the structure may actually have frequencies at or near $\sin\beta = 0$. The solution to the problem lies in realizing that β is directly proportional to the length L of the beam element. The problem can thus be solved by dividing the beam into two sections and representing each section by an individual circuit. To illustrate the approach, an undamped simply-supported beam is arbitrarily divided into two elements with a length ratio of $\frac{4}{6}$ (Figure 4). With reference to the figure, the continuity conditions in slope and moment (voltage and current) at the common boundary is preserved under the cascade connection of the two basic circuits. The loop equation then yields

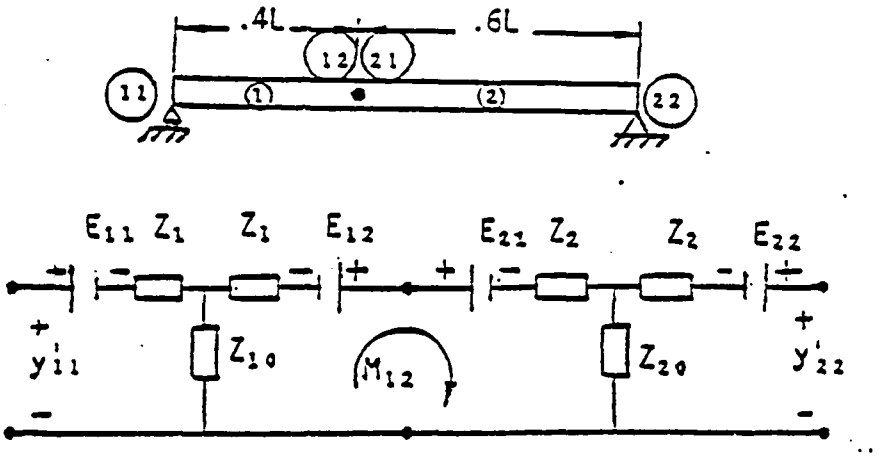

Figure 4. Simply-supported beam represented with two elements and its Analog Circuit

$$(Z_1 + Z_{10} + Z_2 + Z_{20})M_{12} - E_{12} + E_{21} = 0 \qquad (2.26)$$

Since deflection is continuous at the interface (i.e., $y_{12} = y_{21}$), it can be shown that

$$E_{12} = \frac{y_{12}\beta_1 S_1'}{2L_1} \qquad E_{21} = -\frac{y_{12}\beta_2 S_2'}{2L_2} \qquad (2.27)$$

where $L_1 = 0.4L$, $L_2 = 0.6L$, $\beta_1 = 0.4\beta$, and $\beta_2 = 0.6\beta$ with $\beta^4 = \rho\omega^2 L^4 / E_d I$. From Newton's third law $V_{12} = V_{21}$, or

$$y_{12} = \frac{-hM_{12}(S_1' + S_2')}{S_1 + S_2} \qquad (2.28)$$

Equations (2.20) and (2.26) through (2.28) can be combined to yield the frequency equation

$$(S_1' + S_2')^2 - (S_1 + S_2)^2 = 0 \qquad (2.29)$$

It is to be noted that for the particular sectioning in this illustration, the same problem will arise at the fifth natural frequency where $\beta_1 = 2\pi$ and $\beta_2 = \pi$. Then the same procedure can be applied by further sectioning he beam. Better initial sectionings are of course possible than the one presented.

2.2.2. Π Circuit

Similar to the case of Equation (2.17) in the T-circuit, Equation (2.15) can be rewritten such that resisting moments and shears are expressed in terms of deflections and slopes; that is,

$$\begin{Bmatrix} M_1 \\ M_2 \\ V_1 \\ V_2 \end{Bmatrix} = \frac{1}{h} \begin{bmatrix} QL/\beta & WL/\beta & Q' & -W' \\ -WL/\beta & -QL/\beta & -W' & Q' \\ Q' & W' & P\beta/L & -P'\beta/L \\ W' & Q' & -P'\beta/L & -P\beta/L \end{bmatrix} \begin{Bmatrix} y_1' \\ y_2' \\ y_1 \\ y_2 \end{Bmatrix} \tag{2.30}$$

where

$$P = (\cosh\beta \sin\beta + \sinh\beta \cos\beta)/\alpha \qquad P' = \frac{\sinh\beta + \sin\beta}{\alpha}$$

$$Q = (\cosh\beta \sin\beta - \sinh\beta \cos\beta)/\alpha \qquad Q' = \frac{\sinh\beta \sin\beta}{\alpha}$$

$$W = \frac{\sinh\beta - \sin\beta}{\alpha} \qquad W' = \frac{\cosh\beta - \cos\beta}{\alpha}$$

$$\alpha = \cosh\beta \cos\beta - 1 \neq 0 \tag{2.31}$$

The first two equations in (2.30) can be rewritten as

$$M_1 = (G + G_0)y_1' - G_0y_2' + I_1 \quad , \quad M_2 = G_0y_1' - (G + G_0)y_2' + I_2 \tag{2.32}$$

where G and I are the analog admittance and current source, respectively, given by

$$G = (Q + W)\frac{EI\beta}{L} \quad , \quad G_0 = \frac{-WEI\beta}{L} \tag{2.33}$$

$$I_1 = (Q'y_1 - W'y_2)/h \quad , \quad I_2 = (Q'y_2 - W'y_1)/h \tag{2.34}$$

Equation (2.32) is the Kirchhoff's current equation for the active three terminal network shown in Figure 5 (Π circuit) with G and I denoting an admittance and a current source, respectively. Moment, M, and slope, y', are again analogous to current and voltage. As an illustration, the cantilever beam of Figure 3 will now be simulated with a Π circuit. The left port of the circuit in Figure 5 is shorted yielding the circuit of Figure 6. The node voltage equation is

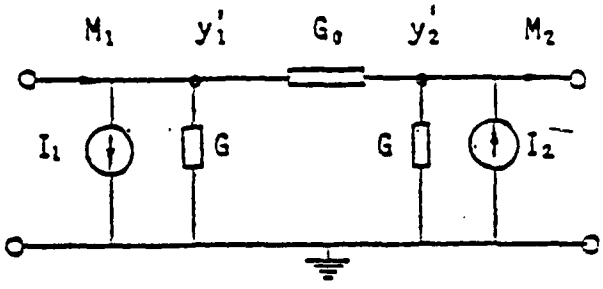

Figure 5. Π-circuit analog of a beam under free vibration

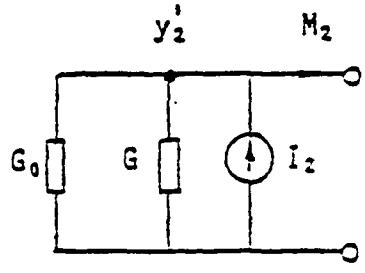

Figure 6. Analog Π-circuit for a Cantilever Beam

$$(G + G_0)y_2' - I_2 = 0 \tag{2.35}$$

The last equation in (2.30) with $y_1 = y_1' = V_2 = 0$ yields

$$y_2 = \frac{LQ'y_2'}{\beta P} \tag{2.36}$$

The characteristic equation is obtained by substituting Equations (2.33, 2.34, 2.36) into (2.35) with the result that

$$Q - \frac{(Q')^2}{P} = 0 \tag{2.37}$$

With reference to (2.31), Equation (2.37) is equivalent to $1 + \cosh\beta \cos\beta = 0$, if $1 - \cosh\beta \cos\beta \neq 0$. When the value of α(Equation 2.31) approaches zero, numerical computation diverges. Similar to the approach in T circuit, the beam can be subdivided into elements as described in the previous section.

2.3. Simulation of Crack with Circuit Analogy

A cracked section in a beam is modeled following the method of fracture hinge [7,8]. The effect of a crack is to introduce local flexibility in the beam. The slope of the mode shape is discontinuous at the cracked section. The crack can thus be mechanically represented by a torsional spring of spring constant κ. The discontinuity in the slope is given by $\Delta y' = \frac{M_c}{\kappa}$, where M_c is the resisting moment at the cracked section. Such a discontinuity is analogous to a voltage drop in the circuit theory, when slope and moment are analogous to voltage and current, respectively. The crack can then be simulated with a resistor of resistance $-1/\kappa$. Hence, a beam with a single crack is represented by two circuits (T or Π) joined by a "crack resistance," $-1/\kappa$.

The derivation of κ is based on equating the energy stored in the torsional spring to the increase in strain energy of the beam due to the crack. For a plane strain crack, this approach yields [7,8].

$$\frac{1}{\kappa} = \frac{3\pi b}{E_d I}(1-\nu^2)\int_0^{\gamma} \lambda\,[f(\lambda)]^2 d\lambda \tag{2.38}$$

where $\gamma = \frac{a}{b}$ is the relative crack depth (Figure 7) and f is the dimensionless stress intensity factor for symmetric cracks given by

$$f(\gamma) = (1-\gamma)^{-1.5}[1.122 - 2.363\gamma + 4.367\gamma^2 - 4.88\gamma^3 + 2.845\gamma^4 - 0.363\gamma^5] \tag{2.39}$$

The analysis of the next chapter will indicate that the crack intensity is quantified by the following nondimensional number:

$$\Theta = \frac{E_d I}{\kappa L} \tag{2.40}$$

Equation (2.38) reveals that Θ is a function of the beam slenderness ratio, $2b/L$, and the relative crack depth, γ. The analysis indicates that as the value of Θ increases, the reduction in the natural frequencies of a beam also increases. Hence, of the two beams with a crack of the same relative depth, at the same relative location, the

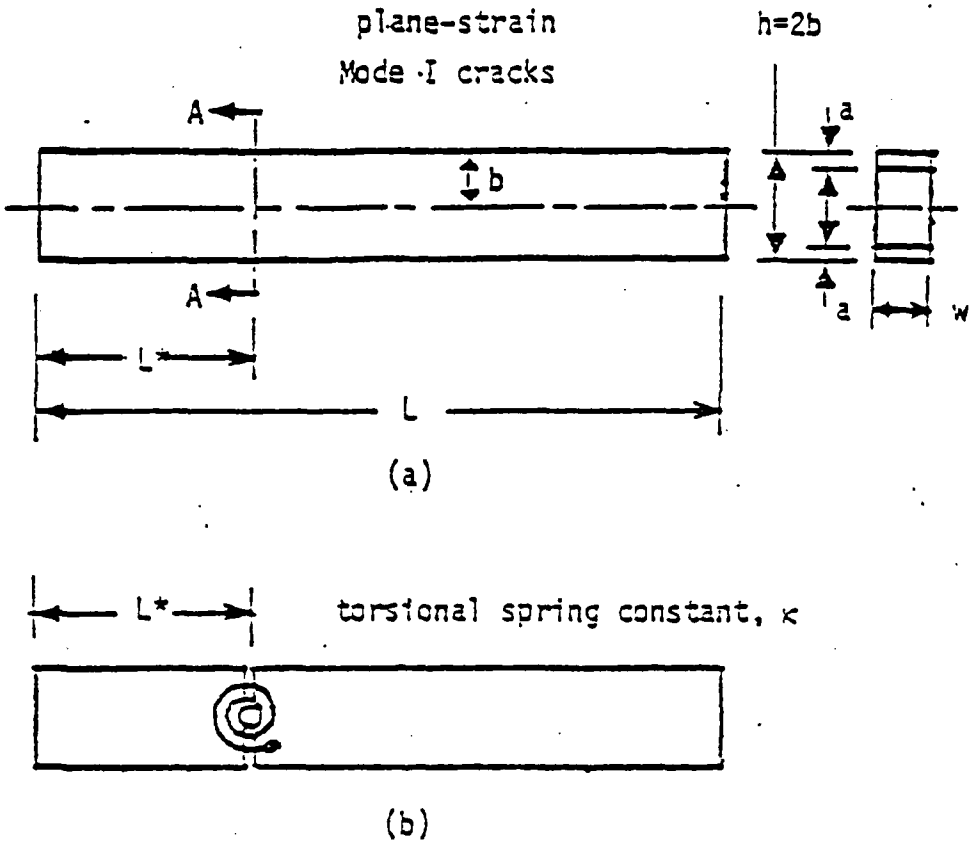

Figure 7. Crack geometry and equivalent fracture hinge

frequencies of the more slender beam will experience smaller changes. Therefore, Θ is called the "sensitivity number".

2.4. Analog Circuit for A Plane Frame

Keropyan and Chegolin presented some examples of the application of electrical analogy circuits to the solution of static and dynamic frame problems [29]. The approaches presented by them to frames with freedom of lateral motion involve an iterative solution or a several step procedure. In the former, the amount of sidesway is guessed and iterated on. In the latter, the frame is first restricted laterally, the reactions at the restrictions are solved for, and the sidesway is then computed. Both of these approaches become complicated and uneconomical for multi-story frames.

Keropyan and Chegolin illustrated the latter approach with a static one-story frame problem. Their examples of dynamic frames involved laterally constrained frames.

This section expounds a generic model of a two-dimensional multi-story frame (Figure 8) with n stories and m spans (thus $m+1$ anchors). Damage diagnosis on such a frame using both the frequency and the transmissibility methods will be developed in later chapters. In the study of the frequency method, free vibration of the frame with and without a crack is analyzed from which the characteristic equation is derived. In the development of the transmissibility method, transverse deflection at a certain location is computed under a sinusoidal excitation force. The analog circuits are the same in both methods with the exception that, in the second method, β is complex and some additions are made to the circuit. In this section the circuit equations are derived in their most general form to be applicable to both methods. A formalized scheme is developed for obtaining the circuit equations of a general frame with or without cracks, from which the modal frequencies or desired kinetic and kinematical quantities can be computed. In the T-circuit analogy, the circuit equations for the structure are developed through the mesh current (moment) equations. Hence, the unknowns are the moments at the frame joints and at the cracks. There are $p-1$ unknown moments at a frame node where p beams join together. Because the moment is continuous across a crack, there is one unknown moment for each crack. It follows that the order of the resulting linear system, which is equal to the number of unknowns, is $[n(3m+1)+k+2]$ for a frame with k cracks and one excitation, one of the unknowns being the value of the kinetic or kinematical quantity at the desired location on the structure. On the other hand, in the Π-circuit analogy, node voltage (slope) equations lead to the circuit equations. Slope is continuous at a frame joint; therefore, there is one unknown slope for each frame joint regardless of the number of beams connected there. However, there are two unknown slopes at each crack location, one on each side of the crack. In other words, slope is discontinuous across a crack. The structure is assumed rigidly fixed at the ground level; hence, the slopes are zero at the anchors. The order of the system is

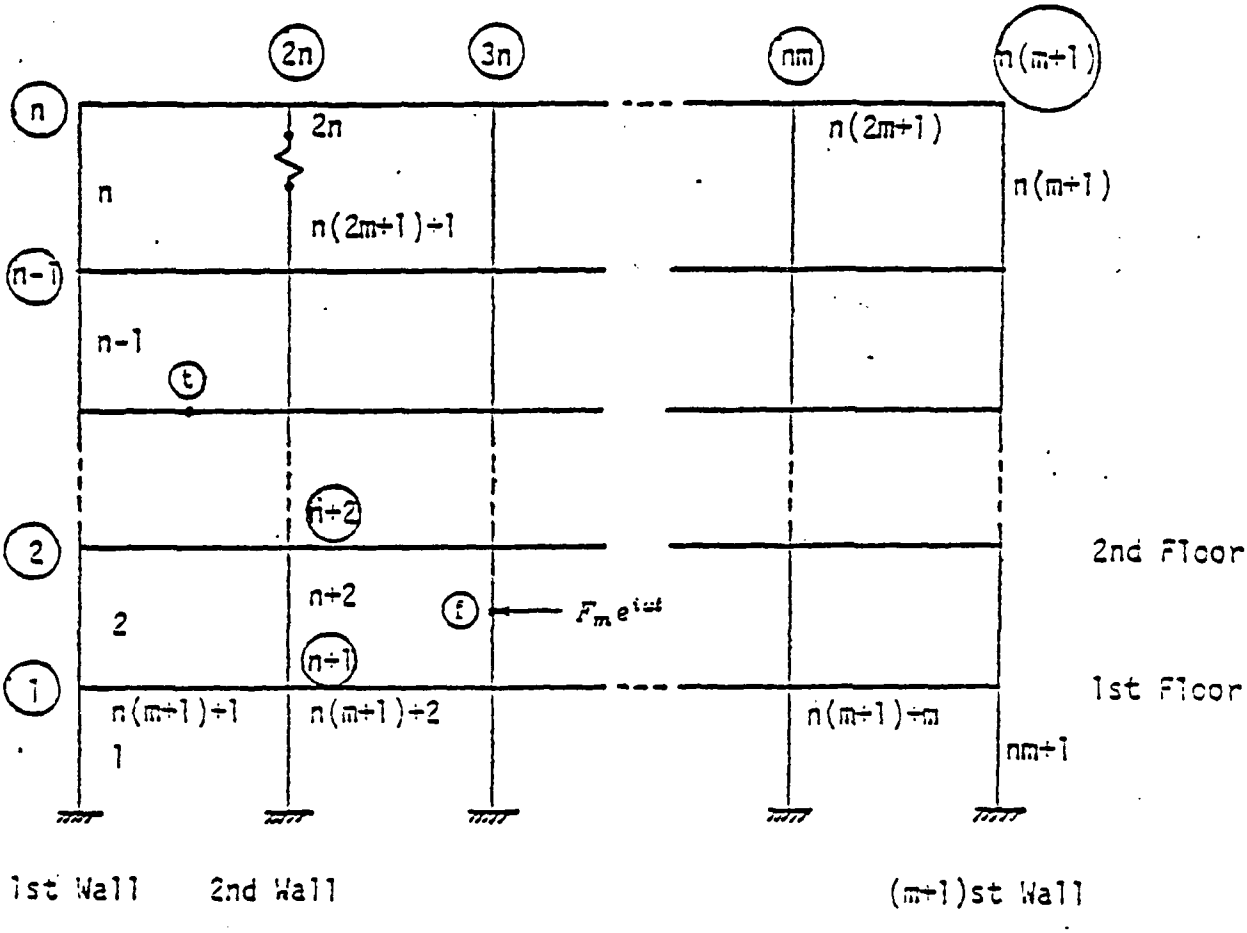

Figure 8. General n-story m-span frame structure

thus $[n(m+1)+2k+2]$ with Π circuits. The Π-circuit analogy is therefore preferred over the T-circuit analogy, since the order of the system for $k < 2mn$ is smaller in the former.

The procedure to obtain the circuit equations of a frame structure are outlined next.

(1) Π circuits simulating individual columns and girders joining at right angles are interconnected such that the boundary conditions at the analog-frame joints are satisfied. (It will be shown that a network diagram need not actually be drawn.)

(2) For each crack present on any element, one more Π circuit and one crack resistance (hence, two more unknown slopes-voltages) are added to the network. A girder or a column with p cracks is thus simulated with $p+1$ circuits connected in cascade via the crack resistance. The first and the $(p+1)th$ circuits are then connected with the rest of the network according to Step 1.

(3) The beam element with the excitation is divided into two elements at the point of application of the excitation and is thus represented by two Π circuits instead of one.

(4) When a kinetic or kinematical quantity is desired at some location on the frame, the corresponding beam element is again divided into two beam elements at the desired location and represented by two Π circuits. Steps 3 and 4 are skipped in the frequency method.

(5) Kirchhoff's current law is written in terms of the node voltages which correspond to the angles of rotation at the frame joints and at the cracks.

(6) Kinetic conditions at each floor level and shear conditions at the cracks, at the excitation location, and at the location where deflection or any other quantity is desired are applied. This allows the lateral motion of the floors to be computed directly.

(7) This step is performed when the frequency method of diagnosis is used. Under free vibration, the coefficient matrix obtained in Step 3 must be singular. If the damage parameters (i.e., location and severity) for each crack are known, the characteristic values of the structure, $\{\beta\}$, can be determined from the zero determinant of the coefficient matrix (the forward problem). If the characteristic values are known, the damage parameters can be solved by using the characteristic equation (the inverse problem).

(8) When the transmissibility method of diagnosis is used, the linear system of equations is solved for the deflections in terms of the excitation force.

The approach taken here results in a formal scheme which can be applied to frame structures without referring to an actual network diagram. Reference is made to Figure 8. The word "wall" will denote the union of all the columns on the same vertical line. Each node and each beam element is identified by a number. Numbers corresponding to the nodes are encircled in the figure. The numbering order for the beam elements begins at the left lowest column, proceeds up through the columns on the first wall, returns back to the second anchor, proceeds up vertically, and continues in that order. Once the columns are finished, girders on each floor are numbered progressively from left to right starting with the first floor and continuing on with the upper floors. Quantities related to a beam element such as G, P, Q, etc. are subscripted by the number of the element. Each node is numbered by the column under the node. If there are v cracks on a column (girder), the original number of the beam element refers to the uppermost (rightmost) segment of the column (girder) which is now represented by $v+1$ beam segments. The other segments are numbered following the largest number in the scheme. Due to discontinuity of slope at a crack, two new nodes are created on the two sides of each crack. The location t on the structure, henceforth referred to as the response station, denotes the location at which deflection or any other quantity is to be computed. One more node is thus created and one more Π circuit is added. Another node is added on the column $2n+2$ where the force is applied. These last two nodes and the beam segments below (to the left of) them are numbered the last in the numbering scheme.

2.4.1. Analog Circuit Equations and Boundary Conditions

a) Nodal Equations:

Figure 9a shows a typical node r at the intersection of column elements r, s and girder elements p, q. In reference to Figures 8 and 9a, the sum of the branch currents entering the node r is set equal to zero. Namely,

$$(y_i' - y_r')G_{p0} + (y_j' - y_r')G_{q0} + (y_k' - y_r')G_{r0} + (y_l' - y_r')G_{s0}$$
$$- y_r'(G_p + G_q + G_r + G_s) + I_{p2} - I_{q1} + I_{r2} - I_{s1} = 0 \qquad (2.41)$$

where $(y_i' - y_r')$ is the analog voltage difference between the nodes i and r and G_{p0} is the conductance which connects these two nodes. The current sources appearing in equation (2.41) are dependent on the transverse deflections of the two ends of the beam elements to which they correspond. Under small deformation theory, vertical deflection of the nodes shown in Figure 8 is, by second order approximation, equal to zero. Thus, in Figure 9a, $y_{p2} = y_{q1} = 0$, where y_{p2} and y_{q1} denote the deflections of the right end of the pth girder and left end of the qth girder, respectively. If, in addition, the nodes i and j do not bound cracks, then $y_{p1} = y_{q2} = 0$. Consequently, $I_{p1} = I_{p2} = I_{q1} = I_{q2} = 0$ from Equation (2.34). On the other and, I_{r2}, for instance, is not zero since, in general, $y_{r1} \neq 0$ and $y_{r2} = y_{s1} \neq 0$ (i.e., sidesway is allowed).

Upon substitution of equation (2.33) into (2.41),

$$-y_r'(\eta_{p1}Q_p + \eta_{q1}Q_q + \eta_{r1}Q_r + \eta_{s1}Q_s) - y_i'\eta_{p1}W_p - y_j'\eta_{q1}W_q$$
$$- y_k'\eta_{r1}W_r - y_l'\eta_{s1}W_s + \left[\frac{L}{EI\beta}\right]_0 (I_{p2} - I_{q1} + I_{r2} - I_{s1}) = 0 \qquad (2.42)$$

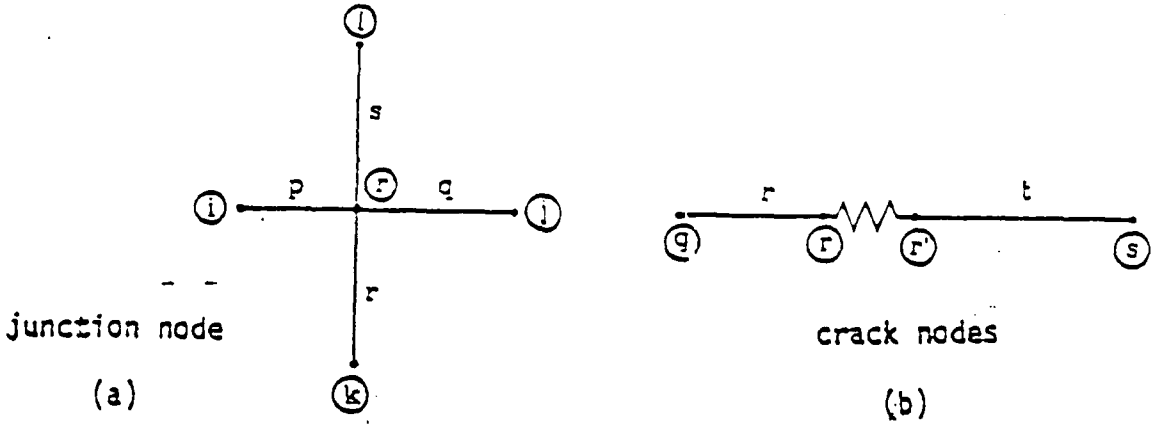

Figure 9. Typical Nodes on the Frame

where $\eta_{t1} = \dfrac{(EI\beta/L)_t}{(EI\beta/L)_0}$ and $\left[\dfrac{EI\beta}{L}\right]_0$ is the characteristic or the reference value chosen for the frame.

In the formation of crack nodes, Figure 9b shows two nodes, r and r', across a crack on a beam element. Kirchhoff's current law is written for the node r:

$$(y_q' - y_r')G_{r0} + (\bar{y}_r' - y_r')(-\kappa) - y_r'G_r + I_{r2} = 0 \qquad (2.43)$$

where $\bar{y}_r'$ is the rotation of the node r' and the conductance $-\kappa$ represents the crack. The nodal equation for the node r' is of a similar form. Equation (2.43) is valid whether the crack is on a girder or a column. The same steps which led to equation (2.42) yield

$$-y_r'\left[\eta_{r1}G_r - \frac{1}{\Theta\beta_0(1+i\delta)}\right] - \bar{y}_r'\left[\frac{1}{\Theta\beta_0(1+i\delta)}\right] - y_q'\eta_{r1}W_r + \left[\frac{L}{EI\beta}\right]_0 I_{r2} = 0 \qquad (2.44)$$

The node t (i.e., the response station) or the node under the force in Figure 8 is the same as that in Figure 9a when the branches p and q are removed. The nodal equation for such a node is then obtained from Equation (2.41) or (2.42) by setting all of the variables with a subscript p and q equal to zero.

b) Boundary and Continuity Conditions:

From the small deformation theory, points on girders on the same floor level will have the same horizontal displacement. Namely,

$$y_{ij} = y_{n+i,j} = y_{2n+i,k} = \cdots = y_{mn+i,j} \quad i = 1,\ldots,n \quad j = 1,2 \qquad (2.45)$$

Also, $y_{i2} = y_{i+1,1}$, $i = 1,\ldots,n-1$. On the other hand, deflection continuity across a crack implies that deflections of the nodes r and r' in Figure 9b are equal. Deflection is continuous at the excitation node and at the node t also (Figure 8). Thus, there are $n+k+2$ unknown deflections associated with the frame, k denoting the total number of cracks on the frame. If the horizontal displacement of the ith floor is designated by y_i ($y_i \equiv y_{i2}$, $i = 1,\ldots,n$), an $[n+k+2]$-vector of displacements and an $[n(m+1)+2k+2]$ - vector of rotations are obtained as

$$\mathbf{y} \equiv \left\{ y_1 \;\; y_2 \;\cdots\; y_n \;\; y_{c_1} \;\cdots\; y_{c_k} \;\; y_f \;\; y_t \right\}^T$$

$$\mathbf{y}' \equiv \left\{ y_1' \;\cdots\; y'_{n(m+1)} \;\; y_{c_1}' \;\; \bar{y}_{c_1}' \;\cdots\; \bar{y}_{c_k}' \;\; y_f' \;\; y_t' \right\}^T \tag{2.46}$$

where y_{c_i} designates the transverse deflection at the ith crack, and y_{c_i}' and $\bar{y}_{c_i}'$ designate the rotations immediately to the left of (below) and to the right of (above) the ith crack which is on a girder (column). The subscripts f and t denote the node under the force and the node t, respectively. The unknown deflections can be related to the rotations via the kinetic equations, defining the sideway motion of the floors, and the shear continuity conditions at the cracks. Cross shears at the column ends are the axial driving forces for the floors. The axial acceleration of a floor, which is composed of all the girders on the same level, is the same as the transverse acceleration of the column ends at the nodes where the columns join the floor. Thus, for the ith floor (Figure 10)

$$\sum_{j=0}^{m} [V_{jn+i,2} - V_{jn+i+1,1}] = \left\{ \sum_{j=p}^{p+m-1} \rho_j L_j + \sum_{j=q}^{q+k_i-1} \rho_j L_j \right\} \omega^2 y_i \tag{2.47}$$

where $p=(m+1)n+(i-1)m+1$ in accordance with the numbering order described earlier and k_i is the total number of cracks on the ith floor. There is one such equation for each floor. The term in the braces on the right-hand side of Equation (2.47) is the total mass of the ith floor. When there is no crack on the ith floor, i.e., $k_i = 0$, the second summation term on the right-hand side is absent. When there is a crack in, for example, girder $p+1$, L_{p+1} denotes the length of the right segment of this girder. Mass $\rho_q L_q$ of the left segment is then included in the second summation term in Equation (2.47). Equation (2.47), upon substitution of the last two equations in (2.30) for shears, will relate deflections to rotations. Figure 11b shows the diagram of a frame with $m=1$, $n=2$, $k=2$. A harmonic load is applied to the frame and a response station, t, is shown. There are ten nodes, ten beam elements (hence ten interconnected Π circuits) and six unknown deflections. The first floor has one crack

on it. The kinetic equation for the first floor with $\rho_2 = \rho_3$, has the form

$$V_{12} + V_{32} - V_{21} - V_{71} = \omega^2 y_1 \rho_3 (L_3 + L_2) \tag{2.48}$$

where, for instance,

$$V_{32} = \frac{1}{h_3}(Q_7' y_3' - P_3 y_1 \beta_3 / L_3)$$

$$V_{71} = \frac{1}{h_7}\left[Q_7' y_3' + \overline{M}_7' y_7' + \frac{(P_7 y_1 - P_7' y_7')\beta_7}{L_7}\right] \tag{2.49}$$

from Equation (2.30) with $y_{31} = y_{31}' = 0$, $y_1 \equiv y_{32} = y_{71}$, $y_3' \equiv y_{32}' = y_{71}'$, $y_7 \equiv y_{72}$, $y_7' \equiv y_{72}'$. Upon substitution of shear expressions, Equation (2.49), and the similar equations for V_{12} and V_{21} into Equation (2.48) the following equation is obtained

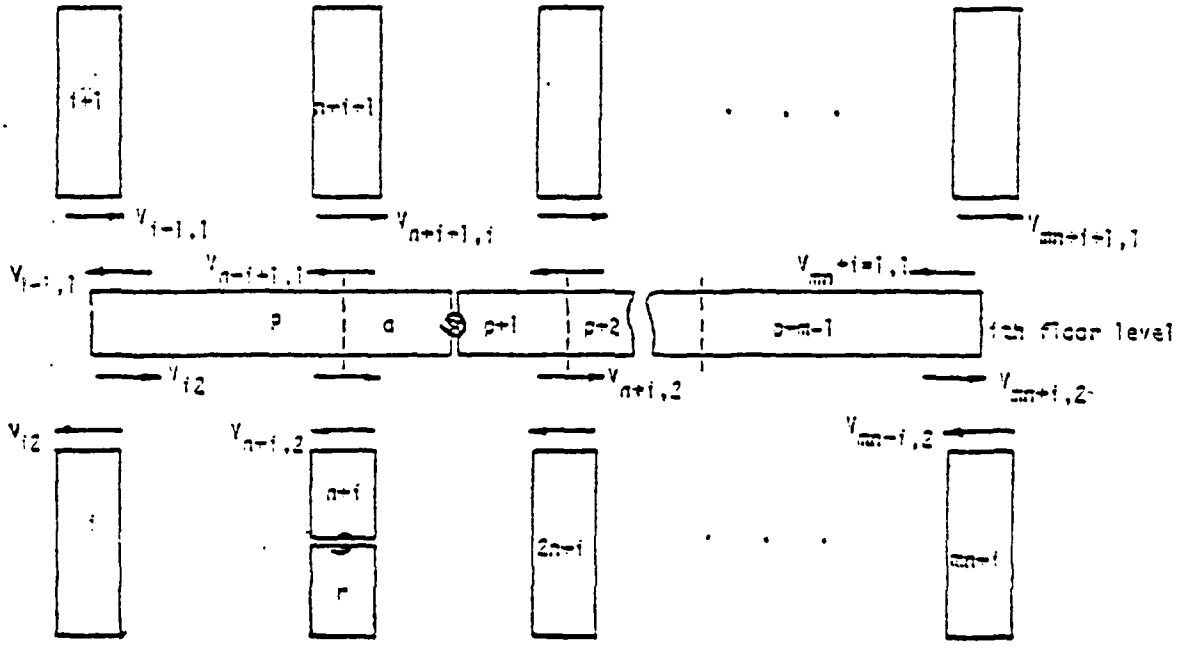

Figure 10. Cross shears in the columns adjoining the ith floor

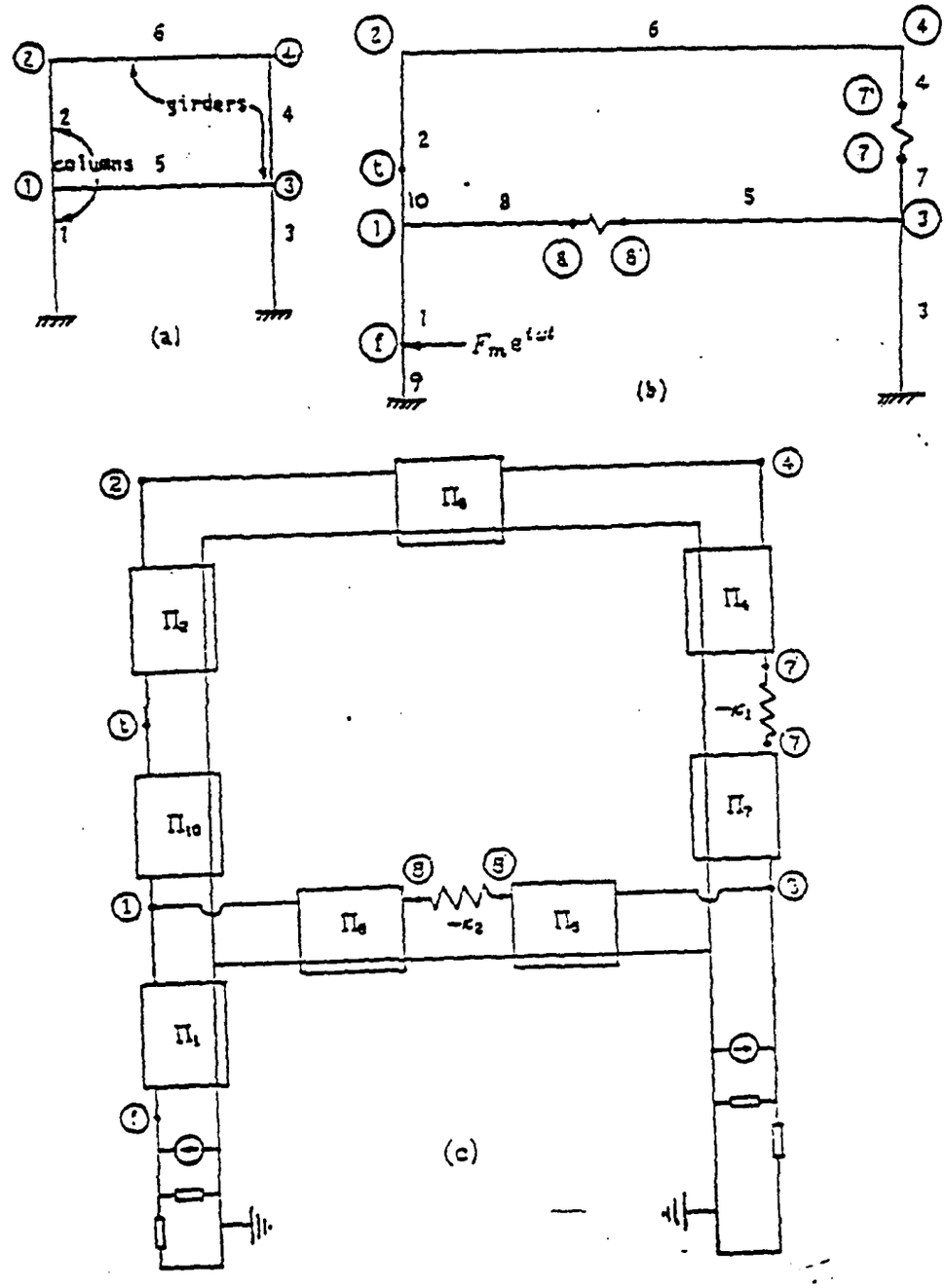

Figure 11. A two-story, single span frame (a) without crack, (b) with two cracks, one excitation and a response station t. (c) Electrical Analog of the frame.

$$\left[\frac{\beta}{L}\right]_0 \Big\{ [\eta_{13}P_1 + \eta_{23}P_2 + \eta_{33}P_3 + \eta_{73}P_7 + \eta_{33}(\beta_3 + \beta_8)]y_1$$

$$- \eta_{23}P_2'y_2 - \eta_{73}P_7'y_7 \Big\} = (\eta_{12}Q_1' - \eta_{22}Q_2')y_1'$$

$$- \eta_{22}W_2'y_2' + (\eta_{32}Q_3' - \eta_{72}Q_7')y_3' - \eta_{72}W_7'y_7' \qquad (2.50)$$

where

$$\eta_{ij} = \frac{(EI)_i \left[\frac{\beta_i}{L_i}\right]^j}{(EI)_0 \left[\frac{\beta_0}{L_0}\right]^j} \qquad (2.51)$$

In Equation (2.51), i is the number of the beam element or the beam segment and j is an exponent. The kinetic equation for the second floor can be developed similarly. Application of shear continuity at a crack will now be demonstrated for the crack on the first floor (Figure 11b). Hence $V_{82} = V_{81}$, or from the last two of Equation (2.30)

$$\frac{1}{h_8}\left(W_8'y_1' + Q_8'y_8' - \frac{P_8y_8\beta_8}{L_8}\right) = \frac{1}{h_3}\left(Q_3'\bar{y}_8' + W_3'y_3' + \frac{P_3y_8\beta_3}{L_3}\right) \qquad (2.52)$$

since $y_{81} = y_{82} = 0$. The following expression is obtained by rearranging Equation (2.52) and noting that $h_3 = h_8$ and $\frac{\beta_3}{L_3} = \frac{\beta_8}{L_8}$:

$$\left[\frac{\beta_3}{L_3}\right](P_3 + P_8)y_8 = W_8'y_1' - W_3'y_3' + Q_8'y_8' - Q_3'\bar{y}_8' \qquad (2.53)$$

Shear continuity at the response station yields an equation similar to (2.53). The shear discontinuity at the excitation location, on the other hand, can be expressed as

$$V_{82} = V_{11} + F_m \qquad (2.54)$$

which yields

$$\left[\frac{\beta_1}{L_1}\right][(P_1 + P_9)y_f - P_1'y_1] = (Q_9' - Q_1')y_f' - W_1'y_1' + h_1F_m \qquad (2.55)$$

c) Matrix Equations for a General Frame Structure:

For the general frame structure, there are n kinetic equations of the form of equation (2.50), $k+1$ shear-continuity equations (k equations for the cracks and one for the response station) of the form of equation (2.53), and one shear discontinuity equation given by (2.55). These $n+k+2$ equations can be arranged in a matrix form to solve for the deflections in terms of the rotations, namely,

$$\mathbf{y} = \left[\frac{L}{\beta}\right]_0 \mathbf{Z}^{-1}\left[\mathbf{X}\mathbf{y}' - h_f F_m \mathbf{e}\right] \tag{2.56}$$

where $\mathbf{e}$ is a column vector whose entries are zero except for the last entry which is unity and h_f is the value pertaining to the beam element with the excitation (for the example of Figure 11, $h_f = h_1$). On the other hand, the nodal equations (2.42) and (2.44) can be arranged in the form

$$\left[\frac{L}{EI\beta}\right]_0 \mathbf{H}_1\mathbf{i} - \mathbf{U}\mathbf{y}' = 0 \tag{2.57}$$

where $\mathbf{i}$ is the vector of current sources and is related to the deflections via Equation (2.34); that is,

$$\mathbf{i} = \frac{1}{h_0}\mathbf{H}_2\mathbf{y} \tag{2.58}$$

After Equation (2.56) is substituted into Equation (2.58), then Equation (2.58) into Equation (2.57), and it is noted that $\mathbf{H}_1\mathbf{H}_2 = \mathbf{X}^T$, the slope equation results:

$$(\mathbf{X}^T\mathbf{Z}^{-1}\mathbf{X} - \mathbf{U})\mathbf{y}' = h_f F_m \mathbf{X}^T\mathbf{Z}^{-1}\mathbf{e} \tag{2.59}$$

This is the general form of the result for any planar frame with any number of cracks on it. The coefficient matrix in (2.59) is symmetric. The individual matrices, in general, have the forms

$$
X = \begin{array}{c}
\begin{matrix} n(m+1) & & & 2k_c & 2k_g & 2 \end{matrix} \\
\left[\begin{array}{ccc|cc|c}
X^{(1)} & \cdots & X^{(m+1)} & F_c & 0 & \\
\hline
E_{c_1} & \cdots & E_{c_{m+1}} & H_c & 0 & \\
\hline
E_{g_1} & \cdots & E_{g_{m+1}} & 0 & H_g & L_1 \\
\hline
\multicolumn{3}{c|}{L_2} & \multicolumn{2}{c|}{} & L_3
\end{array}\right]
\end{array}
\tag{2.60}
$$

$$
U = \begin{array}{c}
\begin{matrix} n(m+1) & 2k_c & 2k_g & 2 \end{matrix} \\
\left[\begin{array}{c|cc|c}
U_0 & A_c & A_g & \\
\hline
A_c^T & B_c & 0 & \\
\hline
A_g^T & 0 & B_g & V_1 \\
\hline
\multicolumn{1}{c|}{V_1^T} & \multicolumn{2}{c|}{} & V_2
\end{array}\right]
\end{array}
\quad
Z = \begin{array}{c}
\begin{matrix} n & k_c & k_g & 2 \end{matrix} \\
\left[\begin{array}{c|cc|c}
Z_0 & C_c & 0 & \\
\hline
C_c^T & D_c & 0 & \\
\hline
0 & 0 & D_g & N_1 \\
\hline
\multicolumn{1}{c|}{N_1^T} & \multicolumn{2}{c|}{} & N_2
\end{array}\right]
\end{array}
\tag{2.61}
$$

with y and y' arranged as in equation (2.48)

$$
y = \begin{Bmatrix} y_0 \\ y_c \\ y_g \\ y_f \\ y_t \end{Bmatrix}
\qquad
y' = \begin{Bmatrix} y_0' \\ y_c' \\ y_g' \\ y_f' \\ y_t' \end{Bmatrix}
\tag{2.62}
$$

where the subscripts c and g refer to cracks on the columns and on the girders, respectively, with k_c and k_g being the total number of cracks on the columns and on the girders ($k = k_c + k_g$). Hence, y_c and y_g, for example, are the vectors of deflections at the column and girder cracks, respectively. y_0 is the vector of the

horizontal floor displacements. y_i and y_f are the transverse deflections at the response station and at the excitation location, respectively. It should be noted that $\mathbf{X}^{(i)}$, $\mathbf{U}_0$, and $\mathbf{Z}_0$ for the case of no crack are modified when cracks are introduced on the frame. The matrices $\mathbf{U}$ and $\mathbf{Z}$ are symmetric.

When the rotations are to be computed, $\mathbf{y}'$ can be solved for from Equation (2.59). When the deflections are needed, $\mathbf{y}'$ can be solved for from (2.57) and substituted into (2.56) from which $\mathbf{y}$ can be obtained. This yields

$$\mathbf{y} = h_f F_m \left[\frac{L}{\beta}\right]_0 (\mathbf{X}\mathbf{U}^{-1}\mathbf{X}^T - \mathbf{Z})^{-1}\mathbf{e} \tag{2.63}$$

With $\mathbf{y}$ and $\mathbf{y}'$ known, resisting moments and shears can be computed from Equation (2.30). When the free vibration of the structure is of interest, $F_m = 0$ and the coefficient matrix on the left-hand side of (2.59) is singular. The determinant of the coefficient matrix then yields the characteristic equation of the structure. A computer program is written to compute the deflections on a general frame structure. The listing of the program is given in Appendix.

A formal procedure will now be described to establish the above matrices without the need to draw the actual analog circuit.

2.5. Procedure to Establish the Matrices

In the following, for simplicity of explanation, properties of the beam elements are assumed uniform throughout the frame except for the lengths. That is, $\eta_{ij} = 1$ for all i, j.

1. To establish the U matrix:

$\mathbf{U}$ is composed of the coefficients of the rotations y_i' in equations such as (2.42) and (2.44). The ith row in the matrix stems from Kirchhoff's current law written for the ith node, the first $n(m+1)$ rows being for the nodes on the frame joints, the next $2k$ rows for the nodes at the cracks, and the last two rows for the nodes at the

excitation and response locations. The procedure to establish the entries of the matrix is outlined below.

a. The diagonal entry u_{ii} will be the sum of the Q values(Equation 2.31) of the beam elements adjoining at the node for which Kirchhoff's current law is being written. If this node is at a crack, then u_{ii} is given by the Q value of the element ending at this node minus the Λ value for the corresponding crack, where $\Lambda = \frac{1}{\Theta\beta_0(1+i\delta)}$. The diagonal entries of B_x and B_y will thus be of the form $(Q_i - \Lambda_r)$. And,

b. The off-diagonal entry u_{ij} will be W_k(Equation 2.31) if the nodes corresponding to the columns i and j of the matrix are linked directly by the kth beam element. If these two nodes are linked by a crack, i.e., they are the nodes on the two sides of a crack, then u_{ij} is given by the M value of the crack. Otherwise $u_{ij} = 0$. Due to symmetry, $u_{ij} = u_{ji}$. The ith row of U_0 in Equation (2.59) is unchanged relative to U_0 of the no-crack ($k=0$) case if the ith node is not adjacent to a cracked element.

2. To establish the Z matrix:

The matrices Z and X stem from the kinetic equations and shear conditions. The first n rows in them represent the kinetic equations governing sidesway of the n floors. The next $k+1$ rows correspond to the shear continuity conditions at the cracks and at the response station. The last row results from the shear discontinuity at the excitation location. Z consists of the coefficients of deflections y_i and its entries can be generated as follows:

a. The diagonal entry z_{ii} for $i=1,2,...n$ will be the sum of the β_k values of all the girder elements on the ith floor plus the sum of the P values(Equation 2.31) of all the columns adjoining at the ith floor. If a column adjacent to the ith floor is cracked, then only the P value of the column segment nearest to that floor will be included. β_k can be expressed in terms of the characteristic value β_0 as $\beta_k = e_k\beta_0$. If the frame is

homogeneous in properties, then $e_k = L_k / L_c$. The diagonal entry z_{ii} for the next k rows (i.e., the diagonal entries of the D matrices) will be the sum of the P values of the two beam segments on the two sides of the corresponding crack. z_{ii} for the last two rows(i.e., the diagonal entries of the N_2 matrix) will be given by the sum of the P values of the two beam segments joining at the excitation node and the response node, respectively.

b. The off-diagonal entry $z_{i,i+1}$ of Z_0 will be the negative of the sum of the P' values(Equation 2.31) of all uncracked columns joining ith and $(i+1)$th floors. $z_{i,i+1} = 0$ if all the columns between those floors are cracked. $z_{ij} = 0$ for $n \geq j \geq i+2$ and $z_{ij} = z_{ji}$. Z_0 is, hence, a tridiagonal symmetric matrix. If any one of the columns adjacent to the ith floor is cracked, then z_{ij} for $1 \leq i \leq n$, $n < j \leq n+k_c$ (i.e., the entries of C_c), will be zero except for that (those) j value(s) which correspond(s) to the deflection(s) at the crack(s) nearest to the ith floor, in which case z_{ij} is equal to the negative of the P' value for the column segment which links the ith floor to that crack. If none of the columns adjacent to the ith floor is cracked, then ith row of C_c is zero, and the ith row of Z_0 is unchanged relative to Z_0 of the no-crack, $k=0$, case.

c. $z_{ij} = 0$ for $1 \leq i \leq n$, $n+k < j \leq n+k+2$, (the entries of N_1), where $k=k_c+k_g$, unless there is an excitation and/or a response station on any column(s) adjacent to the ith floor> In the latter case, z_{ij} is given by the negative of the P' value for the column segment linking the ith floor to the excitation or the response node.

d. $z_{i,i+1}$ for $n < i \leq n+k_c$ (the entries of D_c) will be zero if there is no other crack between the $(i-n)$th column crack and the floor level above this crack. Otherwise, $z_{i,i+1}$ will be equal to the negative of the P' value for the column segment which links the $(i-n)$th and the $(i-n+1)$th cracks.

e. $z_{i,i+1}$ for $n+k_c < i \leq n+k_g$ (the entries of D_g) will be zero if there is no other crack between $(i-n-k_c)$th girder crack and the wall to the right of this crack.

Otherwise $z_{i,i+1}$ will be equal to the negative of the P' value for the girder segment which links the $(i-n-k_z)$th crack and the crack on its right.

Hence, D_c and D_g are diagonal if at most one crack exists on each beam element. If more than one crack exists on any column or girder, then D_c and/or D_g are accordingly tridiagonal symmetric matrices.

f. z_{ij} for $n < i \leq n+k$, $n+k < j \leq n+k+2$ (the entries of N_1) will be nonzero only when the corresponding crack is neighboring an excitation or response node, in which case z_{ij} is equal to the negative of the P' value for the beam segment linking the crack to the excitation or the response node.

3. To establish the X matrix

X consists of the coefficients of rotations y_i' in equations such as (2.50), (2.53) and (2.55). A square submatrix $X^{(k)}$ in Equation (2.58) corresponds to rotations of the frame joints on the kth wall (Figure 8).

a. The diagonal entry $x_{ii}^{(k)}$ of $X^{(k)}$, which stems from the kinetic equation for the ith floor, will be given by the Q' value(Equation 2.31) of the column (column segment) under the frame-joint node $n(k-1)+i$ minus the Q value of the column (column segment) above the same node. If there is no cracked column on the kth wall, then $x_{ii}^{(k)} = Q'_{n(k-1)+i} - Q'_{n(k-1)+i+1}$ for $i=1,\ldots,n-1$ and $x_{nn}^{(k)} = Q'_{nk}$.

b. The off-diagonal entry $x_{i,i+1}^{(k)} = -W'_{n(k-1)+i+1}$, that is, the negative of the W' value for the column above node $n(k-1)+i$ for $i=1,\ldots,n-1$ if the column of the kth wall between the ith and $(i+1)$th floors (i.e., the column above node $n(k-1)+i$) has neither a crack, nor an excitation, nor a response station on it. Otherwise $x_{i,i+1}^{(k)} = 0$, and that entry on the ith row of F_c or L_1 which corresponds to the rotation of the crack node or the excitation or the response node nearest to and above the node $n(k-1)+i$ will be equal to the negative of the W' value of the column segment linking the node $n(k-1)+i$ and the said crack, excitation or response node. $x_{ij}^{(k)} = 0$ for

$j \geq i+2$ and $x_{ij}^{(k)} = -x_{ji}^{(k)}$ for $i \neq j$. (The entries of each $X^{(k)}$ are numbered independently of the other submatrices.) $X^{(k)}$ is thus diagonal if each column of the kth wall has at least one crack. Otherwise it is tridiagonal. $X^{(k)}$ is unchanged relative to $X^{(k)}$ of the no-crack ($k=0$) case if there is no crack on the kth wall.

If the column below node $n(k-1)+i$ is cracked, or has an excitation or a response node, then that entry on the ith row of F_c or L_1 which corresponds to the rotation of the crack node, or the excitation or the response node nearest to and below the node $n(k-1)+i$ will be equal to the W' value of the column segment linking the two nodes. Except for this and the above mentioned cases, entries of F_c are zero.

c. The E matrices in Equation (2.58) couple the crack nodes with the frame-joint nodes. Rows $n+1$ through $n+k$ of X (i.e., E, H and L_1 matrices) are filled in as follows: The entry on the matrix column which corresponds to the rotation of the node on the left (or lower) side of the crack, at which the shear continuity condition is being written, is equal to the Q' value of the girder (or column) segment which links this node to the one on its left (or below it). The entry corresponding to the node on the right (or upper) side of the crack is equal to minus the Q' value of the segment linking this node to the node on its right (or above it). These two entries are within the submatrix H_g (or H_c). The entry corresponding to the node on the left-hand side of (or below) the left (or lower) crack-node is equal to the W' value of the segment linking these two nodes. Finally, the entry corresponding to the node on the right-hand side of (or above) the right-side (or upper) crack-node is equal to the negative of the W' value of the segment linking the two nodes. These two entries can be within the submatrices E, H or L_1 depending on whether there are one or more cracks on a girder (column) and on whether the excitation and response nodes are neighbors with any crack. $E_{c_k} = 0$ if there is no crack on the kth wall; $E_{g_k} = 0$ if there is no crack on any of the girders adjacent to the kth wall.

d. The diagonal entries of L_3 are given by the difference of the Q values of the two beam segments on the left (or lower) and right (or upper) side of the excitation or response nodes. L_3 is a diagonal submatrix if the excitation and response nodes are not neighbors. Only those entries of L_2 corresponding to the nodes nearest to the excitation or the response node are nonzero and are given by the W value, or the negative of it, depending on whether the node in question is on the left- or right-hand side, respectively, of the excitation or the response node.

4. Corrections for the general case:

If beam properties are not uniform throughout the frame (each column or girder still has uniform properties within itself), then the following corrections are necessary:

a. Multiply each term in the U matrix, except the Λ terms, by the corresponding η_1 value, that is, Q_p and W_p by η_{p1}.

b. Multiply each term in the first n rows of the X matrix by the corresponding η_2 value, that is, Q_p' and W_p' by η_{p2}.

c. Multiply each term in the first n rows of the Z matrix by the corresponding η_3 value, that is, P_p and P_p' by η_{p3} and β_r by η_{r3}.

d. Multiply the ith row of Z, $n+1 \le i \le n+k+2$, by $\lambda_l = \frac{\beta_l / L_l}{\beta_0 / L_0}$ where l is the number of the beam element with the crack for which the ith row represents the shear continuity condition, or of the beam element with the excitation or the response station.

The above procedure will now be illustrated with an example.

Example: The three matrices will be written for the frame in Figure 11.

a. Frame without cracks (Fig. 11a) with different beam properties (each beam is uniform within itself).

$$U=\begin{array}{c} \begin{matrix} y_1' & y_2' & y_3' & y_4' & y_f' & y_i' \end{matrix} \\ \begin{bmatrix} \eta_{11}Q_1+\eta_{21}Q_{10}+\eta_{51}Q_5 & 0 & \eta_{51}W_5 & 0 & \eta_{11}W_1 & \eta_{21}W_{10} \\ 0 & \eta_{21}Q_2+\eta_{51}Q_5 & 0 & \eta_{61}W_6 & 0 & \eta_{21}W_2 \\ \eta_{51}W_5 & 0 & \eta_{21}Q_3+\eta_{41}Q_4+\eta_{51}Q_5 & \eta_{41}W_4 & 0 & 0 \\ 0 & \eta_{61}W_6 & \eta_{41}W_4 & \eta_{41}Q_4+\eta_{61}Q_5 & 0 & 0 \\ \eta_{11}W_1 & 0 & 0 & 0 & \eta_{11}(Q_1+Q_5) & 0 \\ \eta_{21}W_{10} & \eta_{21}W_2 & 0 & 0 & 0 & \eta_{21}(Q_2+Q_{10}) \end{bmatrix} \end{array} \tag{2.54}$$

$$Z=\begin{array}{c} \begin{matrix} y_1 & y_2 & y_f & y_i \end{matrix} \\ \left[\begin{array}{cc|cc} \eta_{13}P_1'+\eta_{23}P_{10}+\eta_{33}P_3+\eta_{43}P_4+\eta_{63}\beta_5 & -\eta_{43}P_4' & -\eta_{13}P_1' & -\eta_{23}P_{10}' \\ -\eta_{43}P_4' & \eta_{23}P_2+\eta_{43}P_4+\eta_{63}\beta_5 & 0 & -\eta_{23}P_2' \\ \hline -\lambda_1P_1' & 0 & \lambda_1(P_1+P_5) & 0 \\ -\lambda_2P_{10}' & -\lambda_2P_2' & 0 & \lambda_2(P_2+P_{10}) \end{array}\right] \end{array} \tag{2.55}$$

$$X=\begin{array}{c} \begin{matrix} y_1' & y_2' & y_3' & y_4' & y_f' & y_i' \end{matrix} \\ \left[\begin{array}{cc|cc|cc} \eta_{12}Q_1'-\eta_{22}Q_{10}' & 0 & -\eta_{32}Q_1'-\eta_{42}Q_4' & -\eta_{42}W_4' & \eta_{12}W_1' & -\eta_{22}W_{10}' \\ 0 & \eta_{22}Q_2' & \eta_{42}W_4' & \eta_{42}Q_4' & 0 & \eta_{22}W_2' \\ \hline -W_1' & 0 & 0 & 0 & Q_5'-Q_1' & 0 \\ -W_{10}' & -W_2' & 0 & 0 & 0 & Q_{10}'-Q_2' \end{array}\right] \end{array} \tag{2.56}$$

where, for convenience, the rotations and the deflections at the nodes are written above the corresponding columns of the matrices. It is noted that, for example, $\eta_{91} = \eta_{11}$ and $\eta_{92} = \eta_{12}$ (Eq. 2.51), that is, the beam segments 9 and 1 are the segments of the same column and, hence, have the same properties.

b. Frame with two cracks (Fig. 11b). The frame is now assumed uniform in properties except for the lengths of the individual columns and girders. Hence, $\eta_{ij} = 1$ and $\varepsilon_i \equiv \frac{\beta_i}{\beta_0} = L\frac{i}{L_0}$. Matrix $\mathbf{U}$ is obtained as

$$
\mathbf{U} = \left[\begin{array}{cccc|cc|cc|cc}
Q_1+Q_{10}+Q_8 & 0 & 0 & 0 & 0 & 0 & W_8 & 0 & W_1 & W_{10} \\
0 & Q_2+Q_9 & 0 & W_9 & 0 & 0 & 0 & 0 & 0 & W_2 \\
0 & 0 & Q_3+Q_5+Q_7 & 0 & W_7 & 0 & 0 & W_5 & 0 & 0 \\
0 & W_6 & 0 & Q_4+Q_6 & 0 & W_4 & 0 & 0 & 0 & 0 \\
\hline
0 & 0 & W_7 & 0 & Q_7-\Lambda_4 & \Lambda_4 & 0 & 0 & 0 & 0 \\
0 & 0 & 0 & W_4 & \Lambda_4 & Q_4-\Lambda_4 & 0 & 0 & 0 & 0 \\
\hline
W_2 & 0 & 0 & 0 & 0 & 0 & Q_8-\Lambda_5 & \Lambda_5 & 0 & 0 \\
0 & 0 & W_5 & 0 & 0 & 0 & \Lambda_5 & Q_5-\Lambda_5 & 0 & 0 \\
\hline
W_1 & 0 & 0 & 0 & 0 & 0 & 0 & 0 & Q_1+Q_9 & 0 \\
W_{10} & W_2 & 0 & 0 & 0 & 0 & 0 & 0 & 0 & Q_2+Q_{10}
\end{array}\right] \qquad (2.67)
$$

It may be noted that the first four elements in the second row of $\mathbf{U}$ are the same as those in the second row in Equation (2.64) (except for the factors η_{j1}). This row is unchanged since node 2 is not linked to any crack node. The last two rows and two columns in Equation (2.64) are enlarged by filling with zeros and again appear as the last rows and columns in (2.67). If the beams had different properties, then each term in $\mathbf{U}$ would be multiplied by the corresponding η_i value except the terms $\Lambda_i = \frac{1}{\Theta_i\beta_0(1+i\delta)}$. In the Λ_i terms, the sensitivity numbers, Θ_i, are subscripted by the

original number of the column or girder on which the corresponding cracks are located. Hence, Θ_4, for instance, refers to the crack located on the column numbered 4 in the uncracked frame (Figure 11). It is also noted that Q_4, W_4, P_4, etc. for the cracked frame have different values from the ones in the no-crack case. The Z and X matrices of the cracked frame are subsequently conjugated as :

$$Z = \left[\begin{array}{cc|cc|cc} P_1+P_{10}+P_3+P_7+\beta_5+\beta_8 & 0 & -P_7' & 0 & -P_1' & -P_{10}' \\ 0 & P_2+P_4+\beta_8 & -P_4' & 0 & 0 & -P_2' \\ \hline -P_7' & -P_4' & P_4+P_7 & 0 & 0 & 0 \\ 0 & 0 & 0 & P_5+P_8 & 0 & 0 \\ \hline -P_1' & 0 & 0 & 0 & P_1+P_9 & 0 \\ -P_{10}' & -P_2' & 0 & 0 & 0 & P_2+P_{10} \end{array}\right] \qquad (2.68)$$

$$X = \left[\begin{array}{cc|cc|cc|cc|cc} Q_1'-Q_{10}' & 0 & Q_3'-Q_7' & 0 & -W_7' & 0 & 0 & 0 & W_1' & -W_{10}' \\ 0 & Q_2' & 0 & Q_4' & 0 & W_4' & 0 & 0 & 0 & W_2' \\ \hline 0 & 0 & W_7' & -W_4' & Q_7' & -Q_4' & 0 & 0 & 0 & 0 \\ W_8' & 0 & -W_5' & 0 & 0 & 0 & Q_2' & -Q_5' & 0 & 0 \\ \hline -W_1' & 0 & 0 & 0 & 0 & 0 & 0 & 0 & Q_9'-Q_1' & 0 \\ W_{10}' & -W_2' & 0 & 0 & 0 & 0 & 0 & 0 & 0 & Q_{10}'-Q_2' \end{array}\right] \qquad (2.69)$$

where $X^{(1)}$ in Equation (2.66) and Equation (2.69) are basically the same since there is no crack on the first wall. The terms $-W_4$ and W_4 in $X^{(2)}$ in Equation (2.66) are replaced by zeros in Equation (2.69), since nodes 3 and 4 are no longer linked directly. As the column under the node 4 is cracked, the node 4 is now linked to the

node 7' by the column segment 4. Therefore, W_4' appears on the second row and second column (which corresponds to $\bar{y}_{7'}$) of $\mathbf{F}_c$. The third row of $\mathbf{X}$ reflects the continuity of shear at the column crack in Figure 11b. The lower crack-node 7 is linked to the node 3 by the column segment 7 and the upper crack-node 7' is linked to the node 4 by the segment 4. Q' and W' values are accordingly placed on the third row. The construction of the matrices for the cracked frame is now complete. Numerical results for the frame will be given in Chapter 3.

CHAPTER 3

THE MODAL FREQUENCY THEORY OF FRACTURE DAMAGE DIAGNOSIS

The modal frequency theory was introduced by Ju et al [7,8] to utilize the measurements of pre- and post-damage modal frequencies in detecting and identifying fracture damage. Each pair of fracture characteristics $(\gamma,e)_k$, the kth crack intensity and location, is defined by a damage function

$$(\gamma,e)_k = G_k(R_i) \tag{3.1}$$

where $R_i = 1 - (\omega_i/\omega_{ui})$ is the modal frequency variation, ω_i and ω_{ui} are respectively the post- and pre-damage frequencies of the ith mode. For k-number of cracks, therefore, (2k + 1) number of measurements of frequency variations are needed for diagnostic solutions. The solution of Equation (3.1) yields the diagnosis of the fracture damage in the structure. The application of the modal frequency theory to the diagnosis of a single crack in simple structures was treated by Ju et al [7,8] with the matrix method. The method in general, for a structure of N-beam elements with k-cracks, requires the solution of a (4N + 2k) by (4N + 2k) matrix. The algorithm becomes excessive for structures of large number of beam elements and/or cracks. The numerical difficulty was overcome with the introduction of a generalized theory of circuit analogy. The theory and its application to multiple-crack problem and to complex planar structure were presented by Akgün and Ju [9,10] and summarized in [11]. The basic modal frequency theory, used alone, will encounter uncertainties, arising from (1) frequency crossover, (2) inadequate measurement of change in modal frequencies and (3)

closely packed cracks. The uncertainty of frequency crossover can be illustrated with two modal frequencies, ω_i and ω_j (without loss of generality let $\omega_i < \omega_j$) at undamaged state. After crack occurs the new modal frequencies are corresponding $\bar{\omega}_i$ and $\bar{\omega}_j$. If the crack occurs near the inflection point of the ith modal shape but if the point happens to be near the maximum moment section of the jth modal shape, $\bar{\omega}_i$ may not differ too much from ω_i. It is conceivable that, for the new modal frequency, we may record $\bar{\omega}_j < \bar{\omega}_i$. In that case, not knowing the actual damage configuration, the diagnostic assemblage of frequencies may well confuse $\bar{\omega}_j$ to be the new frequency of the ith mode and $\bar{\omega}_i$ to be the new frequency of the jth mode. The phonomenon is a frequency crossover; the diagnostic result may be disastrous. Such phenomenon is most likely to occur in complex structures, for which there are pairs of modal frequencies with close values. The problem of frequency crossover cannot be handled deterministically by the modal frequency theory. But the transmissibility theory presented in the sequal should alleviate this very uncertainty. The rest of the chapter will address the uncertainties of multiple cracks, which can only be resolved by probabilistic means. The uncertainties can be adequately illustrated with a simple beam structure with k-number of cracks.

A beam with k cracks can be represented by k + 1 circuits joined by resistors simulating the cracks. The unknowns in the T-circuit analogy are the moments (currents) at the cracks and at the ends of the beam. Hence, there are k + 1 unknowns. On the other hand, the unknowns in the Π-circuit analogy are the slopes at the ends of the beam and at the cracks. There are two unknown slopes at each crack. Hence, the order of the system is larger with Π circuits. The T-circuit analog derived in Section 2.2.1 is found to be more suitable for multiple-crack analysis. This section develops the

characteristic frequency equation for the general case, establishes the conditions under which multiple cracks become equivalent to a single crack, and illustrates the inverse problem with k = 1. The beam is undamped and β and all other variables are, therefore, real.

3.1. Cantilever Beam with Multiple Cracks

Figure 12 depicts the analog circuit for a cantilever beam with k cracks. Continuity of moments at the cracked sections is preserved via the continuity of electrical currents through the "crack resistors", $-1/\kappa_i$. The order of the system of mesh current equations is k + 1. Namely,

$$(Z_1 + Z_{10})M_1 - Z_{10}M_2 + E_{11} = 0$$

$$-Z_{i-1,0}M_{i-1} + (Z_{i-1} + Z_{i-1,0} + Z_i + Z_{i,0} - 1/\kappa_i)M_i - E_{i-1,2} + E_{i,1} = 0$$

$$i = 2,\ldots k$$

$$-Z_{k0}M_k + (Z_k + Z_{k0} + Z_{k+1} + Z_{k+1,0} - 1/\kappa_k)M_{k+1} - E_{k2} + E_{k+1,1} = 0 \qquad (3.2)$$

From Equation (2.21), the analog voltage sources $\{E_{i,j}\}$ are:

$$\begin{Bmatrix} E_{11} \\ E_{12} \\ E_{21} \\ E_{22} \\ \cdot \\ \cdot \\ \cdot \\ E_{k2} \\ E_{k+1,1} \end{Bmatrix} = \frac{\beta}{2L} \begin{bmatrix} T_1' & 0 & 0 \ldots & 0 & 0 & 0 \\ S_1' & 0 & 0 \ldots & 0 & 0 & 0 \\ -S_2' & T_2' & 0 \ldots & 0 & 0 & 0 \\ -T_2' & S_2' & 0 \ldots & 0 & 0 & 0 \\ \cdot & \cdot & \cdot \ldots & \cdot & \cdot & \cdot \\ \cdot & \cdot & \cdot \ldots & \cdot & \cdot & \cdot \\ \cdot & \cdot & \cdot \ldots & \cdot & \cdot & \cdot \\ 0 & 0 & 0 \ldots & -T_k' & S_k' & 0 \\ 0 & 0 & 0 \ldots & 0 & -S_{k+1}' & T_{k+1}' \end{bmatrix} \begin{Bmatrix} y_1 \\ y_2 \\ y_3 \\ y_4 \\ \cdot \\ \cdot \\ \cdot \\ y_k \\ y_{k+1} \end{Bmatrix} \qquad (3.3)$$

where y_i is the deflection of the ith cracked section and y_{k+1} is the deflection of the free end. These deflections are solved for by imposing the shear boundary and continuity conditions. That is,

$$V_{i2} = V_{i+1,1} \quad , \quad i = 1,2,\ldots,k$$

$$V_{k+1,2} = 0 \tag{3.4}$$

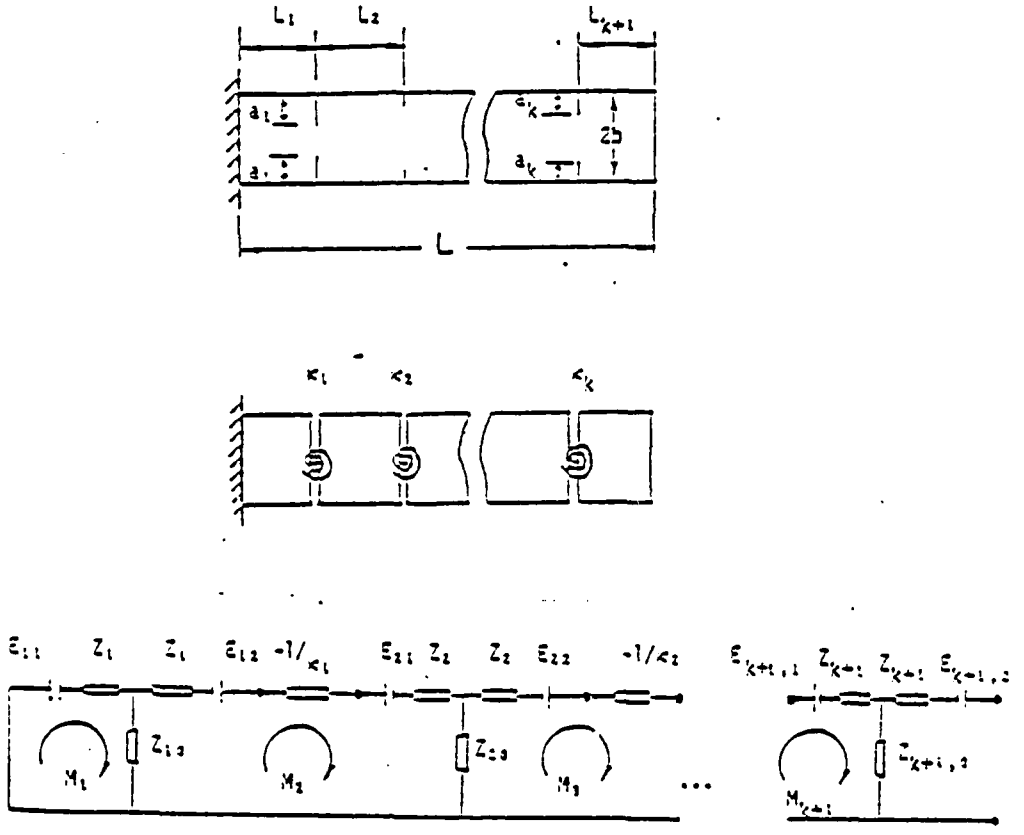

Figure 12. Cantilever beam. (a). With k symmetrical cracks.
(b) Equivalent fracture-hinge model. (c) T-circuit analog.

where the first subscripts refer to the numbers of the elements within the beam and the second subscripts 1 and 2 denote the left and right ends of the corresponding element. Substitution of the last two equations in (2.17) into (3.4) yields

$$(1/h)\ \mathbf{Z}\mathbf{y} = \mathbf{X}\mathbf{m} \tag{3.5}$$

where y and m are vectors of deflections and mesh currents, and Z and X are square matrices of order k+1 given by

$$\mathbf{Z} = \begin{bmatrix} S_1+S_2 & T_2 & 0 & 0 & \cdots & 0 & 0 \\ T_2 & S_2+S_3 & T_3 & 0 & \cdots & 0 & 0 \\ 0 & T_3 & S_3+S_4 & T_4 & \cdots & \cdot & \cdot \\ \cdot & \cdot & \cdot & \cdot & \cdots & \cdot & \cdot \\ \cdot & \cdot & \cdot & \cdot & \cdots & \cdot & \cdot \\ \cdot & \cdot & \cdot & \cdot & \cdots & 0 & T_{k+1} \\ 0 & 0 & 0 & 0 & \cdots & T_{k+1} & S_{k+1} \end{bmatrix} .$$

$$\mathbf{X} = \begin{bmatrix} T_1' & -S_1' & -S_2' & T_2' & 0 & \cdots & 0 \\ 0 & T_2' & -S_2' & -S_3' & T_3' & \cdots & \cdot \\ 0 & 0 & T_3' & -S_3' & -S_4' & \cdots & \cdot \\ \cdot & \cdot & \cdot & \cdot & \cdot & \cdots & \cdot \\ \cdot & \cdot & \cdot & \cdot & \cdot & \cdots & T_k' \\ \cdot & \cdot & \cdot & \cdot & \cdot & \cdots & -S_k' \ -S_{k+1}' \\ 0 & 0 & 0 & 0 & \cdots & & T_{k+1}' \end{bmatrix} \tag{3.6}$$

Hence, Z is a tridiagonal symmetric matrix and X is an upper triangular band matrix with a band width of 3. y can be solved for from Equation (3.5), provided Z is non-singular. That is,

$$\mathbf{y} = h\mathbf{Z}^{-1}\mathbf{X}\mathbf{m} \tag{3.7}$$

Substitution of (3.7) into (3.3), and then the result into (3.2) along with the analog resistances from Equation (2.20) gives

$$(X^T Z^{-1} X - U)m = 0 \tag{3.8}$$

where

$$U = \begin{bmatrix} S_1 & T_1 & 0 & \cdots & 0 & 0 \\ T_1 & S_1+S_2+2\theta_1\beta & T_2 & \cdots & . & . \\ 0 & T_2 & S_2+S_3+2\theta_2\beta & \cdots & . & . \\ . & . & . & \cdots & . & . \\ . & . & . & \cdots & . & . \\ . & . & . & \cdots & . & T_k \\ 0 & 0 & 0 & \cdots & T_k & S_k+S_{k+1}+2\theta_k\beta \end{bmatrix} \tag{3.9}$$

with θ_j being the sensitivity number for the jth crack given by Equation (2.40). θ_j is based on the total length of the beam.

For non-trivial solutions of (3.8), the determinant of the coefficient matrix, which is symmetric, must vanish, yielding the characteristic equation

$$\det(X^T Z^{-1} X - U) = 0 \tag{3.10}$$

When the crack spacings $\{e_j\}$ and sensitivities $\{\theta_j\}$ are known, the natural frequencies can be computed from Equation (3.10). In computing the matrices in equation (3.10), the variables S_i, T_i, S'_i, T'_i (Equation 2.18) pertaining to the ith beam segment are computed using $e_i\beta = (L_i/L)\beta$ where β is based on the total length of the beam.

3.2. Damage Diagnosis with a Single Crack

Damage diagnosis using the present model is accomplished with the knowledge of frequencies after the damage has occurred. Since the characteristic equations of structures are in terms of dimensionless characteristic values $\{\beta\}$ from the measured frequencies $\{\beta\}$ can be computed from

$$\beta = L\left(\frac{\rho\omega^2}{EI}\right)^{1/4} \tag{3.11}$$

When three measurements of frequency are available for the case k = 1 (single crack), exact location, e, and severity, θ, of the crack can be determined. The procedure will be illustrated with the cantilever beam problem developed in the previous section. The coefficient matrix in equation (3.8), with k = 1, is of the form

$$X^T Z^{-1} X - U = \begin{bmatrix} h_{11} & h_{12} \\ h_{12} & h_{22}-2\theta\beta \end{bmatrix} \equiv H(\beta,e,\theta) \tag{3.12}$$

where the $\{\beta\}$ values in equation (3.12) are the post-damage values computed from equation (3.11). The damage characteristics e and θ are to be determined from the determinant of H, which can be written as

$$\det[H(\beta,e,\theta)] = \det[H(\beta,e,0)] - 2\theta\beta h_{11} = 0 \tag{3.13}$$

where $e = L_1/L$ is the normalized crack location. It is noted that when β assumes the pre-damage values β_u, $\det[H(\beta,e,0)]$ is equal to 0; that is, this term is the characteristic equation for the undamaged ($\theta = 0$) beam. There are three equations emerging from Equation (3.13) for the three known characteristic values. A numerical code for damage diagnosis has been

developed in which e is varied through the range (0,1). θ is computed, for a given e, using the first known characteristic value in Equation (3.13), namely,

$$\theta(e) = \frac{\det[H(\beta^{(1)},e,0)]}{2\beta^{(1)}h_{11}} \tag{3.14}$$

where the superscript on β denotes which characteristic value is used. Then with the second known characteristic value, $\beta^{(2)}$,

$$\det[H(\beta^{(2)},e,\theta)] = 0 \tag{3.15}$$

where the value of θ is now substituted from Equation (3.14). A zero-searching routine is used to find the roots of Equation (3.15) which, in general, yields multiple solutions for e. $\beta^{(3)}$ can then be used to locate the crack. With e known, θ is computed from (3.14).

In the case when the beam deviates somewhat from the Bernoulli-Euler theory or when the material properties are uncertain, computing $\{\beta\}$ from Equation (3.11) may not be suitable. The knowledge of modal frequencies prior to the damage is then necessary. Since ω and ω_u are proportional to β^2 and β_u^2, respectively, where ω_u and β_u are the values for the pre-damage structure, and ω and β are the post-damage values, the following relation holds:

$$\beta = \beta_u \left(\frac{\omega}{\omega_u}\right)^{1/2} \tag{3.16}$$

It is assumed in (3.16) that the proportionality constant between ω_u and β_u^2 does not change after the damage has occurred. The characteristic equations do not involve any material properties and β_u can be computed from

the characteristic equation for the undamaged structure. With ω_u and ω measured in the field, $\{\beta\}$ can then be computed from Equation (3.16) and the above procedure can again be employed to determine e and θ. Only the beam length L, the Poisson's ratio ν, and the slenderness ration (b/L) are required to determine the actual crack location L_1 and the crack depth a (Equation 2.40). Since ν is nearly the same for most metals, the theory becomes independent of the specific material of the structure if the material is a metal, if the damage is presented in terms of L_1 and a, and if $\{\beta\}$ are computed from Equation (3.16). The theory is totally independent of the material properties and dimensions if the damage is presented in terms of e and θ. The data are more conveniently presented versus the relative frequencies (ω/ω_u) or the relative frequency changes $(1 - \omega/\omega_u)$ rather than versus the absolute frequencies, whether $\{\beta\}$ are computed from Equation (3.11) or (3.16). In this report, relative changes are chosen as the means to convey the numerical results.

In practice, the responses of structures deviate from the Bernoulli-Euler theory. It is therefore more accurate to compute $\{\beta\}$ from Equation (3.16). Equation (3.16), in effect, adjusts the parameters of the specific structure such that the structure frequencies match those predicted by the Bernoulli-Euler theory.

In practice, especially for structures whose frequencies are close to each other, the reduction in a certain frequency due to damage may be small while the reduction in the next frequency may drop below that of the former. This phenomenon is called crossover. When crossover occurs and when one is not aware that it has occurred, the correspondence established between the pre-damage and the post-damage values of the frequencies will be in error. If, in such a case, one used Equation (3.16), which involves the ratio of the pre- and post-damage values of the frequencies, the computed charac-

teristic values will be incorrect. On the other hand, if Equation (3.11), which involves the structural properties, is used, a knowledge of the pre-damage frequencies is not required. Hence, it becomes immaterial which pre-damage frequency a certain measured post-damage frequency corresponds to; the important point is that there are some frequency values available which satisfy the post-damage characteristic equation (Equation 3.13). If the structural properties are uncertain, they can be identified by measuring one frequency prior to the damage. That is, the constant K in the relation $\beta_u = K\sqrt{\omega_u}$ can be determined by measuring one ω_u and computing the corresponding β_u from the pre-damage characteristic equation. The same constant can later be used to compute all the needed post-damage frequencies ω by means of $\beta = K\sqrt{\omega}$. In this case, however, the R_j values cannot be used to present the data, since the ordering of the post-damage frequencies according to the magnitudes of their values does not correspond to the pre-damage ordering, unless the fact that crossover has occurred is known.

3.3. Uncertainties of Closely Packed Multiple Cracks

Under certain conditions, the effect of multiple cracks is not distinguishable from that of a single crack. In this section, these conditions are investigated. For this purpose, equivalence of two cracks on a simply-supported beam to a single crack is first established analytically. Numerical results for larger numbers of cracks are then presented. It is established that, when equivalence holds, solution to the inverse problem of damage diagnosis cannot differentiate between single and multiple cracks.

Figure 13a depicts a simply-supported beam with a single crack and its T-circuit analog. The mesh equation together with the Equations (2.20) and (2.21) yield

$$-(S_1 + S_2 + 2\theta\beta)M - (S_1' + S_2')\, y/h = 0 \tag{3.17}$$

where M and y are the resisting moment and deflection at the cracked section, respectively. The continuity condition $V_{12} = V_{21}$ at the crack allows y to be solved for in terms of M. The characteristic equation for a beam with a single crack is thus

$$\frac{(S_1' + S_2')^2}{(S_1 + S_2)} - (S_1 + S_2 + 2\theta\beta) = 0 \tag{3.18}$$

For the case of two cracks, with reference to Figure 13b, the characteristic equation is obtained in the form of Equation (3.10) with

$$X = \begin{bmatrix} -S_1'-S_2' & T_2' \\ T_2' & -S_2'-S_3' \end{bmatrix}, \quad Z = \begin{bmatrix} S_1+S_2 & T_2 \\ T_2 & S_2+S_3 \end{bmatrix}$$

$$U = \begin{bmatrix} S_1+S_2+2\theta_1\beta & T_2 \\ T_2 & S_2+S_3+2\theta_2\beta \end{bmatrix} \tag{3.19}$$

When it is assumed that the spacing between the cracks is sufficiently small, that is, $e_2 = L_2/L = \varepsilon$; the following approximations are obtained.

$$\cosh e_2\beta \approx 1 + \frac{(\varepsilon\beta)^2}{2}, \quad \sinh e_2\beta \approx \varepsilon\beta + \frac{(\varepsilon\beta)^3}{6}$$

$$\cos e_2\beta \approx 1 - \frac{(\varepsilon\beta)^2}{2}, \quad \sin e_2\beta \approx \varepsilon\beta - \frac{(\varepsilon\beta)^3}{6} \tag{3.20}$$

It then follows from Equation (2.18) that

$$S_2 \approx \frac{2\varepsilon\beta}{3}, \; T_2 \approx \frac{\varepsilon\beta}{3}, \; S_2' = T_2' \approx \frac{2}{\varepsilon\beta}, \tag{3.21}$$

After (3.21) is substituted into (3.19) and the necessary operations are performed, the matrix of coefficients in (3.8) is obtained as

$$X^T Z^{-1} X - U = \frac{1}{d}\left\{ \frac{4}{(\varepsilon\beta)^2}(S_1 + S_3)\begin{bmatrix} 1 & -1 \\ -1 & 1 \end{bmatrix} + \begin{bmatrix} h_{11} & h_{12} \\ h_{12} & h_{22} \end{bmatrix}\right\} \tag{3.22}$$

where

$$d = S_1 S_3 + \frac{2}{3}(S_1 + S_3)(\varepsilon\beta) + \frac{(\varepsilon\beta)^2}{3}$$

$$h_{11} = \frac{4}{\varepsilon\beta}(2 + S_1' S_3) + \left[(S_1')^2 S_3 + 4S_1' - S_1 S_3(S_1 + 2\theta_1\beta)\right]$$

$$h_{12} = -\frac{2}{\varepsilon\beta}(4 + S_1' S_3 + S_1 S_3') - 2(S_1' + S_3')$$

$$h_{22} = \frac{4}{\varepsilon\beta}(2 + S_1 S_3') + \left[S_1 (S_3')^2 + 4S_3' - S_1 S_3(S_3 + 2\theta_2\beta)\right] \tag{3.23}$$

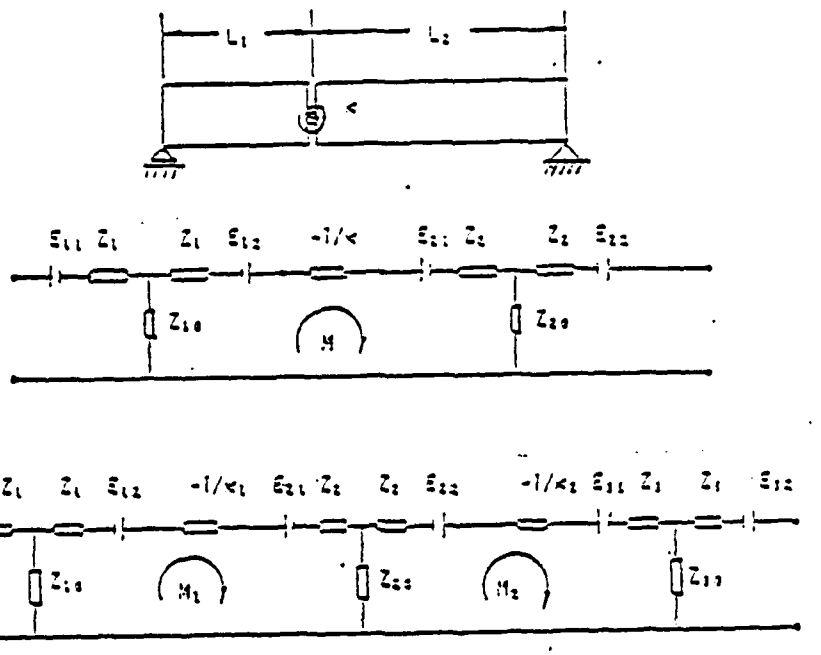

Figure 13. Simply-supported beam. a) With a single crack and its circuit analog. b) Analog circuit for a simply-supported beam with two cracks.

The above analysis is valid at points where S_1, S_1', S_3, S_3' are of smaller order of magnitude than $1/\varepsilon\beta$. The characteristic equation for the two crack case is thus

$$\det(X^T Z^{-1} X - U) = \frac{4S_1 S_3}{(\varepsilon\beta)^2}\{(S_1' + S_3')^2 - (S_1 + S_3)\left[S_1 + S_3 + 2(\theta_1 + \theta_2)\beta\right]\} + O(1/\varepsilon\beta) = 0 \tag{3.24}$$

For small values of e_2, a comparison of Equations (3.18) and (3.24) reveals that S_1, S_1', S_2, S_2' in Equation (3.18) are nearly equal to S_1, S'_1, S_3, S'_3, respectively, in Equation (3.24). The difference between the characteristic equations for one- and two-crack cases is of the order of the product $e_2\beta$. (The difference is proportional to β and is, therefore, larger for higher modes.) The effective sensitivity number for the two cracks approximates, as shown in (3.18) and (3.24), the sum of the individual sensitivity numbers, that is, $\theta \approx \theta_1 + \theta_2$. Thus, closely spaced multiple cracks, in general, cannot be differentiated from a single equivalent crack. Numerical data for different crack configurations indicate the same result.

Similar results are present for a clamped-clamped beam. Numerical results for a cantilever beam indicate that the first few characteristic values of a beam with closely spaced multiple cracks are, in general, close to those of a beam with an equivalent single crack whose sensitivity number, θ_{eq}, is aproximately equal to the sum of the individual sensitivity numbers of the cracks on the original beam. Furthermore, the location of the equivalent crack is generally within the region where the group of cracks is located. In conclusion, equivalence of closely spaced cracks to a single crack implies that, in the process of damage diagnosis, it is impossible to distinguish between closely spaced multiple cracks and a single crack.

Figure 14 typically illustrates the lower limit of crack spacing for a cantilever beam when uniformly spaced multiple cracks become, as a whole, indistinguishable from a single crack. In Figure 3, as in subsequent illustrations, each crack assumes a sensitivity number θ_i of value 0.174 which is taken to be a major crack in a beam of slenderness ratio of 0.05 (corresponding to a relative crack depth $\gamma = a/b$ of 0.6). The equivalence is based on equal values in the first two modal frequency changes and a tolerance of 0.1% in the third mode characteristic values, i.e., $|\beta_{eq}^{(3)} - \beta_{ac}^{(3)}| \leq 0.001$, where the subscripts eq and ac denote the values for the equivalent single crack and the actual damage configuration, respectively. If the tolerance level in $\beta_{eq}^{(3)}$ is increased, the curves in Figure 14 will shift upward. As the number of cracks increases, they must be more closely spaced to be representable by a single crack. The lower limit of spacing depends on where the group of cracks is located. At the built-in end and at $e_1 = 0.6$, more widely spaced cracks can become indistinguishable than at $e_1 = 0.1$. The lower limit of spacing is dependent also on θ_i values. For example, when $e_1 = 0.1$, $k = 2$ and $\theta_1 = \theta_2 = 0.01$ (corresponding to $\gamma = 0.2$ for $b/L = 0.05$), the smallest crack spacing for which the double-crack damage becomes indistinguishable from a single-crack damage is $e_2 = 0.025$.

Figure 15 illustrates the relative frequency changes, R_j, for a cantilever beam with two closely-spaced cracks of $\theta = .174$ each. A very similar set of curves is obtained if $\{R_j\}$ is plotted for a cantilever with one crack of $\theta_{eq} = .348$. For any given number of cracks on a cantilever beam, the largest decrease in the fundamental frequency occurs when all the cracks are groupd at the built-in end. On the other hand, for $\theta_{eq} \geq .3$, the greatest change in the second frequency is observed at a location 4). Such information can be utilized to set rough guidelines for damage diagnosis.

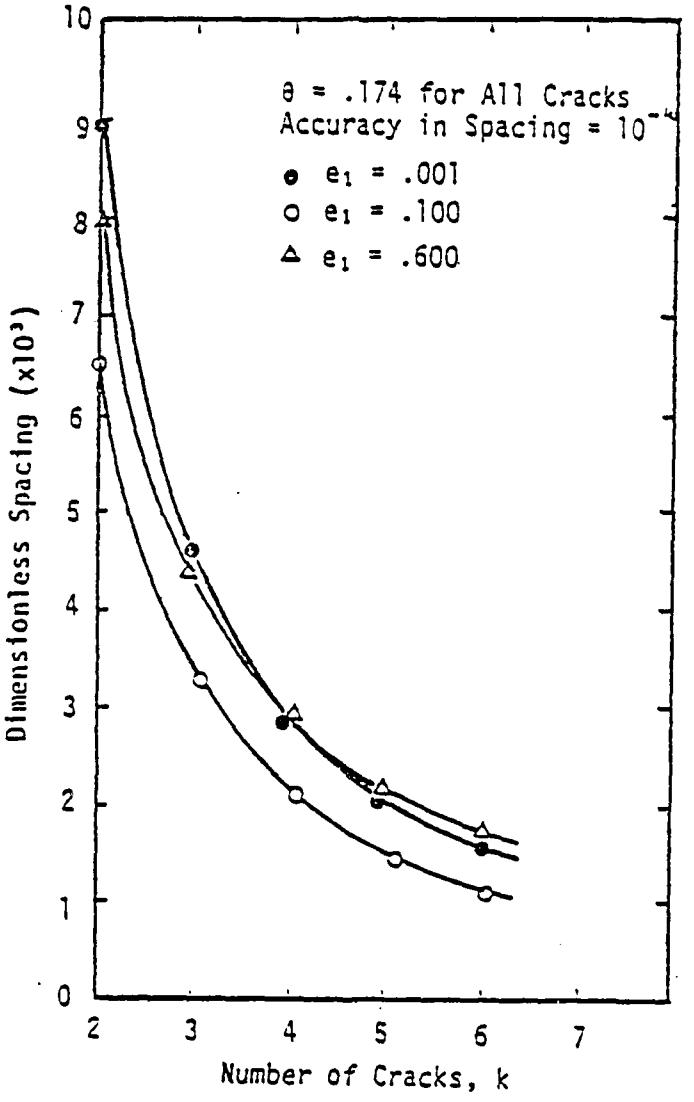

Figure 14. Lower limit of crack spacing for multiple cracks.

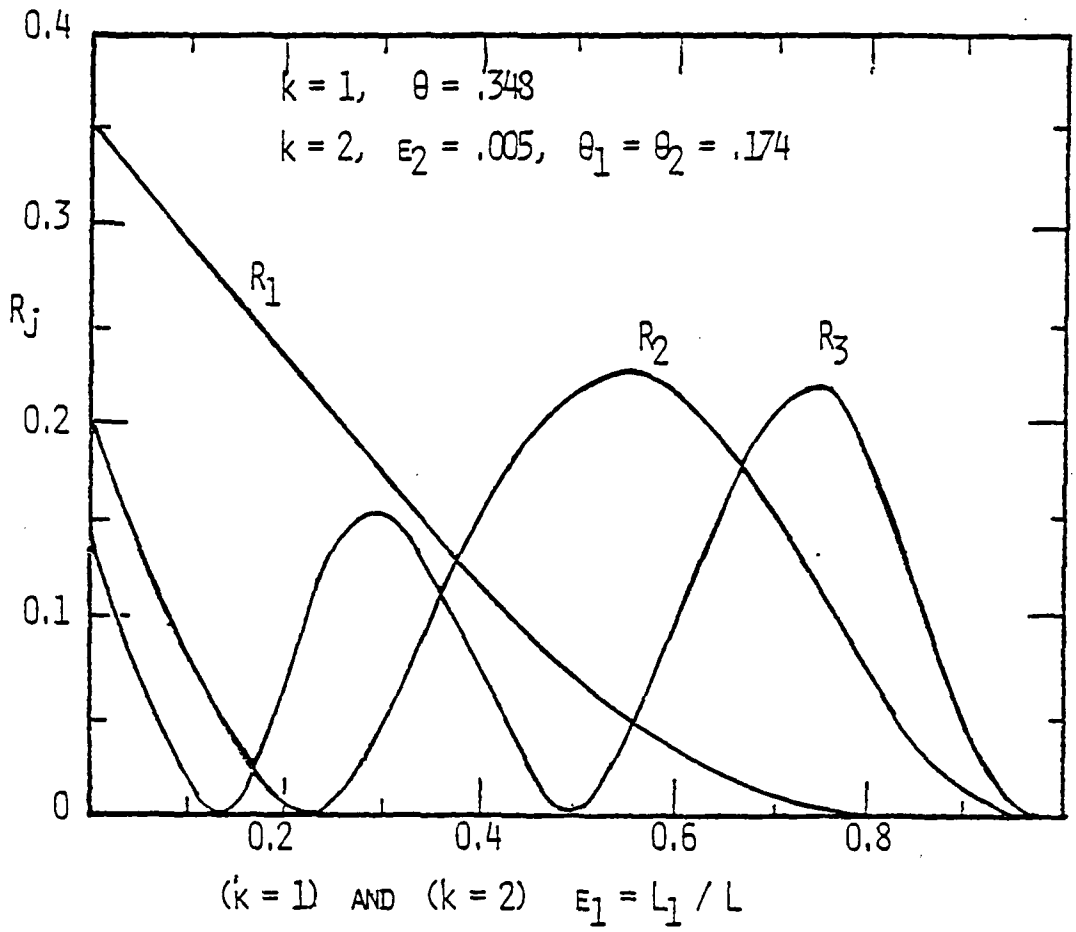

Figure 15. Relative frequency changes for a cantilever with two cracks.

It is clear that probabilistic methods must be resorted to in diagnosis of multiple cracks when an insufficient number of frequency measurements are available. Nevertheless, some qualitative conclusions may be reached with the help of Figure 14 which is independent of material properties. In particular, when a solution has been obtained for a single crack and a decision has to be made between a single crack and a group of closely-spaced less severe cracks, one may argue that formation of a single crack is more likely. In other words, a small mode I type crack is likely to propagate under bending rather than other cracks forming nearby. On the other hand, one severe and several minor cracks may exist distributed along a structure in which case the objective is to be able to diagnose the major crack. Guidelines may be established qualitatively based on the frequency change curves for a cantilever beam, Figure 15, in which case we may propose that

a. If R_1 is considerably smaller than R_2 and/or R_3, then the (major crack(s)) is at a normalized distance greater than ~0.45 from the built-in end (Fig. 15). In addition, (i.) if R_2 is considerably larger than R_3, the crack is located around 0.45-0.65 relative to the built-in end (see Section 6.0 below); (ii.) if R_3 is larger than R_2, the crack is at a distance greater than ~0.7 or; (iii.) if R_2 and R_3 are comparable, then there may be one major crack at 0.65-0.70, or two major cracks one each in the peak regions of the R_2 and R_3 curves.

b. If R_2 is significantly smaller than both R_1 and R_3, the crack is in the region 0.2-0.3, or there may be a (major) crack at 0.2-0.3 and another (major) one at a distance greater than 0.8, the latter being more likely if R_3 is greater than R_1.

c. If R_1 is significantly larger than both R_2 and R_3, and R_2 and R_3 are rather small, the crack is at 0.1-0.2.

d. If the values of R_1, R_2 and R_3 are comparable, several possibilities exist. To list a few, there may be a number of cracks distributed over the beam (Section 3.5 below); the crack may be at 0.35-0.40; or there may be a crack at 0.0-0.3 and a few others at locations greater than ~0.5.

In the present study, only the first three natural frequencies are assumed measurable. The peak locations of R_2 and R_3 curves in Figure 15 are weak functions of θ increases. For example, as θ is increased from 0.01 to 0.50 (effective value for a few closely spaced cracks), the peak of the R_2 curve shifts from the location 0.530 to 0.563 while the second peak of the R_3 curve shifts from 0.710 to 0.760. Similar guidelines for different structures can be established based on minimum and maximum frequency changes although the procedure may become tedious for more complicated structures.

3.4. *Uncertainty From Inadequate Measurements*

To illustrate the uncertainties involved in damage diagnosis when the three R_j values are comparable in value, the following relative frequency changes are assumed to have been computed from the measured frequencies of a cantilever beam: $R_1 = .0579$, $R_2 = .0586$, $R_3 = .0591$. It is to be determined whether the damage mainly consists of one major crack.

The (actual) characteristic values are computed from

$$\beta_{ac}^{(j)} = \beta_u^{(j)} \, (1 - R_j)^{1/2}$$

where $\{\beta^{(j)}\}$ are the undamaged characteristic values, the first three of which for a cantilever are (1.8751, 4.6941, and 7.8548). From (22), in particular, $\beta_{ac}^{(3)} = 7.6192$. The first two actual characteristic values yield one solution for a single crack located at $e_{eq} = .372$ with $\theta_{eq} = .128$ (corresponding to a relative crack depth of $\gamma = .55$ for a slenderness ratio of $b/L = .05$). These equivalent values are then used in the forward problem

with k = 1 eqs. 3.6, 9, 10 (10, 11, 14, 16) to determine the third characteristic value due to the equivalent crack. The computation thus yields $\beta_{eq}^{(3)} = 7.6176$. Then, $\beta_{ac}^{(3)} - \beta_{eq}^{(3)} = .0016$. If we assume that the accuracy in $\beta_{ac}^{(3)}$ is not better than ±.0016, the equivalent single crack solution may be accepted as the true damage diagnosis. On the other hand, the given R_j data were actually generated in a forward problem with ten cracks of equal intensity (θ was taken to be .01 [i.e., $\gamma = .2$] for all the cracks) located such that $e_1 = .001$, $e_i = .094$ for $i = 2,3,\ldots,10$. Thus, in this case, even though the actual and equivalent $\beta^{(3)}$ values match closely, a firm diagnosis cannot be reached.

3.5. Effect of Minor Cracks Associated with a Major Crack.

For the purpose of illustrating the effect, it is sufficient to use the forward problem formulation in which the locations and intensities of the cracks are known. The characteristic values $\beta^{(j)}$ are determined from Equation (3.10). The relative frequency changes are then determined from the characteristic values, namely,

$$R_j = 1 - \left(\frac{\beta^{(j)}}{\beta_u^{(j)}} \right)^2 . \tag{3.25}$$

a. First the analysis will start with one crack (Fig. 16a), i.e., k = 1, at e = .54 (in the peak region of the R_2 curve, Figure 15) with $\theta = .174$ ($\gamma = .6$). The relative frequency changes are then computed as $R_1 = .029$, $R_2 = .137$, $R_3 = .014$.

b. Now, in addition to the crack in part (a), there are five more cracks of intensity $\theta = .0026$ ($\gamma = .1$) each, distributed on the cantilever such the $e_1 = e_2 = e_3 = e_5 = .1$, $e_4 = .24$, and $e_6 = .09$ (Fig. 16b). The actual characteristic values are computed as $\beta^{(1)} = 1.840$, $\beta^{(2)} = 4.351$, and

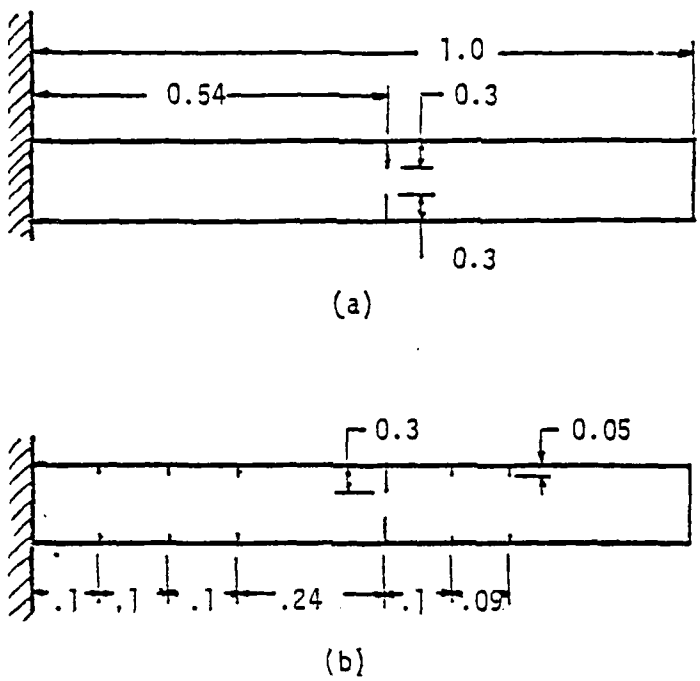

Figure 16. Cantilever with one and six cracks.

$\beta^{(3)} = 7.768$ from which $R_1 = .037$, $R_2 = .141$, $R_3 = .022$. If these values of R_j were obtained from actual measured frequencis from which the damage were to be diagnosed (the inverse problem), $\beta^{(1)}$ and $\beta^{(2)}$ are used to find a solution for a single crack, which is $(e_{eq}, \theta_{eq}) = (.51\ .183)$. This single crack would produce $\beta^{(3)}_{eq} = 7.845$ or $R_{3eq} = .0024$.

c. The same case as in (b) except θ_i are changed to .01 ($\gamma = .2$) with the major crack remaining the same, i.e., $\theta_4 = .174$. Hence, the depths of the minor cracks are doubled. The corresponding frequency changes in the forward problem are $R_1 = .058$, $R_2 = .151$, $R_3 = .043$. If the same R_1 and R_2 are in turn used in the inverse problem of damage diagnosis with k = 1, we obtain $(e_{eq}, \theta_{eq}) = (.47, .224)$, $\beta^{(3)}_{eq} = 7.830$, $R_{3eq} = .0064$.

The above cases indicate that the value of R_2 did not change significantly wnen minor cracks were added to the beam. If this were an actual damage diagnosis problem, in which case only $\{\beta^{(j)}\}$ and $\{R_j\}$ would be known from the measured data, then a decision would have to be made about the computed (e_{eq}, θ_{eq}). In case (b), $R_3 = .022$ whereas $R_{3eq} = .0024$. In cas (c), $R_3 = .043$, but $R_{3eq} = .0064$. Hence, based only on comparison of R_{3eq} with the actual values of R_3, the solutions for (e_{eq}, θ_{eq}) would be rejected. Nevertheless, the equivalent damage parameters in both cases closely identify the major crack located at the distance of .54 from the built-in end with $\theta = .174$. When there is no minor crack on the beam, as in case (a), (e_{eq}, θ_{eq}) would be computed as (.54, .174). The effect of the minor cracks on (e_{eq}, θ_{eq}) is thus seen to be small. Hence, it is concluded that, when the given R_j values exhibit a pattern such as in this example, the discrepancy in R_3 and R_{3eq} or in $\beta^{(3)}_{ac}$ and $\beta^{(3)}_{eq}$ can be ignored when the interest is in diagnosing the major crack.

3.6. Peak Modal Response

It is to be demonstrated that, when multiple cracks exist on a beam, a crack which is located in the peak region of an R_j curve affects the corresponding frequency, ω_j, the most.

a. Given k = 1, e_1 = 0.001, θ_1 = 0.174. The frequency changes are computed as (the forward problem) R_1 = 0.234, R_2 = 0.162, R_3 = 0.125.

b. A second crack is added to case (a) such that e_2 = 0.546 (i.e., near the peak region of the R_2 curve of a single crack as in Figure 15) and θ_2 = 0.174. Then R_1 = 0.246, R_2 = 0.272, R_3 = 0.162.

c. A third crack is added to case (b) such that e_3 = 0.185 (i.e., near a peak region of the R_3 curve of the single crack in Fig. 15) and θ_3 = 0.174 [parameter values in cases (a-b) are preserved]. Then R_1 = 0.247, R_2 = 0.273, R_3 = 0.167. In case (b), the greatest decrease relative to case (a) occurred in the second frequency, whereas in case (c) it was the third frequency that suffered the largest decrease relative to case (b) although this decrease was insignificant for θ_3 = 0.01. The example illustrates the effect of crack location and intensity on the frequencies and confirms the usefulness of curves such as Figure 15 to diagnosis of damage as outlined in the guidelines presented earlier.

It should be noted that the sensitivity number θ is a measure of how sensitive the natural frequencies are to given crack depth and location as a function of the slenderness ratio. Decrease in natural frequencies is greater for larger values of θ. Between two cracked beams with the same crack location and relative crack depth, θ for the more slender one will be smaller giving rise to smaller R_j values. For example, for γ = 0.6, (and ν = 0.3), θ = 0.0697 when b/L = 0.02 and θ = 0.0174 when b/L = 0.005. Thus, in practice it is relatively harder to diagnose damage in slender beams. On

the other hand, two beams of the same slenderness ratio and Poisson's ratio, but of different materials, experience the same relative decrease in frequencies for the same crack location and relative depth.

CHAPTER 4

TRANSMISSIBILITY THEORY OF DAMAGE DIAGNOSIS

In this chapter, a new method is proposed for diagnosing damage in large structures. The method utilizes the changes in transmissibilities at several locations, called the response stations, on the structure. The method is developed by computing the transmissibility changes for known crack configurations and comparing the magnitudes of the changes at different response stations. The equations derived in Chapter 2 through the electrical analogy of a damped frame structure are used in the computations.

4.1. Transmissibility and Relative Transmissibility Change

In this study, transmissibility is defined as the magnitude of the ratio of acceleration at a response station to the force applied at an arbitrary location on the structure (Fig. 17). Namely,

$$T \equiv \left|\frac{\ddot{y}_t}{F}\right| \tag{4.1}$$

where y_t is the complex deflection at the response station of interest. When the force is sinusoidal, that is, $F=F_m e^{i\omega t}$, the deflection becomes

$$y_t = y e^{i\omega t} = y_m e^{i[\omega t-\phi]} \tag{4.2}$$

where y is the complex modal shape, y_m is the amplitude of transverse deflection, and ϕ is the phase angle. y_m and ϕ are functions of location and excitation frequency. ϕ is zero for an undamped structure. Transmissibility for sinusoidal excitation is then given by

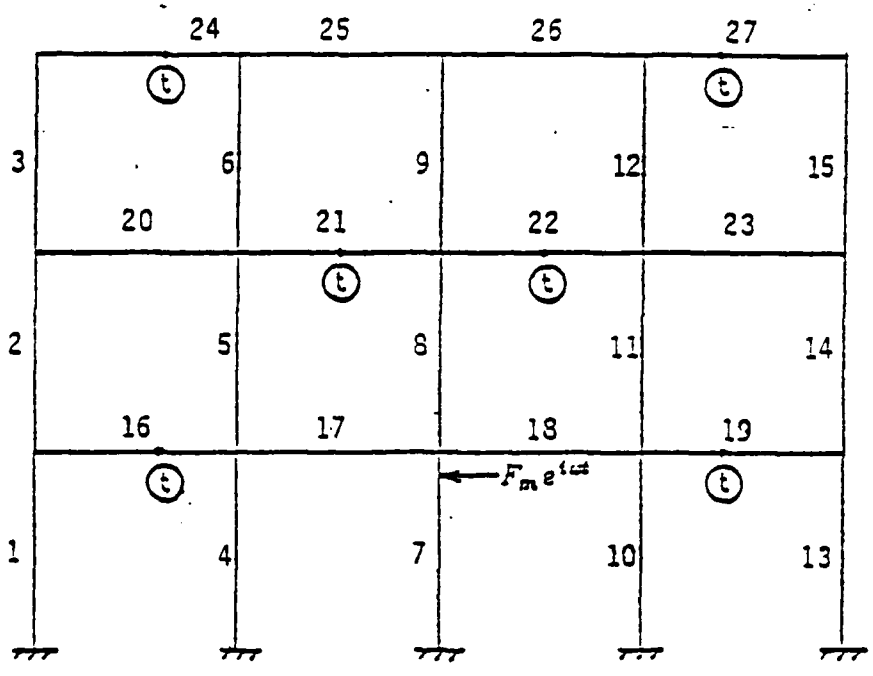

Figure 17. A three-story four-span frame.

$$T = \frac{\omega^2 y_m}{F_m} \tag{4.3}$$

The amplitude of deflection, y_m, at the response station can be computed from Equation (2.63) for any plane frame with and without a crack, when the crack location and the sensitivity number, Θ, are known. In practice, transmissibilities can be measured periodically or after a strong motion event and compared to baseline values to diagnose the damage. To facilitate a diagnosis method, the relative transmissibility change is introduced as follows:

$$R_T = \frac{T_c - T_o}{T_o} = \frac{T_c}{T_o} - 1 \tag{4.4}$$

where the subscripts c and o indicate the transmissibilities with and without the crack, respectively. When the structure is excited at the same frequency and with the same force magnitude before and after the damage, R_T becomes

$$R_T = \frac{y_{m_2}}{y_{m_1}} - 1 \tag{4.5}$$

An undamped structure has node points, that is, points with zero transverse deflection at all times. If, for such a structure, the response station is at a node point of the undamaged modal shape, then $y_{m_1} = 0$. If, on the other hand, it is at a node point of the post-damage modal shape, then $y_{m_2} = 0$. In general, then,

$$-1 < R_T < \infty \tag{4.6}$$

Damped structures, in general, do not have true node points. Every point on the structure deflects somewhat during a period of the excitation. R_T, however, still has minimum and maximum values with respect to the location of the response station. To facilitate referral to such locations, the following definition is introduced. A pseudo-node point, PNP, of a damped structure is a point with locally minimum amplitude of transverse deflection. Thus, R_T is maximum at the PNPs of the undamaged structure and minimum at those of the damaged structure.

Relative transmissibility change is a function of the excitation location and frequency, the location of the response station, and the crack location and severity, as well as the structural parameters. It is desirable to have large values of relative transmissibility changes for as small cracks as possible. This may be accomplished by optimizing the parameters which can be controlled.

4.2. Optimum Parameter Values

It is found that exciting a frame structure on a column rather than on a girder is more advantageous for diagnosis purposes. A 3x4 structure (i.e., $n=3$, $m=4$) is shown in Figure 17. The frames studied throughout this chapter are uniform unless stated otherwise; namely, all of the beam elements which make up the frames are of equal length and have the same material and geometric properties. Figure 18 illustrates the variation of the relative transmissibility change at a response station as a function of the excitation location which is varied along the leftmost wall of the frame. Each third of the abscissa corresponds to one of the columns on that wall, with

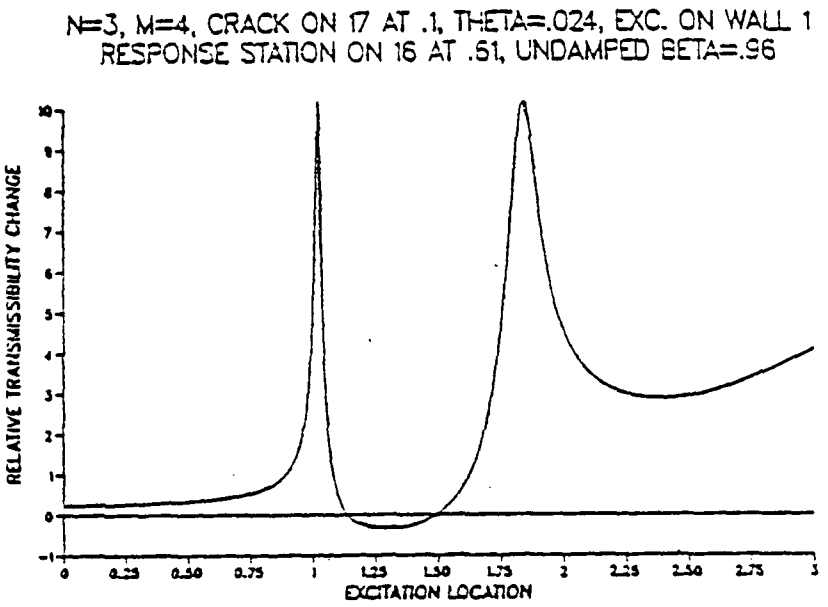

Figure 18. Relative transmissibility change vs excitation location.

distance measured from the anchor up. The response station is on girder 16 at a normalized distance of 0.61 measured from the left end. The crack is on girder 17 at a distance of 0.1 from the left end of that girder. Sensitivity number, Θ, for the crack is 0.024 (Eq. 2.40). Damping factors, δ, (Eq. 2.2) for the structure is taken to be 0.01. The undamped β value, β_d, which is a function of the excitation frequency (Eq. 2.8), is 0.96, nearly the same as the first undamped characteristic value of the structure. The figure indicates that the relative transmissibility change for a given crack is largest when the excitation is applied near a frame joint.

Figure 19 illustrates the dependence of the relative transmissibility change, R_T, on the excitation frequency expressed in terms of the undamped β value. Other variables have the values given above with the excitation applied on column 1 at a distance of 0.95 from the ground. R_T is seen to have peaks near the natural modal frequencies of the structure. Thus, it is concluded that structures should be tested near resonance.

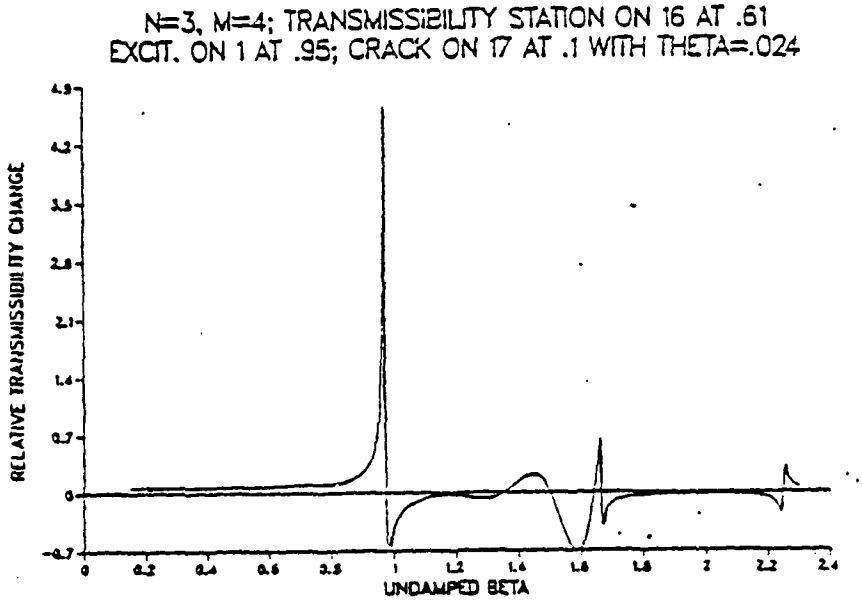

Figure 19. Relative transmissibility change vs frequency.

The amplitudes of dimensionless transverse deflections, $|y^*|$, along girder 16 with and without a crack on girder 17 are shown in Figure 20, where dimensionless deflection for the uniform frame is defined by

$$y^* \equiv \frac{EI\beta^3}{L^3 F_m} y = \frac{L\rho\omega^2}{\beta F_m} y \tag{4.7}$$

with y given by Equation (2.63). A computer program is written to compute the dimensionless deflections on a frame with uniform material properties, but different beam lengths in general. The listing of the program is given in Appendix.

For an undamped (i.e., δ=0) structure, the curves in Figure 20 would be called modal shapes. The pseudo-node point, PNP, of the girder is observed to have shifted after the damage. The curves in Figure 20 also represent the transmissibilities (Eq. 4.3) with and without the crack as a function of the location of the response station on girder 16. These two curves yield the R_T curve in Figure 21 which indicates that R_T takes its minimum and maximum values at the PNPs of the post-damage and pre-damage structure, respectively. Figure 22 shows the variation of R_T as a function of

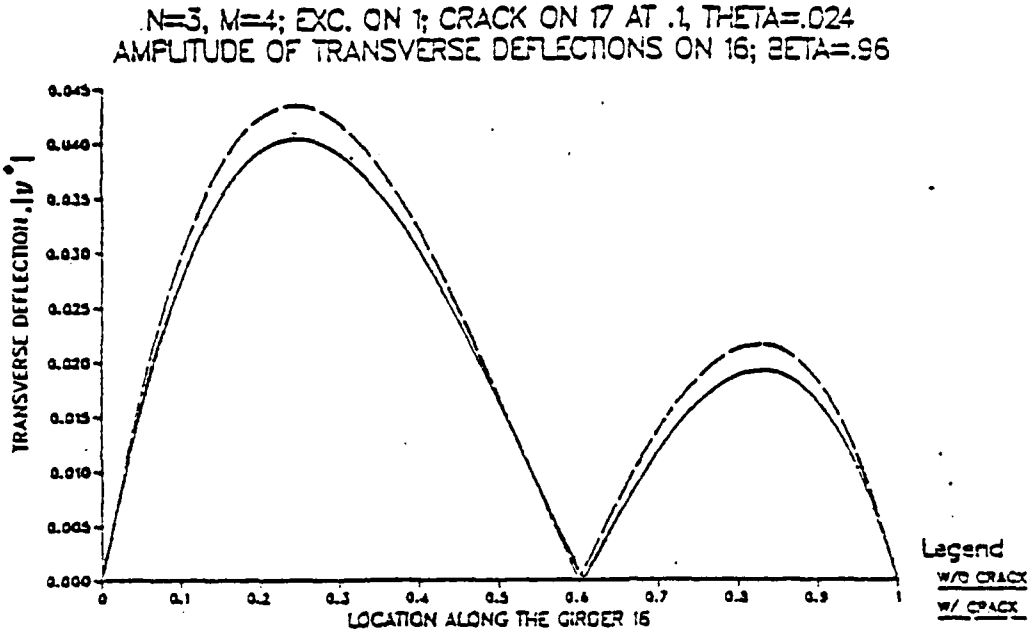

Figure20. Transverse deflections on girder 16.

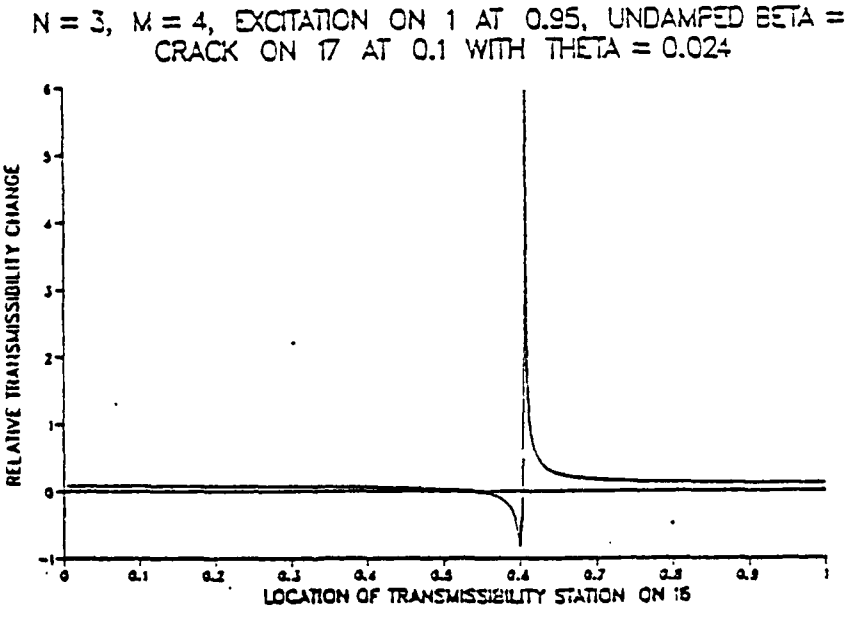

Figure 21. Relative transmissibility change vs response location.

the location of the response station on 16 when there is a crack on column 4.

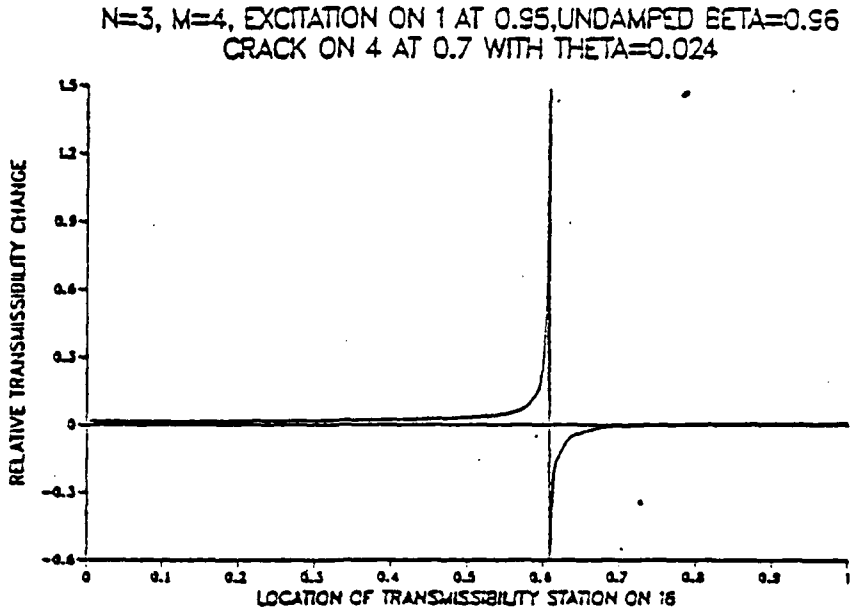

Figure 22. Relative transmissibility change vs response location.

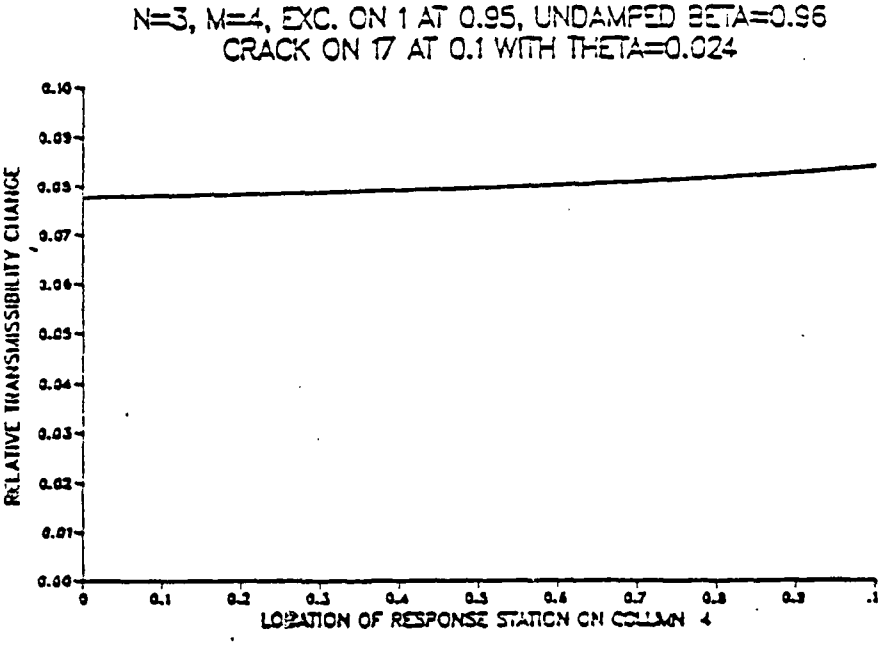

Figure 23. Relative transmissibility change vs response location.

At lower natural frequencies, the columns of the structure do not have pseudo-node points. Figure 23 shows that, at the fundamental frequency (i.e., β_d=0.96), R_T remains nearly constant when the location of the response station is varied along the column 4.

In summary, then, R_T can be maximized when the excitation is on a column near a joint and at a resonant frequency and when the response station(s) is(are) near the PNP(s) of a girder(s).

Table 1 lists the PNP locations at the fundamental frequency, on some of the girders of the frame in Figure 17 In the table, ξ_f denotes the excitation location on the respective column. All of the distances are normalized and measured relative to the lower (left) end of the respective column (girder). As the table indicates, a PNP location is highly insensitive to the excitation location and to the value of the damping factor.

4.3. The Number of Response Stations

It is desirable, from a practical point of view, to accomplish damage diagnosis with a minimum number of transducers. This number is related to the objectives of a diagnosis process. In theory, a transducer may be installed on every girder and the crack can be isolated to within a beam element. In the light of the high sensitivity of the transmissibility changes to the response location in the vicinity of the PNPs and the uncertainties involved in practice, however, the objective in this study is to isolate a crack to within one or two cells of a frame structure. A local method, such as an ultrasonic technique, may then be utilized to determine the exact location of the crack. With this objective in mind, the six response stations on the frame of Figure 17 were chosen. These stations are on girders 16, 19, 21, 22, 24, and 27. Numerical results indicate that, in general, response at a measuring station is most significantly affected when the crack is at a frame cell neighboring the station. In Figure 17 station 26, for example, has four neighboring cells while station 21 has six. The criterion used here for selecting the stations is that each station has at most two

neighboring cells in common with those of another station. This implies that every other girder on a floor level has a station on it and that every other girder is skipped as one moves vertically up the frame. The number of transducers (response stations) required is, then, $\frac{nm}{2}$ when nm is even and $\frac{1+nm}{2}$ when nm is odd, where n is the number of stories and m is the number of spans. The selection of stations in Figure 17 violates the above criterion, even though the number of stations is still six. Most of the numerical computations were carried out with the configuration of Figure 17 therefore, the development of the method is based on that configuration.

TABLE 1

PNPs of Some Girders (No crack)

β_d = .96; ξ_f = .95 unless noted otherwise

δ	Girder 16 Column with the excitation			
	1	7	11 (ξ_f =.55)	15
.01	.6062	.6084	.6084	.6083
.30	.5994	...	...	.6079
.30*	.5932	...	...	.6016

δ	Girder 24 Column with the excitation			
	1	3	6	7
.01	.6183	.6140	.6249	.6187

δ	Other Girders(excitation on 7) Girder No.			
	19	21	22	27
.01	.3916	.4895	.5105	.3813

* (With a crack of Θ=.024 on girder 17 at a distance of .1)

4.4. Selection of the Column for Excitation

Figures 24-27 show the relative transmissibility change curves resulting from four different excitation locations when the other parameter values are kept the same. Transmissibility change at station 27 for a crack on girder 17 is small in all the cases; therefore, the corresponding curve is omitted. The figures indicate that the trends of R_T values, for the given response stations, are highly insensitive to the excitation location. A trend of relative transmissibility changes is defined as the order, with respect to the magnitudes, of the relative transmissibility changes for a given crack configuration. The word "trend", however, will be used in a more qualitative manner rather than with an implication of a precise ordering of numbers. For a crack on a certain beam element, for instance, two response stations may exhibit the largest transmissibility changes without one response clearly overwhelming the other, in which case the trend will be described as such. From Figures 28-31, then, the trend of R_T values for a crack on girder 17 is such that

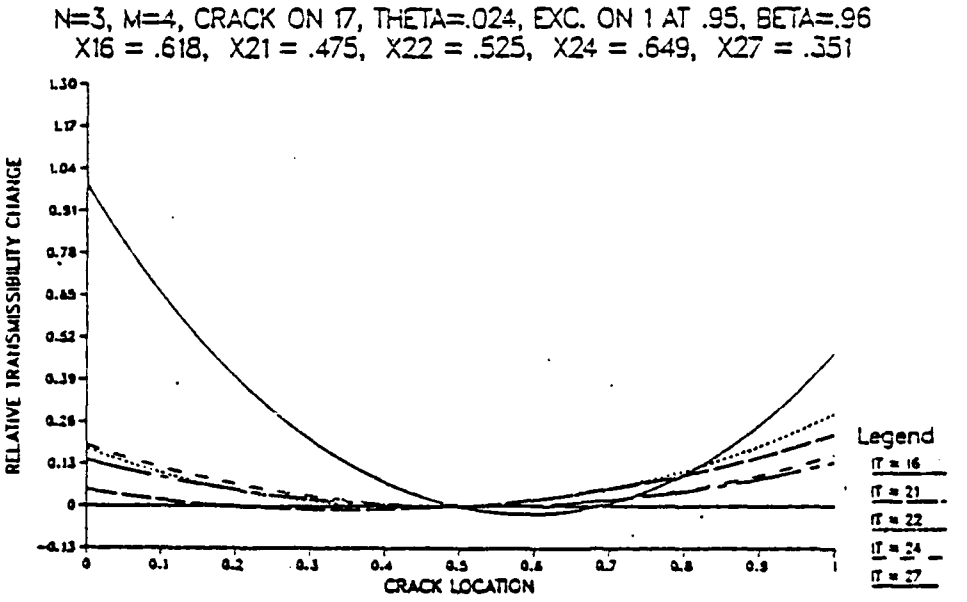

Figure 24. Relative transmissibility change vs crack location(excitation on 1).

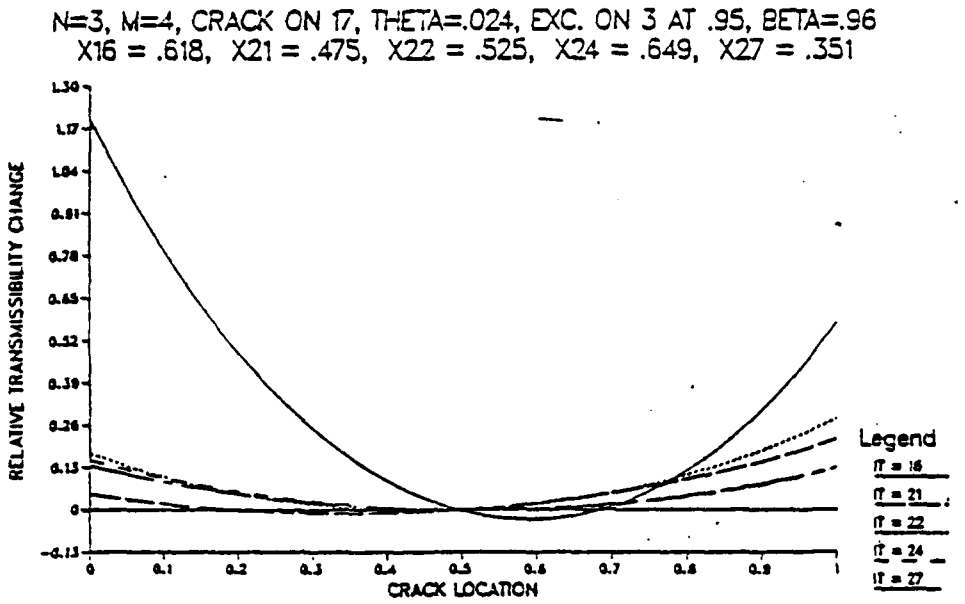

Figure 25. Relative transmissibility change vs crack location(excitation on 3).

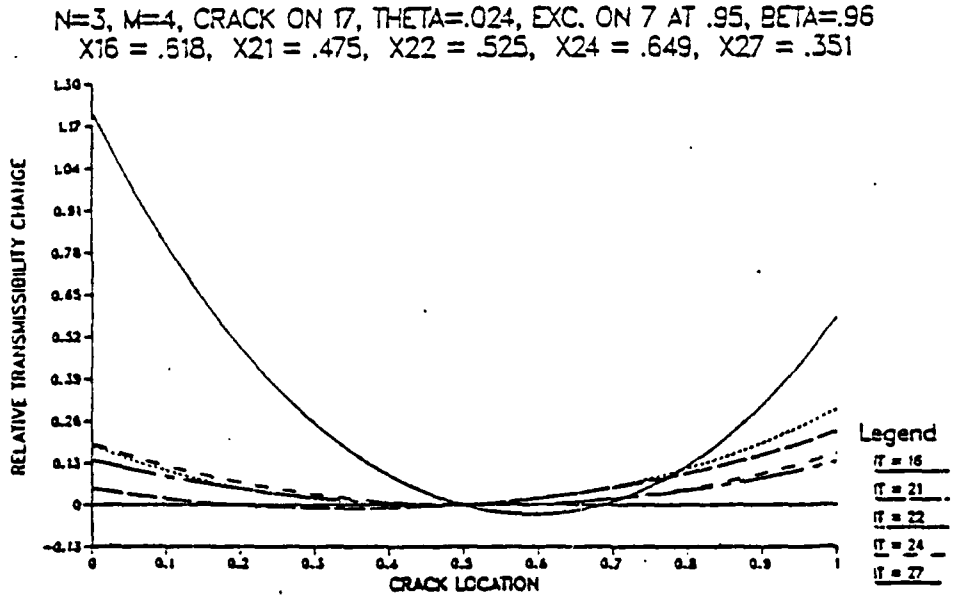

Figure 26.Relative transmissibility change vs crack location(excitation on 7).

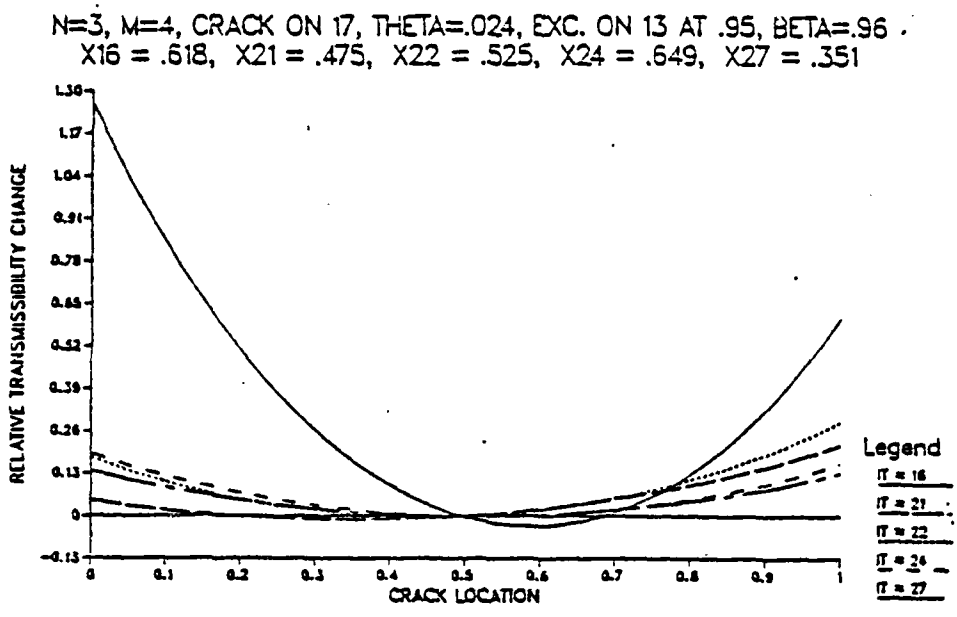

Figure 27. Relative transmissibility change vs crack location(excitation on 13).

station 16 displays a much more significant transmissibility change than the other stations over a large portion of the range of the crack location. However, when the response stations are very close to the PNPs, unlike in the figures, the trends may be more sensitive to the excitation location. It should be noted that relative transmissibility changes and transmissibilities themselves change as the excitation location is varied. The interest of this study, however, is in the trends rather than the absolute values. In what follows, the general trends of R_T values will be studied by exciting the structure on column 7 at a distance of 0.95 from the ground and by studying only the left half of the frame and utilizing the symmetry.

4.5. Selection of Response Locations Relative to the PNPs

Figures 21 and 22 demonstrate that relative transmissibility changes are highly sensitive to the response location in the vicinity of the PNPs. In practice, however, it may not be possible to determine the exact location of a PNP. On the other hand, it may not be desirable to install a transducer at a PNP either since the acceleration or

deflection there may be too small to be measurable. Transducers then must be installed at some distance from the PNPs and yet must be close enough to the PNPs to yield large R_T values. For some crack configurations, installing the transducers to the right of the pre-damage PNP yields better results (Fig.21), whereas for others installing them to the left is better (Fig. 22). This is due to the fact that PNPs may shift to the right or left after the damage. The situation may be improved by installing two transducers in the vicinity of a PNP in close proximity to each other. Such a measure is likely to increase the probability of obtaining a large R_T value for a given crack.

4.5.1. The Amount of Shift of the Response Stations Relative to the PNPs

Table 2 lists the amplitudes of dimensionless deflections of selected girders on the undamaged frame in the vicinity of PNPs as well as the lateral deflections of the floor levels for the frame of Figure 17 with the excitation on column 7. The undamped β value, β_d, is 0.96 (i.e., at the fundamental frequency). The amplitude of complex deflection can be shown to be

$$|y^*| = \frac{L\rho\omega^2}{\beta_d F_m}(1+\delta^2)^{1/2}\,|y| \tag{4.8}$$

from Equations (4.7) and (2.8), where $|y|$ is the physical deflection. An empirical formula for the fundamental frequency of multistory buildings is $\omega_1 = \frac{20\pi}{n}$ in rad/s [33], which is the Uniform Building Code formula, where n is the number of stories. For a three story building, then, $\omega_1 \approx 21$ rad/s. If it is assumed that the amplitude of the force, F_m, is approximately equal to the weight, $L\rho g$, of one beam element, where g is the gravitational constant, equation (4.8) can be written as

$$|y^*| \approx 1.2|y| \quad , \quad |y| \text{ in inches.} \tag{4.9}$$

Eddy-current displacement transducers are capable of measuring deflections less than 10^{-3} inch (0.025 mm). If this value is accepted as the base, $|y^*|$ must be of the order 10^{-3} in order for $|y|$ to be measurable. From Table 4, then, the locations of the response stations are determined to be at the points away from the PNPs, where $|y^*|$

TABLE 2

Deflections at Selected Locations

Excitation on column 7 at .95

$\beta_d = .96, \quad \delta = .01$

Sidesway of the Floors	
Floor	$\lvert y^* \rvert$
1	0.436
2	0.909
3	1.157
at the excitation	0.422

In the vicinity of the girder PNPs		
Girder	Location	$\lvert y^* \rvert \times 10^3$
16	.588	3.04
	.598	1.53
	.6084(PNP)	0.008
	.618	1.40
	.628	2.83
21	.475	1.32
	.4895(PNP)	0.014
	.505	1.41
24	.589	1.14
	.6187(PNP)	0.003
	.649	1.09

reaches a value of at least 10^{-3}. This translates into a shift, away from the respective PNP, of 0.01 for girders 16 and 19, 0.015 for 21 and 22, and 0.03 for 24 and 27. The response locations used in Figures 24-27 were based on these shift values. As the response stations are moved further away from the PNPs, R_T values get smaller and become comparable in value as a result of which the trends are gradually lost. For example, when the locations of the response stations are $\xi_{16} = 0.85$, $\xi_{19} = 0.15$, $\xi_{21} = 0.20$, $\xi_{22} = 0.80$, $\xi_{24} = 0.85$, and $\xi_{27} = 0.15$, all of which are measured from the left end of the respective girder, all of the relative transmissibility changes for a given crack are either small (less than 10%) or close in

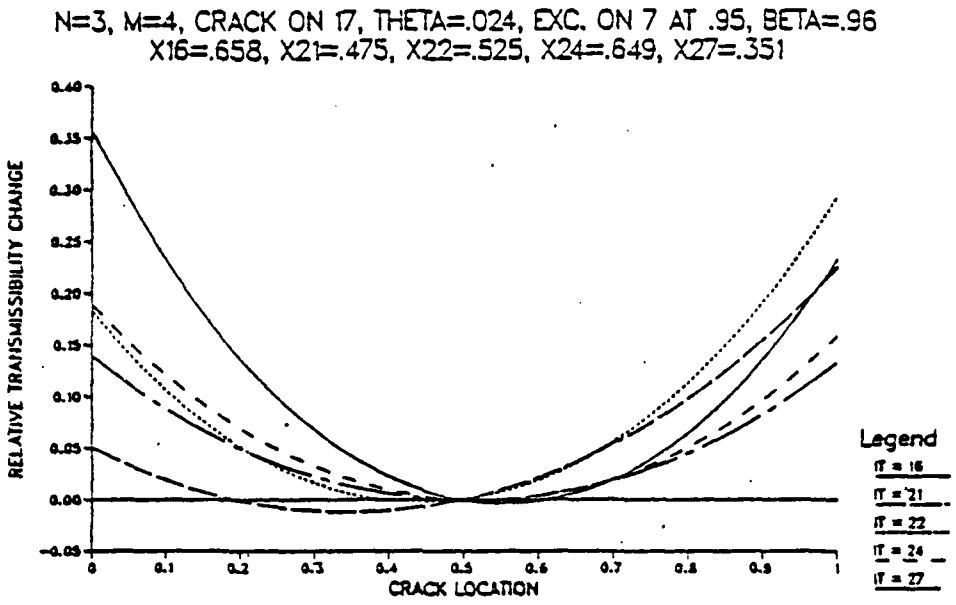

Figure 28. Relative transmissibility change vs crack location.

value. On the other hand, moving the response stations closer to the PNPs increases the possibility of diagnosis as the trends become more definitive.

It is desirable to know how far away from the PNPs the trends still persist. Figure 28 illustrates that at a distance of 0.05 from the PNP of girder 16, the trend for a crack on girder 17 is still clear, when the crack is on the left half of the frame and when the other response stations are kept at the same locations as in Figures 24-27. Further away from the PNP, however, the trend starts becoming less clear-cut.

4.5.2. The Direction of Shift of the Response Stations Relative to the PNPs

Another question related to the optimum location of the response stations relative to the PNPs is that of which direction to shift the response stations. Tables 3 and 4 list the relative transmissibility changes at the six response stations as a function of the crack location. In Table 3, the response stations on girders 16 and 19 are shifted from the corresponding PNPs by a distance of 0.01 away from the center, while those on 21 and 22 are shifted by a distance of 0.015 toward the center and the

TABLE 3

Relative Transmissibility Changes vs Crack Location

Excitation on column 7 at a distance of .95, β_d = .96, δ = .01, Θ = .024.

Response Locations :

ξ_{16} = .598 ξ_{21} = .505 ξ_{24} = .589
ξ_{19} = .402 ξ_{22} = .495 ξ_{27} = .411

(ξ_c = crack location, RS : response station)

1) Crack on column 1

ξ_c	RS 16	RS 19	RS 21	RS 22	RS 24	RS 27
0.001	-0.440	0.239	0.257	0.224	0.179	0.235
0.100	-0.221	0.163	0.171	0.153	0.128	0.160
0.200	-0.067	0.103	0.104	0.096	0.087	0.101
0.300	0.027	0.059	0.056	0.054	0.054	0.057
0.400	0.071	0.028	0.023	0.025	0.030	0.026
0.500	0.067	0.008	0.004	0.007	0.013	0.008
0.600	0.018	0.000	-0.001	0.000	0.002	0.000
0.700	-0.076	0.003	0.007	0.003	-0.003	0.003
0.800	-0.214	0.016	0.028	0.016	-0.002	0.017
0.900	-0.400	0.040	0.061	0.040	0.005	0.041
0.999	-0.635	0.074	0.107	0.073	0.017	0.076

2) Crack on column 2

ξ_c	RS 16	RS 19	RS 21	RS 22	RS 24	RS 27
0.001	-0.454	0.043	0.028	0.049	0.116	0.038
0.100	-0.301	0.024	0.021	0.029	0.058	0.022
0.200	-0.177	0.011	0.015	0.015	0.019	0.010
0.300	-0.081	0.003	0.008	0.005	-0.001	0.003
0.400	-0.013	0.000	0.002	0.000	-0.002	0.000
0.500	0.029	0.002	-0.005	0.000	0.013	0.001
0.600	0.046	0.007	-0.012	0.004	0.044	0.005
0.700	0.037	0.017	-0.019	0.011	0.091	0.012
0.800	0.004	0.030	-0.027	0.021	0.153	0.022
0.900	-0.052	0.045	-0.036	0.035	0.228	0.035
0.999	-0.132	0.064	-0.045	0.050	0.315	0.049

TABLE 3
(continued)

3) Crack on column 4

ξ_c	RS 16	RS 19	RS 21	RS 22	RS 24	RS 27
0.001	1.203	0.349	0.172	0.269	0.370	0.328
0.100	0.680	0.221	0.123	0.175	0.231	0.209
0.200	0.321	0.128	0.083	0.105	0.131	0.121
0.300	0.096	0.063	0.052	0.056	0.062	0.060
0.400	-0.018	0.022	0.028	0.023	0.020	0.022
0.500	-0.035	0.003	0.009	0.005	0.001	0.003
0.600	0.039	0.002	-0.005	-0.000	0.003	0.002
0.700	0.207	0.020	-0.014	0.007	0.027	0.018
0.800	0.475	0.058	-0.019	0.028	0.072	0.052
0.900	0.858	0.117	-0.021	0.063	0.141	0.106
0.999	1.372	0.200	-0.020	0.113	0.238	0.181

4) Crack on column 5

ξ_c	RS 16	RS 19	RS 21	RS 22	RS 24	RS 27
0.001	1.205	0.171	0.560	0.205	0.015	0.133
0.100	0.773	0.103	0.287	0.115	0.025	0.080
0.200	0.450	0.054	0.107	0.053	0.026	0.043
0.300	0.219	0.022	0.008	0.015	0.022	0.018
0.400	0.067	0.004	-0.021	-0.001	0.011	0.004
0.500	-0.016	0.000	0.017	0.003	-0.005	-0.000
0.600	-0.034	0.008	0.118	0.026	-0.028	0.005
0.700	0.012	0.029	0.285	0.067	-0.058	0.019
0.800	0.124	0.061	0.521	0.128	-0.097	0.042
0.900	0.306	0.107	0.835	0.210	-0.146	0.074
0.999	0.563	0.165	1.231	0.315	-0.207	0.115

5) Crack on girder 16

ξ_c	RS 16	RS 19	RS 21	RS 22	RS 24	RS 27
0.001	0.588	0.269	0.299	0.283	0.346	0.256
0.100	-0.987	0.170	0.174	0.174	0.223	0.162
0.200	-0.017	0.098	0.087	0.096	0.133	0.092
0.300	0.470	0.048	0.032	0.043	0.069	0.044
0.400	0.534	0.016	0.002	0.012	0.027	0.015
0.500	0.211	0.002	-0.004	-0.000	0.004	0.001
0.600	-0.489	0.002	0.013	0.006	-0.001	0.003
0.700	-0.651	0.018	0.054	0.030	0.011	0.020
0.800	-0.050	0.051	0.119	0.073	0.041	0.053
0.900	1.398	0.102	0.214	0.139	0.092	0.105
0.999	3.826	0.174	0.344	0.232	0.167	0.177

TABLE 3
(continued)

6) Crack on girder 17

ξ_c	RS 16	RS 19	RS 21	RS 22	RS 24	RS 27
0.001	-0.841	0.190	0.215	0.098	0.085	0.135
0.100	-0.569	0.112	0.146	0.069	0.050	0.083
0.200	-0.354	0.056	0.091	0.045	0.025	0.045
0.300	-0.190	0.019	0.049	0.025	0.008	0.018
0.400	-0.073	0.001	0.019	0.010	0.000	0.004
0.500	0.003	0.000	-0.001	-0.000	0.000	0.000
0.600	0.036	0.017	-0.010	-0.007	0.008	0.007
0.700	0.032	0.052	-0.008	-0.010	0.025	0.026
0.800	-0.015	0.107	0.005	-0.009	0.050	0.056
0.900	-0.108	0.182	0.029	-0.004	0.084	0.098
0.999	-0.252	0.280	0.065	0.004	0.129	0.155

ones on 24 and 27 by a distance of 0.03 away from the center. In Table 4, the shifts are in the opposite directions by the same amounts. Table 3 shows only the cases when the crack is on a beam element in the neighborhood of response station 26, that is, on 1, 2, 4, 5, 16, or 17. A negative transmissibility change which is large in magnitude is considered significant. From Table 3, then, the changes at station 16 are the most significant among all the stations, when the crack is on an element neighboring station 16. It is preferable, however, to choose a response station at a location where transmissibility (or deflection) increases after the damage, which increases the measurability of post-damage deflections. When Table 3 is compared with the corresponding segments of Table 4, it is observed that it is more advantageous to shift response station 16 to the right for a crack on elements 1, 2, 16, and 17, and to the left for a crack on 4 and 5. Figure 20 clearly illustrates the case for a crack on girder 17. In the analysis which follows, response station is taken to be located to the right of the respective PNP since this is more advantageous for more elements. As mentioned earlier, if one transducer is mounted on each side of a PNP, the prospects of diagnosis are significantly improved. Similar computations and comparisons were carried out for crack locations on other beam elements. The results are summarized in Table 5 which shows the preferred directions of shift

AD-A172 732 STRUCTURE DYNAMIC THEORIES OF FRACTURE DIAGNOSIS(U) NEW 2/2
MEXICO UNIV ALBUQUERQUE DEPT OF MECHANICAL ENGINEERING
F D JU 03 MAR 86 ME-134(85)AFOSR-993-2 AFOSR-TR-86-0890
UNCLASSIFIED AFOSR-85-0085 F/G 20/11 NL

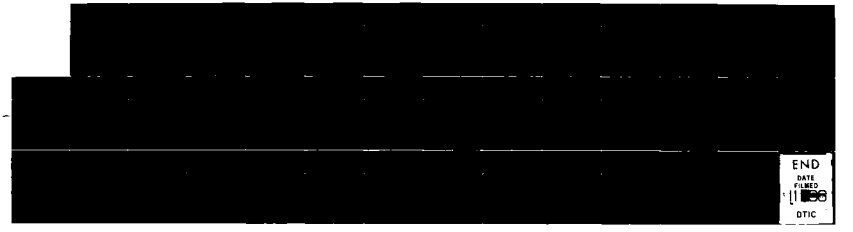

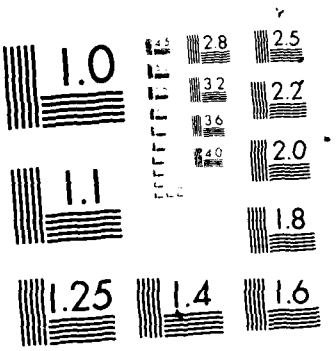

TABLE 4

Relative Transmissibility Changes vs Crack Location

Excitation on column 7 at a distance of .95, β_d = .96, δ = .01, Θ = .024.

Response Locations :

ξ_{16} = .618 ξ_{21} = .475 ξ_{24} = .649
ξ_{19} = .382 ξ_{22} = .525 ξ_{27} = .351

(ξ_c = crack location, RS : response station)

1) Crack on column 1

ξ_c	RS 16	RS 19	RS 21	RS 22	RS 24	RS 27
0.001	0.921	0.220	0.196	0.233	0.277	0.225
0.100	0.546	0.150	0.139	0.160	0.183	0.154
0.200	0.272	0.095	0.093	0.102	0.111	0.098
0.300	0.087	0.054	0.057	0.059	0.059	0.056
0.400	-0.019	0.025	0.031	0.028	0.023	0.027
0.500	-0.053	0.008	0.012	0.009	0.004	0.008
0.600	-0.018	0.000	0.001	0.001	-0.001	0.000
0.700	0.084	0.003	-0.002	0.002	0.008	0.002
0.800	0.253	0.015	0.001	0.014	0.032	0.014
0.900	0.491	0.037	0.011	0.035	0.069	0.036
0.999	0.801	0.068	0.027	0.066	0.121	0.067

2) Crack on column 2

ξ_c	RS 16	RS 19	RS 21	RS 22	RS 24	RS 27
0.001	0.565	0.051	0.074	0.051	-0.015	0.055
0.100	0.365	0.030	0.037	0.028	-0.000	0.032
0.200	0.208	0.014	0.013	0.013	0.008	0.015
0.300	0.092	0.005	0.000	0.003	0.008	0.005
0.400	0.014	0.000	-0.001	-0.000	0.002	0.000
0.500	-0.028	0.001	0.008	0.002	-0.010	0.001
0.600	-0.034	0.006	0.027	0.010	-0.029	0.007
0.700	-0.008	0.016	0.056	0.022	-0.054	0.017
0.800	0.054	0.029	0.093	0.038	-0.086	0.031
0.900	0.146	0.046	0.138	0.059	-0.125	0.049
0.999	0.286	0.065	0.191	0.082	-0.169	0.071

TABLE 4
(continued)

3) Crack on column 3

ξ_c	RS 16	RS 19	RS 21	RS 22	RS 24	RS 27
0.001	-0.031	0.007	0.043	0.012	0.134	0.006
0.100	-0.019	0.003	0.024	0.006	0.052	0.002
0.200	-0.008	0.001	0.010	0.002	0.008	0.000
0.300	0.000	0.000	-0.000	-0.000	0.000	0.000
0.400	0.006	0.001	-0.006	-0.000	0.024	0.001
0.500	0.011	0.002	-0.008	0.001	0.077	0.003
0.600	0.013	0.005	-0.007	0.003	0.153	0.005
0.700	0.013	0.008	-0.004	0.005	0.249	0.010
0.800	0.011	0.011	0.001	0.008	0.358	0.013
0.900	0.008	0.014	0.008	0.012	0.476	0.016
0.999	0.003	0.017	0.016	0.015	0.595	0.019

4) Crack on column 4

ξ_c	RS 16	RS 19	RS 21	RS 22	RS 24	RS 27
0.001	-0.653	0.285	0.477	0.367	0.267	0.308
0.100	-0.321	0.184	0.290	0.231	0.176	0.198
0.200	-0.104	0.109	0.157	0.132	0.107	0.116
0.300	0.020	0.057	0.068	0.064	0.058	0.059
0.400	0.067	0.022	0.017	0.022	0.025	0.023
0.500	0.046	0.004	-0.003	0.002	0.005	0.004
0.600	-0.041	0.000	0.007	0.003	-0.001	0.001
0.700	-0.194	0.011	0.048	0.024	0.005	0.014
0.800	-0.422	0.036	0.120	0.066	0.023	0.043
0.900	-0.736	0.077	0.227	0.132	0.054	0.090
0.999	-0.846	0.135	0.373	0.223	0.100	0.156

5) Crack on column 5

ξ_c	RS 16	RS 19	RS 21	RS 22	RS 24	RS 27
0.001	-0.987	0.147	-0.272	0.129	0.308	0.188
0.100	-0.650	0.086	-0.111	0.084	0.168	0.110
0.200	-0.392	0.043	-0.012	0.050	0.073	0.056
0.300	-0.201	0.016	0.033	0.025	0.017	0.021
0.400	-0.067	0.002	0.030	0.008	-0.004	0.003
0.500	0.019	0.001	-0.018	-0.002	0.006	0.001
0.600	0.057	0.011	-0.111	-0.006	0.047	0.013
0.700	0.050	0.032	-0.251	-0.005	0.118	0.040
0.800	-0.004	0.066	-0.444	0.001	0.223	0.081
0.900	-0.109	0.111	-0.694	0.012	0.362	0.138
0.999	-0.271	0.168	-0.974	0.029	0.539	0.211

TABLE 4
(continued)

6) Crack on column 6

ξ_c	RS 16	RS 19	RS 21	RS 22	RS 24	RS 27
0.001	0.106	0.036	-0.424	-0.017	-0.307	0.021
0.100	0.064	0.020	-0.274	-0.015	-0.141	0.012
0.200	0.034	0.009	-0.155	-0.011	-0.036	0.006
0.300	0.012	0.002	-0.064	-0.006	0.010	0.002
0.400	0.000	0.000	-0.001	-0.000	0.001	0.000
0.500	-0.004	0.001	0.036	0.007	-0.060	-0.001
0.600	-0.001	0.005	0.048	0.014	-0.168	-0.000
0.700	0.008	0.012	0.036	0.022	-0.320	0.001
0.800	0.023	0.021	0.003	0.029	-0.510	0.002
0.900	0.043	0.031	-0.051	0.035	-0.735	0.004
0.999	0.067	0.043	-0.122	0.041	-0.981	0.005

7) Crack on column 7

ξ_c	RS 16	RS 19	RS 21	RS 22	RS 24	RS 27
0.001	0.414	0.414	0.192	0.192	0.317	0.317
0.100	0.254	0.254	0.136	0.136	0.203	0.203
0.200	0.139	0.139	0.092	0.092	0.119	0.119
0.300	0.062	0.062	0.057	0.057	0.060	0.060
0.400	0.016	0.016	0.030	0.030	0.022	0.022
0.500	-0.002	-0.002	0.010	0.010	0.003	0.003
0.600	0.005	0.005	-0.004	-0.004	0.001	0.001
0.700	0.039	0.039	-0.013	-0.013	0.016	0.016
0.800	0.099	0.099	-0.017	-0.017	0.048	0.048
0.900	0.188	0.188	-0.016	-0.016	0.099	0.099
0.999	0.301	0.301	-0.012	-0.012	0.164	0.164

8) Crack on column 8

ξ_c	RS 16	RS 19	RS 21	RS 22	RS 24	RS 27
0.001	0.279	0.279	0.525	0.525	0.132	0.132
0.100	0.175	0.175	0.269	0.269	0.083	0.083
0.200	0.098	0.098	0.099	0.099	0.046	0.046
0.300	0.044	0.044	0.006	0.006	0.021	0.021
0.400	0.012	0.012	-0.020	-0.020	0.006	0.006
0.500	-0.002	-0.002	0.019	0.019	-0.001	-0.001
0.600	0.001	0.001	0.119	0.119	0.000	0.000
0.700	0.021	0.021	0.282	0.282	0.009	0.009
0.800	0.059	0.059	0.512	0.512	0.025	0.025
0.900	0.114	0.114	0.813	0.813	0.049	0.049
0.999	0.188	0.188	1.199	1.199	0.079	0.079

TABLE 4
(continued)

9) Crack on column 9

ξ_c	RS 16	RS 19	RS 21	RS 22	RS 24	RS 27
0.001	0.014	0.014	0.428	0.428	0.065	0.065
0.100	0.006	0.006	0.269	0.269	0.029	0.029
0.200	0.001	0.001	0.146	0.146	0.007	0.007
0.300	-0.001	-0.001	0.056	0.056	-0.002	-0.002
0.400	0.000	0.000	-0.002	-0.002	0.000	0.000
0.500	0.003	0.003	-0.030	-0.030	0.014	0.014
0.600	0.008	0.008	-0.032	-0.032	0.037	0.037
0.700	0.014	0.014	-0.008	-0.008	0.068	0.068
0.800	0.020	0.020	0.038	0.038	0.107	0.107
0.900	0.028	0.028	0.104	0.104	0.151	0.151
0.999	0.035	0.035	0.186	0.186	0.199	0.199

10) Crack on girder 16

ξ_c	RS 16	RS 19	RS 21	RS 22	RS 24	RS 27
0.001	3.230	0.279	0.255	0.273	0.211	0.288
0.100	1.399	0.173	0.174	0.175	0.126	0.180
0.200	0.241	0.097	0.112	0.102	0.065	0.101
0.300	-0.365	0.045	0.064	0.051	0.026	0.048
0.400	-0.501	0.014	0.030	0.019	0.004	0.015
0.500	-0.209	0.001	0.006	0.002	-0.002	0.001
0.600	0.506	0.005	-0.008	0.001	0.008	0.004
0.700	0.525	0.026	-0.012	0.014	0.033	0.024
0.800	0.247	0.066	-0.008	0.044	0.075	0.063
0.900	-0.754	0.127	0.007	0.091	0.137	0.123
0.999	1.799	0.212	0.032	0.159	0.222	0.207

11) Crack on girder 17

ξ_c	RS 16	RS 19	RS 21	RS 22	RS 24	RS 27
0.001	1.212	0.080	0.051	0.184	0.190	0.140
0.100	0.805	0.056	0.019	0.107	0.121	0.088
0.200	0.487	0.037	-0.002	0.051	0.069	0.049
0.300	0.251	0.021	-0.011	0.016	0.032	0.022
0.400	0.090	0.009	-0.010	-0.001	0.009	0.006
0.500	-0.003	-0.000	0.001	0.001	-0.000	-0.000
0.600	-0.029	-0.007	0.022	0.020	0.003	0.004
0.700	0.012	-0.010	0.054	0.057	0.020	0.019
0.800	0.123	-0.011	0.098	0.114	0.051	0.045
0.900	0.310	-0.009	0.155	0.193	0.097	0.083
0.999	0.580	-0.004	0.226	0.295	0.160	0.134

TABLE 4
(continued)

12) Crack on girder 20

ξ_c	RS 16	RS 19	RS 21	RS 22	RS 24	RS 27
0.001	0.239	0.123	0.456	0.170	0.348	0.123
0.100	0.168	0.080	0.240	0.102	0.250	0.081
0.200	0.110	0.047	0.089	0.053	0.168	0.048
0.300	0.064	0.023	-0.002	0.019	0.102	0.024
0.400	0.029	0.007	-0.036	0.001	0.049	0.008
0.500	0.005	0.000	-0.016	-0.002	0.009	0.001
0.600	-0.009	0.002	0.058	0.010	-0.019	0.001
0.700	-0.013	0.011	0.186	0.035	-0.035	0.009
0.800	-0.007	0.029	0.371	0.076	-0.039	0.025
0.900	0.009	0.055	0.618	0.133	-0.031	0.049
0.999	0.036	0.090	0.929	0.207	-0.012	0.082

13) Crack on girder 21

ξ_c	RS 16	RS 19	RS 21	RS 22	RS 24	RS 27
0.001	-0.037	0.084	0.091	-0.188	-0.129	0.094
0.100	-0.030	0.052	-0.833	-0.086	-0.094	0.056
0.200	-0.023	0.027	-0.003	-0.017	-0.064	0.029
0.300	-0.015	0.011	0.403	0.020	-0.038	0.010
0.400	-0.008	0.002	0.395	0.025	-0.017	0.000
0.500	0.000	0.000	-0.018	-0.001	0.001	0.000
0.600	0.008	0.006	-0.343	-0.059	0.014	0.009
0.700	0.017	0.019	-0.297	-0.149	0.023	0.027
0.800	0.026	0.040	0.125	-0.271	0.029	0.055
0.900	0.035	0.069	0.932	-0.425	0.029	0.092
0.999	0.044	0.106	2.127	-0.616	0.025	0.139

14) Crack on girder 24

ξ_c	RS 16	RS 19	RS 21	RS 22	RS 24	RS 27
0.001	0.003	0.017	0.016	0.015	0.592	0.019
0.100	0.001	0.011	0.015	0.011	0.223	0.012
0.200	-0.001	0.007	0.014	0.008	-0.031	0.006
0.300	-0.001	0.003	0.011	0.005	-0.166	0.002
0.400	-0.001	0.001	0.007	0.003	-0.181	-0.000
0.500	-0.001	0.000	0.002	0.001	-0.075	-0.000
0.600	0.001	0.000	-0.004	-0.001	0.150	0.001
0.700	0.003	0.002	-0.011	-0.002	0.325	0.005
0.800	0.007	0.004	-0.019	-0.002	0.150	0.011
0.900	0.011	0.008	-0.028	-0.003	-0.311	0.018
0.999	0.015	0.013	-0.038	-0.002	-0.957	0.027

TABLE 4
(continued)

15) Crack on girder 25

ξ_e	RS 16	RS 19	RS 21	RS 22	RS 24	RS 27
0.001	0.017	0.008	-0.022	0.020	0.454	-0.020
0.100	0.011	0.005	-0.018	0.010	0.317	-0.009
0.200	0.007	0.003	-0.015	0.003	0.201	-0.001
0.300	0.004	0.002	-0.010	-0.001	0.108	0.003
0.400	0.001	0.000	-0.005	-0.002	0.040	0.003
0.500	-0.000	-0.000	0.000	0.000	-0.002	-0.000
0.600	-0.000	0.000	0.007	0.006	-0.019	-0.008
0.700	0.001	0.001	0.013	0.014	-0.009	-0.020
0.800	0.003	0.002	0.020	0.025	0.026	-0.035
0.900	0.006	0.004	0.027	0.039	0.087	-0.053
0.999	0.011	0.006	0.034	0.056	0.171	-0.075

relative to the PNPs (to the left or to the right) for all the beam elements on the left half of the frame. The preferred direction of shift is indicated only when the cracked beam element is in the neighborhood of the response station in question. From Table 5, it is concluded that response stations 16 and 24 should be shifted to the right and station 21 to the left of the respective PNPs of the undamaged frame.

4.6. Development of the General Trends

In this section the transmissibility method will be developed with the 3x4 frame of Figure 17. The procedure used is to vary the location of a single crack of known sensitivity number throughout the frame, on each column and girder in turn, and to compute the relative transmissibility change at each one of the six response stations corresponding to each crack location. Trends of relative transmissibility changes as a function of the crack location are then established, which can serve as a diagnosis procedure in a practical situation wherein the crack location is unknown and the transmissibility changes are known from measured data.

4.6.1. Exciting the Frame at its Fundamental Frequency

Relative transmissibility changes computed for the frame excited at the fundamental frequency are shown in Table 4. Table 4 is arranged in 15 groups in each

TABLE 5

Direction of Shift of the Response Stations

(IND = No. of the beam element with the crack,

RS: Response Station,

R: Shift the response station to the right of the PNP,

L: Shift the response station to the left of the PNP.)

IND	RS		
	16	21	24
1,2,7,16,17	R	...	...
4,5	L	...	...
5,21	...	R	...
8,9,20	...	L	...
3,24,25	...	...	R
6	...	...	L

of which numerical data for a crack on a particular beam element is presented. Crack location in each group of data is varied from the lower (left) end of the element to the upper (right) end for a column (girder). Significant R_T values are shown framed in the table, "significance" being determined by the following criteria.

i) An R_T value whose magnitude is greater than 0.1 is considered significant.

ii) If all or most of the response stations indicate significant transmissibility changes for a certain crack location, but some of them indicate much larger changes than others, then only the larger R_T values are framed. Examples can be seen in data groups 1 and 4.

iii) If several response stations indicate significant and comparable transmissibility changes for a certain crack, the overall trend of transmissibility changes for that crack is considered insignificant. An example in Table 4 is the case of a crack on column 4 at a location of 0.2 from the ground. All of the R_T values for that crack have magnitudes between 0.10 and 0.16. Such a crack may be detectable, but is not diagnosable.

A crack is considered diagnosable if it can be located within one or two cells of the frame; that is, if the trend of R_T values for that crack is as described in (ii) above. Thus, the ranges of crack locations 0.-0.29 and 0.71-1. on column 1, and the ranges 0.-0.26 and 0.54-1. on column 6, for example, are diagnosable. The diagnosable regions of all the beam elements in Table 4 and the response stations exhibiting significant transmissibility changes in each one of those regions are summarized in Table 6. Also shown are the percentages of the lengths of the beam elements which are diagnosable. The following conclusions are drawn from Table 6.

i) The response station(s) closest to the crack exhibit the most significant transmissibility change(s) with the exception that stations 24 and 27 experience larger changes than stations 21 and 22 for a crack on column 7. However, since stations 16 and 19 exhibit the most significant changes, the diagnosability of a crack on 7 is unaffected. For a crack in region 0.91-0.92 of girder 16, the most significant changes, which are about 0.13, are experienced at stations 19, 24, and 27, which may cause a misdiagnosis.

ii) Beam elements with diagnosable regions larger than 75% are 5, 6, 16, 21, and 24, the last three of which have response stations on them. Both ends of the columns 5 and 6, on the other hand, adjoin the end of a girder with a response station. That is, column 5 is neighbors with girders 16 and 21, and column 6 is with 21 and 24.

iii) All of the regions near the joints are diagnosable, with the small exception of the region 0.-0.02 at the left end of girder 21. In that region, response station 22 exhibits the most significant transmissibility change which may cause a misdiagnosis.

iv) The mid-regions of all the elements, with the exception of those carrying a response station, are undiagnosable. At the fundamental frequency, these regions are usually regions of low stress or low resisting moment. Slope discontinuity in those regions is, therefore, small for a given crack depth (Section 2.3), which reduces the effect of the crack on the structural response.

TABLE 6

Summary of the Diagnosable Regions from Table 4

IND = no. of the beam element with the crack

DR = diagnosable region on the beam

RS = response station(s) exhibiting the most significant relative transmissibility change(s)

PD = total percentage of the beam length which is diagnosable

IND	DR	RS	PD(%)
1	.00 - .29 .71 - 1.0	16 16	58
2	.00 - .29 .85 - 1.0	16 16,21,24	44
3	.00 - .04 .53 - 1.0	24 24	51
4	.00 - .13 .64 - 1.0	16,21 16	49
5	.00 - .38 .59 - .67 .67 - 1.0	16 21 21,24	79
6	.00 - .14 .14 - .25 .50 - 1.0	21,24 21 24	76
7	.00 - .14 .80 - 1.0	16,19,24,27 16,19	34
8	.00 - .20 .58 - 1.0	21,22,16,19 21,22	82
9	.00 - .25 .78 - .89 .89 - 1.0	21,22 24,27 24,27,21,22	47
16	.00 - .21 .26 - .51 .54 - .79 .83 - .91 .91 - .92 .92 - 1.0	16 16 16 16 19,24,27 16	87
17	.00 - .39 .80 - .84 .84 - 1.0	16 16,22,21 16	59

TABLE 6
(continued)

IND	DR	RS	PD(%)
20	.00 - .14 .14 - .30 .63 - 1.0	21,24 24 21	67
21	.00 - .02 .02 - .03 .03 - .19 .22 - .47 .53 - .71 .71 - .74 .74 - .81 .81 - 1.0	22 22,21 21 21 21 21,22 22 21,22	91
24	.00 - .15 .25 - .47 .58 - .81 .85 - 1.0	24 24 24 24	75
25	.00 - .31 .92 - 1.0	24 24	39
Diagnosability for the whole frame = 62.7 % .			

The overall diagnosability of the frame excited at its fundamental frequency can be computed by adding all the percentages in Table 6, multiplying the sum by two, subtracting the percentages for 7 through 9 once and dividing the result by the total number of beam elements, 27. This yields a diagnosability for the whole frame of 62.7%. In other words, the mid-regions of all the beam elements which are undiagnosable make up the 37.3% of the total frame area.

4.6.2. Exciting the Frame at the Third Modal Frequency

The previous section indicated that mid-regions of the beam elements, which are regions of low resisting moment at the fundamental frequency, are undiagnosable. If the frame is excited at a higher modal frequency yielding different complex modal shapes and moment distributions, more segments of the frame become diagnosable. The PNPs and corresponding dimensionless deflections for the frame excited at the second and third modal frequencies are summarized in Table 7.

TABLE 7

PNPs at the Second and Third Modal Frequencies (undamaged frame)

Excitation on column 7 at .95

(Girders 19, 22, 27 are symmetrical with 16, 21, 24.)

β_d = 1.72			
girder no.	16	21	24
PNP location	.6765	.4798	.6441
$\|y^*\| \times 10^4$ at PNP	.52	3.2	3.4
β_d = 2.25			
girder no.	16	21	24
PNP location	.6091	.3265	.7174
$\|y^*\| \times 10^3$ at PNP	1.6	.72	1.2

It will be assumed that the response stations are at the same locations as in the previous section. Then, at the second modal frequency, the dimensionless deflections at the response stations on girders 21 and 24 are too small to be measurable (Part 1 of Table 7). This is a result of the fact that the PNPs at the first two modal frequencies are close to each other for both girders. The PNP of girder 16 at the second frequency, however, is relatively far from that at the fundamental frequency. The situation is reversed at the third modal frequency (Part 2 of Table 7). It is expected that exciting the frame at the third frequency will alter the modal shape more significantly than exciting it at the second frequency, thus making more additional regions of the frame diagnosable.

Computations similar to those of the previous section were carried out at the third modal frequency. Regions which become diagnosable in addition to those in Table 6 are presented in Table 8. Also shown are the regions which may, at the fundamental frequency, be misdiagnosed and are now diagnosable correctly at the third frequency. Those are the regions 0.-0.14 on column 7, 0.91-0.92 on girder 16,

and 0.-0.05 on girder 21. Table 8 indicates that the general trend established at the fundamental frequency is preserved to a large extent at the third frequency. That is, a crack affects the transmissibility at the closest response station the most. Exceptions are for the cases of a crack on elements 3 and 24, in which station 16 exhibits the most significant transmissibility changes for the regions shown, rather

TABLE 8

Additional Diagnosable Regions at the Third Modal Frequency

All of the parameters same as in Table 4 except β_d=2.25.

Nomenclature same as in Table 6 with prefix A denoting additional

IND	ADR	RS	APD(%)
1	.47 - .71	16	24
2	.29 - .47 .55 - .73 .78 - .85	16 16 16	43
3	.04 - .51	16	47
4	.13 - .29 .47 - .64	16 16	33
5	.38 - .47 .51 - .59	16 16	17
6	.26 - .41	21	15
7	.00 - .14* .63 - .80	16,19 16,19	17
8	.20 - .29 .56 - .58	16,19 21,22	11
9	.25 - .47	21,22	22
16	.23 - .26 .51 - .52 .79 - .81 .91 - .92*	16 16 16 16	6
21	.00 - .03*	21	...
24	.15 - .25	16	10
17,20,25	APD less than 1%		

* (not included in APD)

than station 24. This is not surprising since station 16 is much closer to the PNP of girder 16 at the third frequency than station 24 is to that of girder 24. On the other hand, it is expected that more additional regions on girder 20, for example, would be diagnosable if station 21 were closer to the PNP of girder 21 at the third frequency.

With the addition of the new diagnosable regions, the diagnosability for the whole frame now becomes 79%, with the diagnosability of the beam elements 7, 8, 9, 17, 18, 20, 23, 25, and 26 remaining below the average. It is also expected that if the criterion stated in Section 4 is fully obeyed in the selection of the beam elements for the response stations, the diagnosability of the structure will increase. According to that criterion, girders 18, 23, and 26 would carry the response stations rather than 19, 22, and 27, respectively.

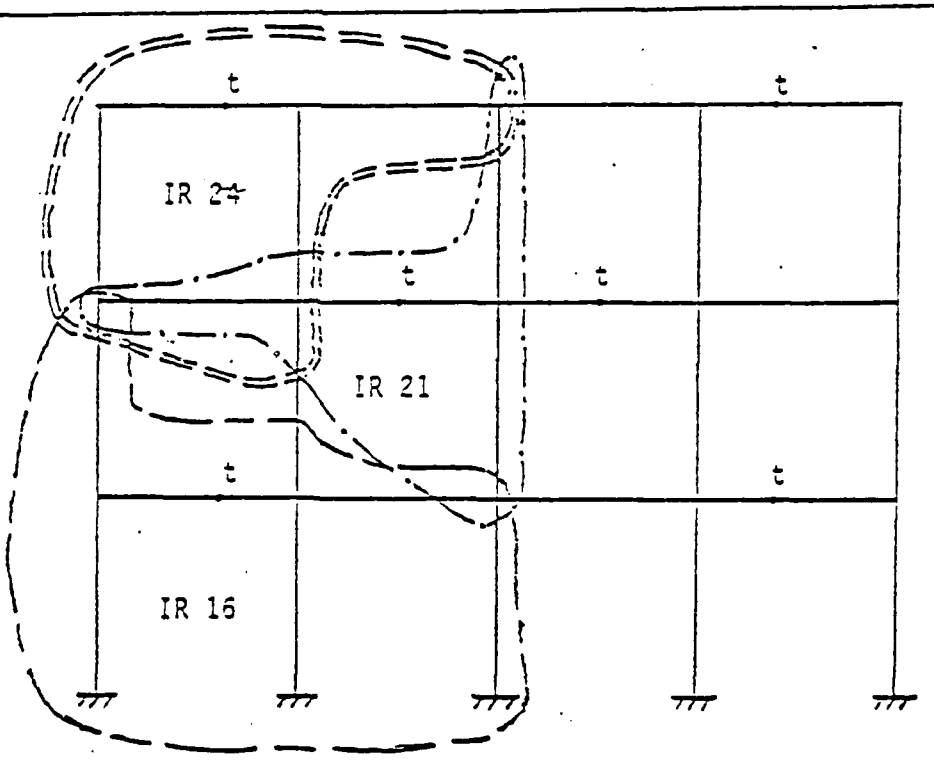

Figure 29. Influence regions on the frame.

The general trends established above are presented in the form of "influence regions" in Figure 29. Influence region of a response station is defined as the region in whose diagnosability the station in question plays the most influential role. In other words, a crack in that region affects the transmissibility at that particular station the most.

4.7. The Effect of Crack Severity on the Trends

The previous computations were carried out for a crack of sensitivity number Θ=0.024 (Eq. 2.40). For beams with slenderness ratios (length to beam-depth ratio) of 10 and 20 and for a Poisson's ratio of 0.3, this Θ corresponds to the relative crack depths of 0.3 and 0.4, respectively. Numerical results show that changing Θ does not have significant effects on the trends. Only the transmissibility changes are reduced or amplified depending on whether Θ is decreased or increased, respectively. As Θ gets smaller (or as the crack gets shallower), however, the diagnosable regions of the beam elements are squeezed toward the frame joints, thereby reducing the diagnosability of the frame. To illustrate the effect, diagnosable regions on beam elements 3, 6, 20, and 24 at the fundamental frequency are computed for a crack of Θ=0.005 and presented in Table 9. This Θ corresponds to the relative crack depths of 0.14 an 0.20 for beams with slenderness ratios of 10 and 20, respectively.

Two different sets of response locations are used in generating Table 9. One set(group 1 of the table) is the same as that used previously. In the second set(group 2), the response stations are moved closer to the PNPs. In both cases, diagnosable regions of the beam elements studied are smaller than those for a crack with Θ=0.024. However, when the response stations move closer to the PNPs, the diagnosability increases significantly. For a crack with Θ=0.001, corresponding to the relative crack depths of 0.062 and 0.088 for slenderness ratios of 10 and 20, no segments of the elements 3, 6, 20, or 24 are diagnosable when the response stations are at the locations given in Table 9. In conclusion, if smaller deflections can be placed closer to the PNPs, larger regions become diagnosable.

TABLE 9

Diagnosable Regions for a Crack with Θ=.005

(Nomenclature same as in Table 8)

1) Parameter values same as in Table 8 except for Θ

IND	DR	RS	PD(%)
3	.90 - 1.0	24	10
6	.78 - 1.0	24	22
20	.84 - 1.0	21	16
24	.92 - 1.0	24	8

2) Parameter values same as in (1) except for the response locations

$\xi_{18} = .613$ $\xi_{21} = .483$ $\xi_{24} = .634$
$\xi_{19} = .387$ $\xi_{22} = .517$ $\xi_{27} = .366$

IND	DR	RS	PD(%)
3	.70 - 1.0	24	30
6	.00 - .12 .67 - 1.0	21 24	45
20	.00 - .08 .72 - 1.0	21,24 21	36
24	.00 - .09 .68 - .74 .88 - 1.0	24 24 24	27

4.8. The Effect of Damping on the Trends

As the damping factor, δ, is increased, the amplitudes of deflections, $|y^*|$, and, therefore, the transmissibilities are reduced. Table 10 lists four groups of relative-transmissibility-change data for a δ value of 0.10. Other parameters are kept the same as in Table 4 which contains data for δ=0.01. The comparison of Table 10 with the corresponding data groups in Table 4 yields the following conclusions:

i) Positive R_T values are invariably reduced as δ increases. An example is the case of a crack on girder 20. Although all of the responses are influenced in this case,

TABLE 10

Relative Transmissibility Changes vs Crack Location

Excitation on column 7 at a distance of .95, β_d = .96, δ = .10, Θ = .024.

Response Locations :

ξ_{16} = .618 ξ_{21} = .475 ξ_{24} = .649
ξ_{19} = .382 ξ_{22} = .525 ξ_{27} = .351

(ξ_c = crack location, RS : response station)

1) Crack on column 3

ξ_c	RS 16	RS 19	RS 21	RS 22	RS 24	RS 27
0.001	-0.037	0.001	0.036	0.006	0.127	-0.001
0.100	-0.021	0.000	0.021	0.003	0.049	-0.001
0.200	-0.009	0.000	0.009	0.001	0.008	-0.000
0.300	0.000	0.000	-0.000	-0.000	0.000	0.000
0.400	0.006	0.000	-0.006	-0.001	0.024	0.001
0.500	0.009	0.000	-0.010	-0.001	0.074	0.001
0.600	0.009	0.001	-0.011	-0.002	0.148	0.002
0.700	0.006	0.001	-0.011	-0.001	0.240	0.003
0.800	0.002	0.001	-0.008	-0.001	0.345	0.004
0.900	-0.004	0.002	-0.004	-0.000	0.457	0.004
0.999	-0.011	0.002	0.001	0.000	0.571	0.005

2) Crack on column 6

ξ_c	RS 16	RS 19	RS 21	RS 22	RS 24	RS 27
0.001	0.074	0.007	-0.429	-0.044	-0.325	-0.008
0.100	0.048	0.004	-0.280	-0.030	-0.153	-0.003
0.200	0.027	0.002	-0.158	-0.018	-0.042	-0.000
0.300	0.011	0.001	-0.065	-0.008	0.008	0.001
0.400	0.000	0.000	-0.001	-0.000	0.001	0.000
0.500	-0.005	-0.000	0.034	0.005	-0.061	-0.002
0.600	-0.006	0.000	0.042	0.009	-0.171	-0.006
0.700	-0.003	0.001	0.024	0.010	-0.325	-0.010
0.800	0.005	0.002	-0.015	0.010	-0.513	-0.016
0.900	0.015	0.004	-0.075	0.008	-0.725	-0.023
0.999	0.029	0.006	-0.150	0.004	-0.883	-0.030

TABLE 10
(continued)

3) Crack on girder 20

ξ_c	RS 18	RS 19	RS 21	RS 22	RS 24	RS 27
0.001	0.115	0.010	0.306	0.052	0.212	0.011
0.100	0.089	0.007	0.155	0.028	0.166	0.008
0.200	0.065	0.005	0.045	0.010	0.121	0.006
0.300	0.043	0.003	-0.021	-0.001	0.080	0.004
0.400	0.023	0.001	-0.041	-0.005	0.042	0.002
0.500	0.005	0.000	-0.016	-0.002	0.009	0.000
0.600	-0.011	-0.000	0.055	0.007	-0.020	-0.001
0.700	-0.023	-0.000	0.171	0.024	-0.045	-0.002
0.800	-0.034	0.001	0.330	0.047	-0.064	-0.003
0.900	-0.041	0.002	0.531	0.076	-0.079	-0.003
0.999	-0.046	0.004	0.768	0.110	-0.089	-0.003

4) Crack on girder 24

ξ_c	RS 16	RS 19	RS 21	RS 22	RS 24	RS 27
0.001	-0.011	0.002	0.001	0.000	0.568	0.005
0.100	-0.009	0.002	0.005	0.001	0.211	0.002
0.200	-0.006	0.001	0.008	0.002	-0.037	-0.000
0.300	-0.004	0.000	0.008	0.002	-0.168	-0.001
0.400	-0.002	0.000	0.006	0.002	-0.181	-0.001
0.500	-0.001	-0.000	0.002	0.001	-0.075	-0.001
0.600	0.001	0.000	-0.004	-0.001	0.149	0.001
0.700	0.002	0.000	-0.012	-0.003	0.323	0.004
0.800	0.003	0.001	-0.022	-0.006	0.146	0.007
0.900	0.004	0.002	-0.034	-0.009	-0.313	0.011
0.999	0.005	0.003	-0.047	-0.012	-0.872	0.015

the most adversely affected transmissibility changes are those at the stations 19 and 27, the farthest two stations from the cracked girder, which were reduced to near zero values. The stations near the crack are not affected so significantly. Example: the case of a crack on girder 24.

ii) Negative R_T values are affected less by an increase in δ. The magnitude of a negative transmissibility change can be amplified or reduced, both not very significantly. Example: R_T values at station 24 for a crack on beam elements 6 and

20.

The diagnosable regions with δ=0.10 are computed and presented in Table 13. When these regions are compared with the corresponding data in Table 6, it is observed that an increase in the damping factor from 0.01 to 0.10 leaves the trends essentially unaffected and reduces the diagnosable regions slightly (between 0 to 6 percentage points for the cases presented in Table 11).

4.9. A Response Station on a Column

At the fundamental frequency, the transmissibility change on a column for a given crack is found to be almost independent of the response location on that column. Relative transmissibility changes at a response station on column 8 for a crack on various beam elements are shown in Table 12. In this example, the excitation is on column 1. Only one crack location on each beam is considered. Beams are grouped based on the closeness of the corresponding R_T values. For example, R_T values for a crack at a location of 0.15 on each of the beams 1, 7, 13 and 16 range from 0.125 to 0.150. The R_T value for a particular crack is nearly the same regardless of where the response station is located on column 8. That nearly constant value for the crack on column 7, for example, is 0.15. Furthermore, the transmissibility changes at a station on column 9 are very close to those on column 8, as well as being nearly constant along the length of column 9.

Table 12 indicates that as the crack is moved to upper levels on the frame, the R_T value on column 8 decreases. There is especially a significant decrease from the first level to the second(Fig. 17). The overall R_T values, however, are not very large. A transducer on a column may, nevertheless, help in diagnosis by differentiating between a crack on the first level and on the upper levels.

4.10. Effect of the Crack Model on the Transmissibility Method

In this study, a Mode-I crack has been modeled as a torsional spring. The crack surface has been assumed to be perpendicular to the neutral axis of the beam

TABLE 11

Diagnosable Regions for a Frame with Heavier Damping

Parameter values same as in Table 6 except $\delta = .10$

Nomenclature same as in Table 8.

IND	DR	RS	PD(%)
3	.00 - .03 .54 - 1.0	24 24	49
8	.00 - .26 .54 - 1.0	21 24	72
20	.00 - .15 .15 - .25 .64 - 1.0	21,24 24 21	61
24	.00 - .14 .25 - .48 .58 - .81 .85 - 1.0	24 24 24 24	75

TABLE 12

Relative Transmissibility Changes at a Response Station on Column 8

δ=.01, excitation on column 1 at .95, β_d = .96

Θ = .024, crack location is .15 on all the beam elements

IND = no. of the beam element with the crack

R_T = relative transmissibility change

IND	1,7,13,16	5,11	20,21,23	6,9	24,25,26	15
R_T	.125 - .150	.069	.034 - .060	.010 - .011	.004 - .008	.002

element on which the crack is located. It can be shown, however, that the trends of relative transmissibility changes are independent of the crack model as long as the crack introduces a reduction in the flexural rigidity of the beam. To this end, a one-story four-span frame excited at the mid-column is analyzed (Figure 30). The fundamental characteristic value of such a uniform frame is 1.687. In the

computations, the frame is excited at a β_d value of 1.68. Damping factor is taken to be 0.01. Two response stations are placed on girders 6 and 8 at the locations 0.69 and 0.56, respectively. (PNPs of these girders for a uniform frame are at 0.681 and 0.551, respectively, when the excitation is on column 3 at a distance of 0.95 from the ground.)

First, the relative transmissibility changes at the two stations of the uniform frame were computed for a crack of Θ=0.01 on girder 9, as the crack location was varied along the girder. It was observed that the station on girder 8 exhibited much more significant transmissibility changes except when the crack was in the mid-region of girder 9. In the latter case, both transmissibility changes were small. Next, the length of girder 9 was assumed to be 20% longer than the lengths of the other columns and girders, which made the former less rigid than the others and qualitatively simulated a crack. With the other parameters kept the same, the transmissibility changes at the two stations relative to the transmissibilities across the undamaged uniform frame were computed. The relative transmissibility changes due to the lengthening of girder 9 were found to be -0.41 and 0.88 at stations 6 and 8, respectively. As the result indicates, softening in a region of a frame structure affects the response at the nearest station the most.

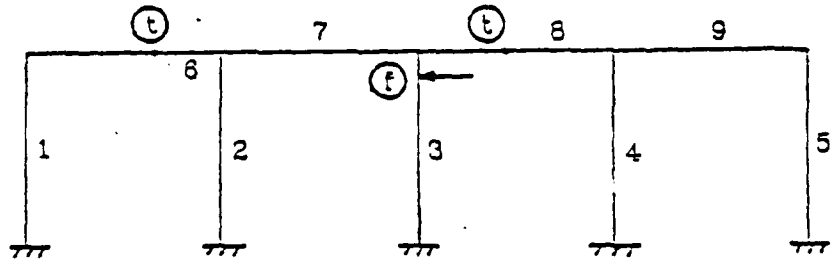

Figure 30. A one-story four-span frame.

CHAPTER 5

Discussion and Conclusions

Nondestructive testing of large-scale structures is still in its infancy. Local methods currently used require a sweeping of the whole structure and can become costly and time-consuming. A global method whereby a structure can be continually monitored and damage can be isolated at least within a section of the structure is needed. Such a method, the transmissibility method, is proposed in this study. The transmissibility method, which is based on the relative transmissibility changes at various response stations, isolates a crack to within one or two cells of a frame structure after which a local method may be used to pinpoint the crack. In the study, the effects of excitation location and frequency, location of response stations, crack location and severity, and damping on the relative transmissibility changes are investigated. General trends of the values of transmissibility changes as a function of these factors are established. In practice, these trends can be used for locating a crack, given the transmissibility changes. The following conclusions are reached from the transmissibility analysis:

i) The most significant transmissibility change is usually observed at a response station in the neighborhood of the crack.

ii) The trends as stated in (i) are highly insensitive to the excitation location.

iii) The trends are insensitive to the crack depth and material properties such as damping.

iv) The trends are highly insensitive to the location of the response stations when the stations are in the vicinity of the PNPs. Trends, however, are lost away from the PNPs, in which case damage may be detected but cannot be located. On the other hand, the closer the response stations to the PNPs, the larger are the transmissibility

changes and the chances of diagnosing a crack.

v) Amplitude of deflections and accelerations are small near the PNPs. Therefore, how close the response stations can be located to the PNPs depends on the signal levels which can be measured.

vi) Cracks at or near the joints of a frame are most easily diagnosable. A crack located away from the joints, in the mid-regions of the beam elements, may not be diagnosable.

vii) Diagnosability of a crack increases if transmissibility data is available at more than one resonant frequency.

Conclusion (vi) is especially encouraging in the light of the fact that structures such as offshore platforms usually fail at the foundation or develop cracks at the welded joints.

The electrical analogy method as developed for frame structures in this study provides an economical test for the analysis of large structures. The responses computed with the analogy are exact insofar as Bernoulli-Euler theory is exact. The structures analyzed in the study are assumed rigidly fixed at the ground level. In the case of non-rigid foundations, foundation flexibility can be accounted for by inserting resistances in the electrical circuit at points corresponding to the anchors[34, pp. 82-85].

The other nondestructive method of damage diagnosis investigated in this study is the frequency method. In complex structures, the changes in modal frequencies due to a crack are small. Therefore, the frequency method is not suitable for such structures. For simple structures such as beams, however, it is a feasible method.

It is shown in the study that closely spaced multiple cracks can be effectively represented by a single crack for which the sensitivity number, Θ, is approximately equal to the sum of the individual sensitivity numbers. Uncertainty exists, however, in diagnosing such a damage as to whether there is only one major crack or several closely spaced minor cracks. Nevertheless, location of the damage can be identified

quite accurately.

In the case of a structure with several cracks, only one of which is severe, it is possible to diagnose the major crack. The contributions of minor cracks to frequency decreases is small compared to that of the severe crack. The relative frequency changes, R_j, in such a situation, exhibit a trend similar to that which would be observed were the major crack the only crack present on the structure. If there is more than one major crack, not closely spaced, on the structure, it is, in general, not possible to diagnose deterministically the damage with only a few R_j values known.

In the frequency method, curves of relative frequency changes, R_j, versus crack location yield valuable information regarding damage diagnosis. It may be possible to estimate damage location, provided there is only one major crack, by only looking at the relative magnitudes of frequency decreases and using the relative-change curves.

In diagnosing damage in a structure using the frequency method, given three post-damage characteristic values, β, the solution is sought for a single crack since there are not enough equations to solve for a large number of cracks. In solving for a single crack (i.e. for e_{eq} and β_{eq}), two measured β values are actually used first. The third measured β value is then compared with the computed counterpart which would be produced by the crack with the characteristic pair (e_{eq} , Θ_{eq}). It is shown that the two β values may not match closely even though the diagnosis is accurate (that is, e_{eq} and Θ_{eq} identify the major crack correctly), the discrepancy possibly being due to the presence of other minor cracks. If the discrepancy is large, then the solution is rejected with the conclusion that there is more than one major crack. On the other hand, the choice of the pair of measured β values to be used in computing e_{eq} and Θ_{eq} may affect the diagnosis. In some cases, choosing the two characteristic values which correspond to the largest two R_j values leads to the correct diagnosis. It is not clear, however, whether there is a right choice in each case.

REFERENCES

[1] Betz, C.E., "A History of Nondestructive Testing: The Magnaflux Corporation," *Materials Evaluation*, 34, 1976, p. 18A.

[2] *ASME B & PV Code*, 1983, Section XI, Division 1, IO-I2.

[3] Rose, J.L., Fuller, M.C., Nestleroth, J.B., Jeong, Y.H., "An Ultrasonic Global Inspection Technique for an Offshore K-Joint," *Society of Petroleum Engineers Journal*, 23, 1983, 358-364.

[4] Fuller, M.D., Nestleroth, J.B., Rose, J.L., "A Proposed Ultrasonic Inspection Technique for Offshore Structures," *Materials Evaluation*, 41, 1983, 571-578.

[5] Yang, J.C.S., Chen, J., Dagalakis, N.G., "Damage Detection in Offshore Structures by the Random Decrement Technique", *J. Energy Resources Technology*, Trans. ASME, 106, 1984,38-42.

[6] Tsai, T., Yang, J.C.S., Chen, R.Z., "Detection of Damages in Structures by the Cross Random Decrement Method," *Proc. 3rd International Modal Analysis Conf.*, Orlando, Florida, 1985, V.II, 691-700.

[7] Ju, F.D., Akgun, M., Wong, E.T., Paez, T.L., "Modal Method in Diagnosis of Fracture Damage in Simple Structures," ASME 103rd Winter Annual Meeting, 1982, Phoenix, AZ, *Productive Applications of Mechanical Vibrations*, ASME Publication, 1982, 113-125.

[8] Ju, F.D., Akgun, M., Paez, T.L., Wong, E.T., *Diagnosis of Fracture Damage in Simple Structures*, AFOSR Scientific Repot, AFOSR-TR-83-0049, Nov. 1982.

[9] Akgun, M., Ju, F.D. and Paez, T.L., "Fracture Diagnosis in Beam Frame Structures Using Circuit Analogy," *Recent Advances in Engrg. Mech.*, V.2, 1983, 767-769.

[10] Akgun, M., Ju, F.D. and Paez, T.L., "Fracture Diagnosis in Structures Using Circuit Analogy," *Proc. Interact. of Non-nuclear Muni. with Struc.*, 1983, 146-150.

[11] Akgun, M., Ju, F.D. and Paez, T.L., "A General Theory of Circuit Analogy in Fracture Diagnosis," *AFOSR Scientific Report*, AFOSR-TR-84-0910, Mar. 1984.

[12] Ju, F.D., "Multiple Fracture Diagnosis in Simple Beams," *ASCE Fall Convention, Appl. Fract. Session*, San Francisco, CA, Oct. 1-5, 1984.

[13] Akgun, M., Ju, F.D. and Paez, T.L., "Transmissibility as a Means to Diagnose Damage in Structures," *Proc. 3rd International Modal Anal. Conf.*, V.II, IMAC, Jan. 1985, 701-707.

[14] Akgun, M. and Ju, F.D., "Transmissibility Method in Structural Fracture Diagnosis," *Proc. 2nd Symp. on Interact. of Non-nucl. Muni. with Struct.*, Apr. 1985, Panama City, FL, 127-131.

[15] Liebowitz, H., "Fracture and Carrying Capacity of Notched Columns," *Fracture*, ed., H. Liebowitz, Academic Press, V.IV, 1969, 113-171.

[16] Bennett, J.G., Ju, F.D., Anderson, C.A., *An Investigation of Failure Mechanisms for HTGR (High Temperature Gas-Cooled Reactor) Core Supports*, LASL Report LA-NUREG-8639-MS, Dec. 1976.

[17] Ju, F.D., Bennett, J.G., Anderson, C.A., "Structural Safety Analysis of HTGR Core Supports," *Advances in Civil Engineering through Engineering Mechanics*, Proc. 2nd EMD Specialty Conference, ASCE, 1977, 427-430.

[18] Hart, G.D., Huang, S., "The Good News of Full-Scale Testing," ASME 103rd Winter Annual Meeting, 1982 Phoenix, AZ, *Productive Applications of Mechanical Vibrations*, ASME publication, 1982, 127-135.

[19] Hetenyi, M., "Deflection of Beams of Varying Cross Section," *J. Appl. Mech.*, 4, 1937, A-49 - A-52.

[20] Thomson, W.T., "Vibration of Slender Bars With Discontinuities in Stiffness," *J. Appl. Mech.*, 16, 1949, 203-207.

[21] Kirmser, P.G., "Effect of Discontinuities on the Natural Frequency of Beams," *Proc. of the American Soc. for Testing and Materials*, 44, 1944, 897-904.

[22] Sato, H., "Free Vibration of Beams With Abrupt Changes of Cross-Section," *J. Sound and Vib.*, 89, 1983, 59-64.

[23] Petroski, H.J., Glazik, J.L., "Effects of Cracks on the Response of Circular Cylindrical Shells," *Nuclear Technology*, 51, 1983, 303-316.

[24] Petroski, H.J., "Simple Static and Dynamic Models for the Cracked Elastic Beam," *Int. J. Fracture*, 17, 1981, R71-R76.

[25] Chondros, T.G., Dimarogonas, A.D., "Identification of Cracks in Welded Joints of Complex Structures," *J. Sound Vib.*, 69, 1980, 531-538.

[26] Gudmundson, P., "Eigenfrequency Changes of Structures Due to Cracks, Notches or Other Geometrical Changes," *J. Mechanics and Physics of Solids*, 30, 1982, 339-353.

[27] Gudmundson, P., "The Dynamic Behavior of Slender Structures With Cross-Sectional Cracks," *J. Mechanics and Physics of Solids*, 31, 1983, 329-345.

[28] Ju, F.D. and Mimovich, M., "Modal Frequency Method in Diagnosis of Fracture Damage in Structures," *4th International Modal Analysis Conference*, Feb. 2-6, 1986, Los Angels.

[29] Keorpyan, K.K., Chegolin, P.M., *Electrical Analogues in Structural Engineering*, 1963. First English Translation, Edward Arnold (Publishers) Ltd., 1967.

[30] Lazan, B.J., *Damping of Materials and Members in Structural Mechanics*, Pergamon Press, 1968, 12,27,38,57.

[31] Snowdon, J.C., *Vibration and Shock in Damped Mechanical Systems*, Wiley, 1968, 3-6.

[32] Clough, R.W., Penzien, J., *Dynamics of Structures*, McGraw-Hill, 1975, 301-302.

[33] Blevins, R.D., *Formulas for Natural Frequency and Mode Shape*, Van Nostrand Reinhold Company, 1979, 179.

APPENDIX

The Program to Compute Dimensionless Deflections in a Frame

```
      SUBROUTINE TRANS(N,M,K,ES,EC,THE,IND,IE,XE,IT,XT,NT,BUN,DAM,
     *                 U,X,XTR,Z,RH,IUR,IXR,WA,WK,IWK)
C
      COMPLEX*16  U(IUR,IUR), XTR(IUR,IXR), Z(IXR,IXR), X(IXR,IUR),
     *            RH(IXR), WA(1), DCMPLX, CDSIN, CDCOS, CDEXP,
     *            B, BI, W, WP, Q, QP, P, PP, EXP1, EXP2, ALF
      REAL*8  XT(NT), ES(1), EC(1), THE(1), WK(1), XE, BUN, DAM, D1, D2, D3, D4
      INTEGER  IT(NT), IWK(1), IND(1), N, M, K, IE, NT, IUR, IXR
C ***************************************************************************
C THIS SUBROUTINE COMPUTES THE DIMENSIONLESS COMPLEX DEFLECTIONS
C AT SELECTED LOCATIONS ON AN NxM PLANAR FRAME STRUCTURE WITH OR
C WITHOUT CRACKS EXCITED AT AN ARBITRARY LOCATION BY A SINUSOIDAL
C FORCE. THE FRAME IS ASSUMED TO HAVE UNIFORM PROPERTIES EXCEPT
C FOR THE FLOOR HEIGHTS AND SPAN WIDTHS. THE BEAM ELEMENTS
C COMPOSING THE FRAME ARE NUMBERED AS EXPLAINED IN SECTION 2.4.
C THE FRAME IS SIMULATED BY Π CIRCUITS.
C
C WRITTEN BY MEHMET A. AKGUN
C DATE LAST REVISED :  APRIL 1985
C
C INPUT :  (ALL OF THE INPUT VARIABLES ARE PRESERVED)
C
C  N     NUMBER OF STORIES OF THE FRAME.
C  M     NUMBER OF SPANS OF THE FRAME (NO. OF ANCHORS - 1).
C  K     NUMBER OF CRACKS ON THE FRAME (ZERO FOR NO-CRACK CASE).
C  ES    A VECTOR OF LENGTH N+M. THE FIRST N LOCATIONS SHOULD CONTAIN
C        THE RELATIVE FLOOR HEIGHTS, L_i / L_c, IN THE ORDER FROM GROUND
C        UP, WHERE L_c IS THE REFERENCE LENGTH CHOSEN FOR THE FRAME AND
C        L_i IS THE HEIGHT OF THE i-th FLOOR. THE LAST M LOCATIONS
C        SHOULD CONTAIN THE RELATIVE SPAN WIDTHS, L_j / L_c, IN THE ORDER
C        FROM LEFT TO RIGHT, WHERE L_j IS THE WIDTH OF THE j-th SPAN.
C  EC    A VECTOR OF LENGTH MAX(1,K) CONTAINING THE RELATIVE CRACK
C        LOCATIONS, LC_i / L_j, WHERE L_j IS THE LENGTH OF THE j-th
C        BEAM ELEMENT WHICH CARRIES THE i-th CRACK. WHEN THE i-th CRACK
C        IS THE ONLY CRACK OR THE FIRST ONE OF A GROUP OF CRACKS ON
C        THE j-th ELEMENT, THE DISTANCE LC_i OF THE CRACK IS MEASURED
C        FROM THE LEFT(LOWER) END OF THE GIRDER(COLUMN) ON WHICH THE
```

```
C          CRACK IS LOCATED. OTHERWISE, LC(I) IS THE DISTANCE BETWEEN THE
C          (I-1)th AND Ith CRACKS. THE ORDERING OF THE CRACK LOCATIONS
C          WITHIN EC SHOULD FOLLOW THE NUMBERING SCHEME EXPLAINED IN
C          SECTION 2.4. NAMELY, FIRST THE LOCATIONS OF THE COLUMN CRACKS,
C          THEN THOSE OF THE GIRDER CRACKS SHOULD BE WRITTEN.
C          0 < EC(I) < 1. EC IS IGNORED WHEN K=0.
C     THE  A VECTOR OF LENGTH MAX(1,K) CONTAINING THE SENSITIVITY
C          NUMBERS, Θ, OF THE CRACKS IN THE SAME ORDER AS EC.
C          THE(I) ≠ 0 for 1 ≤ I ≤ K. IGNORED WHEN K=0.
C     IND  A VECTOR OF LENGTH MAX(1,K) CONTAINING THE NUMBERS OF THE
C          BEAM ELEMENTS ON WHICH THE CRACKS ARE LOCATED, ORDERED IN
C          CORRESPONDENCE WITH EC. IND(1) ≤ IND(2) ≤ ... ≤ IND(K).
C     IE   THE NUMBER OF THE BEAM ELEMENT ON WHICH THE EXCITATION IS
C          APPLIED.
C     XE   THE RELATIVE LOCATION OF THE EXCITATION, LE/L(IE), WHERE LE
C          IS THE DISTANCE TO THE EXCITATION FROM THE LEFT(LOWER) END
C          OF THE GIRDER(COLUMN) ON WHICH THE EXCITATION IS APPLIED.
C          L(IE) IS THE LENGTH OF THAT GIRDER(COLUMN). 0 < XE < 1 .
C     NT   TOTAL NUMBER OF RESPONSE STATIONS ON THE FRAME.
C     IT   A VECTOR OF LENGTH NT CONTAINING THE NUMBERS OF THE BEAM
C          ELEMENTS WHICH HAVE A RESPONSE STATION ON THEM. ONLY ONE
C          RESPONSE STATION PER BEAM ELEMENT IS ALLOWED.
C          IT(1) < IT(2) < ... < IT(NT).
C     XT   A VECTOR OF LENGTH NT CONTAINING THE RELATIVE LOCATIONS,
C          LT(J)/L(IT(J)), OF THE RESPONSE STATIONS ON THE
C          CORRESPONDING BEAM ELEMENTS, WHERE L(IT(J)) IS THE LENGTH
C          OF THE PARTICULAR BEAM ELEMENT.
C     BUN  UNDAMPED BETA VALUE.
C     DAM  DAMPING FACTOR.
C     IUR  N*(M+1) + 2*K + NT + 1. THE ORDER OF MATRIX U.
C     IXR  N + K + NT + 1. THE ORDER OF MATRIX Z.
C
C OUTPUT:
C
C     RH   A COMPLEX VECTOR OF LENGTH IXR CONTAINING THE NONDIMENSIONAL
C          TRANSVERSE DEFLECTIONS, y*. THE FIRST N LOCATIONS CONTAIN THE
C          LATERAL DISPLACEMENTS OF THE N FLOORS, ORDERED FROM THE FIRST
```

```
C       FLOOR UP. THE NEXT K LOCATIONS CONTAIN THE DEFLECTIONS AT THE
C       CRACKS, ORDERED IN ACCORDANCE WITH EC. THE DEFLECTIONS AT THE
C       RESPONSE STATIONS ARE CONTAINED IN THE NEXT NT LOCATIONS. THE
C       LAST LOCATION CONTAINS THE DEFLECTION AT THE EXCITATION POINT.
C       THE CHANGES IN TRANSMISSIBILITIES CAN BE OBTAINED BY COMPUTING
C       THE AMPLITUDES OF DEFLECTIONS AT THE RESPONSE STATIONS WITH
C       AND WITHOUT THE CRACK(S).
C
C WORK ARRAYS:
C
C  U    A COMPLEX ARRAY OF ORDER  IUR X IUR.
C  X    A COMPLEX ARRAY OF ORDER  IXR X IUR.
C  XTR  A COMPLEX ARRAY OF ORDER  IUR X IXR.
C  Z    A COMPLEX ARRAY OF ORDER  IXR X IXR.
C  WA   A COMPLEX VECTOR OF LENGTH IUR*(IUR + 2).
C  WK   A REAL VECTOR OF LENGTH  IUR.
C  IWK  AN INTEGER VECTOR OF LENGTH  K + 2*NT + 1.THE FIRST K LOCATIONS
C       ARE RESERVED FOR THE MULTIPLICITIES OF THE CRACKS ON A BEAM
C       ELEMENT. THE NEXT  NT + 1  LOCATIONS SOMETIMES CONTAIN CRACK
C       INDICES WHEN A CRACK AND A RESPONSE STATION OR THE EXCITATION
C       ARE LOCATED ON THE SAME BEAM ELEMENT. THE NUMBERS OF THE
C       ROWS IN Z MATRIX WHICH CORRESPOND TO THE DEFLECTIONS AT
C       THE RESPONSE STATIONS ARE SAVED IN THE LAST NT LOCATIONS.
C
C REQUIRED IMSL ROUTINES :
C
C   LEQ2C (COMPLEX LINEAR EQUATION SOLVER) AND OTHER ROUTINES CALLED BY IT.
C   LEQ2C FACTORS THE COEFFICIENT MATRIX INTO THE L-U DECOMPOSITION
C   OF A ROWWISE PERMUTATION OF A AND SOLVES THE SYSTEM. LEQ2C COMPUTES
C   THE RESIDUALS AND USES ITERATIVE IMPROVEMENT UNTIL THE SOLUTION
C   IS ACCURATE TO MACHINE PRECISION. (REF: IMSL LIBRARY REFERENCE
C   MANUAL, 9TH ED., V.2, CHPT. L, IMSL, INC., 1982.)
C
C REQUIRED FORTRAN FUNCTION SUBPROGRAMS :
C
C   CDSIN, CDCOS, CDEXP, DCMPLX, DSQRT, DMIN1, DMAX1.
C
```

```
C ERROR CONDITIONS :
C
C   IF IE = IT(J) FOR ANY J AND ABS(XE - XT(J)) IS SMALLER THAN
C   5.D-4 OR IF IND(I) = IE OR IT(J) FOR ANY I AND J AND
C   EC(I) = XE OR XT(J) , THE SUBROUTINE RETURNS TO THE CALLING PROGRAM.
C ***********************************************************************
C
C COMPUTE THE DAMPED B VALUE
C
      D1 = DSQRT(1.D0+DAM**2)
      D2 = .5D0/DSQRT(D1)
      D3 = .5D0*DSQRT(.5D0+.5D0*D1)/D1
      B = BUN*DCMPLX(DSQRT(D2+D3),-DSQRT(D2-D3))
C
C FIND THE MULTIPLICITY OF CRACKS ON EACH CRACKED ELEMENT
C
      IWK(1) = 1
      IF (K .LE. 1) GO TO 5
      J3 = 1
      KM1 = K - 1
      DO 4 J1 = 1, KM1
      IF (IND(J1+1) .NE. IND(J1)) GO TO 3
      IWK(J3) = IWK(J3) + 1
      GO TO 4
    3 J3 = J3 + 1
      IWK(J3) = 1
    4 CONTINUE
C
C CLEAR THE MATRICES
C
    5 DO 8 J1 = 1, IUR
      DO 6 I1 = 1, IXR
    6 X(I1,J1) = 0.D0
      DO 7 I1 = 1, IUR
    7 U(I1,J1) = 0.D0
    8 CONTINUE
      DO 9 J1 = 1, IXR
```

```
      DO 9 I1 = 1, IXR
    9 Z(I1,J1) = 0.D0
      NMP1 = N*(M+1)
C
C SET VARIABLES
C
      JET = 1
      KR = 1
      J = 1
      J3 = 1
      J4 = NMP1 + 1
      J8 = IWK(1)
      JADD = 0
      NTP1 = NT + 1
      DO 12 L = 1, NTP1
   12 IWK(K+L) = 0
      ICOMP = 4
      NOW = 1
      LU = M + 1
      IU = N
C
C ESTABLISH THE MATRICES
C
   15 DO 230 L = 1, LU
      I1 = JADD
      J1 = L
      DO 220 I = 1, IU
      I2 = I
      J2 = J
      IF (ICOMP .EQ. 0) J2 = I*N + L
      IGIRD = 1
      D3 = 0.D0
      IF (IND(KR) .NE. J .OR. KR .GT. K) GO TO 120
      D1 = EC(KR)
      IF (IE .NE. J) GO TO 20
      D2 = XE
      IF (NOW .GT. NT .OR. IE .NE. IT(NOW)) GO TO 40
```

```
      IF (DABS(XE - XT(NOW)) .LT. 5.D-4) GO TO 240
      D2 = DMIN1(XE,XT(NOW))
      D3 = DMAX1(XE,XT(NOW))
      GO TO 40
   20 IF (NOW .GT. NT .OR. IT(NOW) .NE. J) GO TO 90
      D2 = XT(NOW)
   40 IF (D1 - D2) 50, 240, 70
   50 BI = EC(KR)*B
      I2 = N + KR
      J2 = J4
      J4 = J4 + 2
      U(J2,J2) = -1.D0/(B*THE(KR)*DCMPLX(1.D0,DAM))
      U(J2,J2+1) = -U(J2,J2)
      U(J2+1,J2) = U(J2,J2+1)
      U(J2+1,J2+1) = U(J2,J2)
      KR = KR + 1
      ASSIGN 190 TO JUMP
      ASSIGN 40 TO JCR
      IF (KR .LE. J8) GO TO 60
      J3 = J3 + 1
      J8 = IWK(J3)
      ASSIGN 80 TO JCR
      GO TO 130
   60 D1 = D1 + EC(KR)
      GO TO 130
   70 BI = (EC(KR) + D2 - D1)*B
      WK(JET) = EC(KR)
      IWK(K+JET) = KR
      EC(KR) = D1 - D2
      J2 = NMP1 + K + K + JET
      I2 = N + K + JET
      JET = JET + 1
      ASSIGN 200 TO JUMP
      D4 = D2
      IF (D3 .EQ. 0.D0) GO TO 71
      ASSIGN 40 TO JCR
      D2 = D3
```

```
      D3 = 0.D0
      GO TO 72
   71 ASSIGN 90 TO JCR
   72 IF (IT(NOW) .NE. IND(KR) .OR. D4 .NE. XT(NOW)) GO TO 73
      IWK(K+NTP1+NOW) = I2
      NOW = NOW + 1
      GO TO 130
   73 I7 = I2
      GO TO 130
   80 BI = (D2 - D1)*B
      I2 = N + K + JET
      J2 = NMP1 + K + K + JET
      JET = JET + 1
      D1 = D2
      ASSIGN 200 TO JUMP
      ASSIGN 110 TO JCR
      IF (D3 .EQ. 0.D0) GO TO 84
      D2 = D3
      D3 = 0.D0
      ASSIGN 80 TO JCR
   84 IF (IT(NOW) .NE. J .OR. D1 .NE. XT(NOW)) GO TO 85
      IWK(K+NTP1+NOW) = I2
      NOW = NOW + 1
      GO TO 130
   85 I7 = I2
      GO TO 130
   90 BI = EC(KR)*B
      I2 = N + KR
      J2 = J4
      J4 = J4 + 2
      U(J2,J2) = -1.D0/(B*THE(KR)*DCMPLX(1.D0,DAM))
      U(J2,J2+1) = -U(J2,J2)
      U(J2+1,J2) = U(J2,J2+1)
      U(J2+1,J2+1) = U(J2,J2)
      KR = KR + 1
      ASSIGN 90 TO JCR
      ASSIGN 190 TO JUMP
```

```
      IF (KR .LE. J8) GO TO 100
      J3 = J3 + 1
      J8 = IWK(J3)
      ASSIGN 110 TO JCR
      GO TO 130
  100 D1 = D1 + EC(KR)
      GO TO 130
  110 BI = (1.D0 - D1)*B
      IGRD = 2
      I2 = I
      J2 = J
      IF (ICOMP .EQ. 0) J2 = I*N + L
      ASSIGN 210 TO JUMP
      GO TO 130
  120 D1 = 0.D0
      IF (IE .NE. J) GO TO 121
      D2 = XE
      IF (NOW .GT. NT .OR. IE .NE. IT(NOW)) GO TO 80
      IF (DABS(XE - XT(NOW)) .LT. 5.D-4) GO TO 240
      D2 = DMIN1(XE,XT(NOW))
      D3 = DMAX1(XE,XT(NOW))
      GO TO 80
  121 IF (NOW .GT. NT .OR. IT(NOW) .NE. J) GO TO 122
      D2 = XT(NOW)
      GO TO 80
  122 BI = B
      IGRD = 3
      ASSIGN 210 TO JUMP
  130 BI = ES(I+JADD)*BI
C
C COMPUTE THE Π-CIRCUIT PARAMETERS
C
      EXP1 = CDEXP(BI)
      EXP2 = CDEXP(-BI)
      W = (EXP1 - EXP2)/2.D0
      WP = (EXP1 + EXP2)/2.D0
      EXP1 = CDSIN(BI)
```

```
      EXP2 = CDCOS(BI)
      ALF = WP*EXP2 - 1.D0
      P = WP*EXP1
      Q = (P - W*EXP2)/ALF
      P = (P + W*EXP2)/ALF
      QP = W*EXP1/ALF
      PP = (W + EXP1)/ALF
      W = (W - EXP1)/ALF
      WP = (WP - EXP2)/ALF
C
      U(J2,J2) = U(J2,J2) + Q
      IF (I1 .EQ. 0) GO TO 160
      U(J1,J1) = U(J1,J1) + Q
      U(J1,J2) = W
      U(J2,J1) = W
      I3 = ICOMP + IGIRD
      GO TO (150,170,180),I3
      Z(I1,I1) = Z(I1,I1) + P
      Z(I1,I2) = Z(I1,I2) - PP
      Z(I2,I1) = Z(I2,I1) - PP
      X(I1,J1) = X(I1,J1) - QP
      X(I1,J2) = -WP
  150 X(I2,J1) = WP
  160 X(I2,J2) = QP
      Z(I2,I2) = Z(I2,I2) + P
      GO TO 180
  170 X(I1,J1) = X(I1,J1) - QP
      X(I1,J2) = -WP
      Z(I1,I1) = Z(I1,I1) + P
  180 J1 = J2
      I1 = I2
      GO TO JUMP,(80, 110, 190, 200, 210)
  190 J1 = J1 + 1
  200 IGIRD = 4
      GO TO JCR,(40, 80, 90, 110)
  210 J = J + 1
  220 CONTINUE
```

```
  230 CONTINUE
      IF (JADD .EQ. N) GO TO 250
      JADD = N
      ICOMP = 0
      LU = N
      IU = M
      GO TO 15
  240 WRITE(6,250)
  250 FORMAT(1X,'LOCATIONS SPECIFIED FOR DIFFERENT THINGS TOO CLOSE')
      RETURN
  260 D1 = 0.D0
      DO 265 I = 1, M
  265 D1 = D1 + ES(N+I)
      BI = B*D1
      DO 266 I = 1, N
  266 Z(I,I) = Z(I,I) + BI
C
C MATRICES ESTABLISHED
C
      DO 270 I = 1, NTP1
      IF (IWK(K+NTP1+1-I) .EQ. 0) GO TO 270
      EC(IWK(K+NTP1+1-I)) = WK(NTP1+1-I)
  270 CONTINUE
      DO 300 J = 1, IXR
      DO 290 I = 1, IUR
  290 XTR(I,J) = X(J,I)
  300 CONTINUE
C
C COMPUTE  U^-1 X^T
C
      IJOB = 0
      CALL LEQ2C(U, IUR, IUR, XTR, IXR, IUR, IJOB, WA, WK, IER)
      IF (IER .NE. 0) RETURN
C
C COMPUTE  Z - XU^-1 X^T
C
      DO 380 J = 1, IXR
```

```
      DO 370 I = 1, J
      BI = 0.D0
      DO 360 I1 = 1, IUR
  360 BI = BI + X(I,I1)*XTR(I1,J)
  370 Z(I,J) = Z(I,J) - BI
  380 CONTINUE
      I1 = IXR - 1
      DO 390 J = 1, I1
      J1 = J + 1
      DO 390 I = J1, IXR
  390 Z(I,J) = Z(J,I)
C
      DO 400 I = 1, IXR
  400 RH(I) = 0.D0
      RH(I7) = 1.D0
C
C COMPUTE  [Z - XU^-1X^T]^-1 RH
C
      IJOB = 0
      I = 1
      CALL LEQ2C(Z, IXR, IXR, RH, I, IXR, IJOB, WA, WK, IER)
      IF (IER .NE. 0) RETURN
C
      NKP1 = N + K + 1
      DO 420 I = NKP1, IXR
  420 WA(I) = RH(I)
      DO 430 I = 1, NT
  430 RH(N+K+I) = WA(IWK(K+NTP1+I))
      RH(IXR) = WA(I7)
      RETURN
      END
```

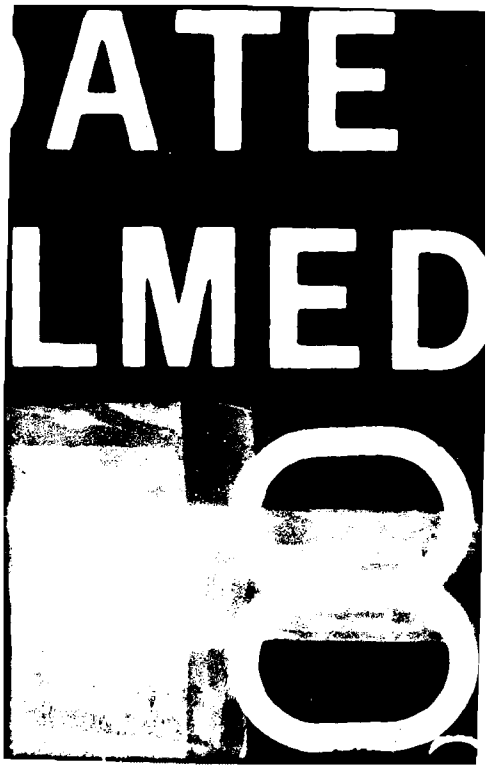
ATE
LMED
8